

Francisco Serrano Alcalde

Finite Element modeling of cell
behavior under different
biophysical stimuli: from passive to
active behavior.

Director/es

Dra. D^a. María José Gómez Benito
Dr. D. José Manuel García Aznar

<http://zaguan.unizar.es/collection/Tesis>

© Universidad de Zaragoza
Servicio de Publicaciones

ISSN 2254-7606



Universidad
Zaragoza

Tesis Doctoral

FINITE ELEMENT MODELING OF CELL BEHAVIOR
UNDER DIFFERENT BIOPHYSICAL STIMULI:
FROM PASSIVE TO ACTIVE BEHAVIOR.

Autor

Francisco Serrano Alcalde

Director/es

Dra. D^a. María José Gómez Benito
Dr. D. José Manuel García Aznar

UNIVERSIDAD DE ZARAGOZA
Escuela de Doctorado

2021

**Finite Element modeling of cell
behavior under different biophysical
stimuli: from passive to active behavior.**



Universidad Zaragoza

Francisco Serrano Alcalde

Aragón Institute of Engineering Research (I3A)

University of Zaragoza

Faculty Advisors:

María José Gómez Benito

José Manuel García Aznar

A thesis submitted for the degree of
Doctor of Philosophy in Biomedical Engineering
September 2021

A mis padres y hermano.

A Irene.

*True success is not the absence of failure, it is the refusal to
surrender.*

~ Lazarus Lake

Agradecimientos

Me gustaría comenzar expresando mi más sincero agradecimiento a mis directores de tesis, M^aJosé y Manu, por haberme guiado todos estos años y haberme animado a embarcarme en este proyecto. Por su apoyo y confianza durante todo este tiempo. Siempre habéis encontrado un hueco para juntarnos y echarme una mano, aunque a veces no haya sido sencillo.

Agradecer también la predisposición de todos los miembros del grupo M2BE por su ayuda en los momentos que lo he necesitado. Y a mis compañeros del Instituto Tecnológico de Aragón, por todas las discusiones que las Tesis y Abaqus nos han brindado.

Por supuesto, quiero agradecer a mis abuelas, tíos y primos por haberme dado ánimos en todo momento. Al *trailrunner*, por tantos kilómetros recorridos y todos los que quedan por completar.

A mis padres y hermano, por haberme apoyado siempre en todas y cada una de mis decisiones, dándome la libertad de equivocarme. Esta Tesis es también vuestra.

A Irene, por haber padecido todo el tiempo que una Tesis requiere, por entenderme y acompañarme en este viaje que acaba de comenzar.

Abstract

Cell mechanobiology is focused on the study of the cells behavior when they are subjected to mechanical loads and the transduction mechanisms involved. It is known that cells are able to adapt to the mechanical environment in which they are, being able to increase or decrease their stiffness depending on the stiffness of the surrounding substrate. In addition, they are able to switch from one migration mode to another, searching for the most efficient way to migrate depending on the mechanical properties of the extracellular matrix in which they are embedded. Nevertheless, this adaptive capacity also allows some tumor cells to change their mechanical properties to invade other organs more efficiently. To do this, cells use different mechanotransduction mechanisms that allow them to make this type of decision depending on what they are sensing mechanically.

Understanding mechanotransduction mechanisms is not a simple task, however, computational models can help to better understand what the cell is sensing to make some of its decisions. For this purpose, there are different types of computational models in the literature, from agent-based models to continuum models, including hybrid models, which have helped to understand part of the mechanotransduction mechanisms, although many of them are still unsolved.

In this PhD Dissertation, we investigate how cells are able to sense different mechanical environments passively and actively. To do so, three different computational models are presented and solved using the Finite Element Method (FEM). Due to the great capacity of cells to adapt to the environment and to be in constant remodeling, the constitutive models of material for each case study are different depending on the predominant behavior. These models show the mechanical response that cells could be sensing under different conditions. The first case corresponds to a passive cell flowing inside a cytometer, where the velocity profile variation produced by a reduction of the channel section deforms the cell. The second one is a single cell using lobopodial migration in a three

dimensional extracellular matrix, where the mechanical properties of the matrix depend on the level of deformation or are constant. Finally, the last case corresponds with the simulation of a cell culture on a plate, where bacterial infection is simulated.

These three models together are intended to give some insight into the different mechanotransduction mechanisms that cells may use to sense their environment and that could trigger important biological mechanisms.

Resumen

La mecanobiología celular se encarga del estudio del comportamiento de las células cuando son sometidas a cargas mecánicas y de los mecanismos de mecanotransducción que éstas tienen. Se sabe que las células son capaces de adaptarse al ambiente mecánico en el que se encuentran, pudiendo aumentar o disminuir su rigidez en función de la rigidez del sustrato que las rodea. Además, son capaces de cambiar de un modo de migración a otro, buscando el modo más eficiente de migrar dependiendo de las propiedades mecánicas de la matriz en la que se encuentren. Sin embargo, esta capacidad de adaptación también permite que algunas células tumorales cambien sus propiedades mecánicas para invadir otros órganos de manera más sencilla. Para ello, las células utilizan diferentes mecanismos de mecanotransducción que les permiten tomar este tipo de decisiones en función de lo que estén sintiendo mecánicamente.

Descifrar y entender los mecanismos de mecanotransducción no es una tarea sencilla, sin embargo, los modelos computacionales ayudan a entender mejor qué está sintiendo la célula para tomar algunas de estas decisiones. Para ello, distintos autores han propuesto diferentes tipos de modelos computacionales, desde modelos basados en agente a modelos continuos, pasando por modelos híbridos, que han ido resolviendo parte de los mecanismos de mecanotransducción, aunque todavía quedan muchos de ellos sin resolver.

En esta Tesis, se estudia cómo las células son capaces de sentir diferentes ambientes mecánicos de manera pasiva y activa. Para ello, se presentan tres modelos computacionales distintos que se resuelven utilizando el Método de los Elementos Finitos (MEF). Debido a la gran capacidad de las células para adaptarse al entorno y estar en constante remodelación, los modelos constitutivos de material para describir cada caso de estudio son diferentes en función del comportamiento predominante. Estos modelos muestran la respuesta mecánica que las células podrían estar percibiendo en diferentes condiciones. El primero

es una célula fluyendo de forma pasiva por el interior de un citómetro donde el cambio en el perfil de velocidad, provocado por el cambio de sección del canal, induce una deformación en la célula. El segundo es una célula migrando de forma lobopodial dentro de una matriz extracelular tridimensional, donde sus propiedades mecánicas dependen o no del nivel de deformación que soporte la matriz. Finalmente, el último de los modelos es un cultivo celular sobre una matriz donde se simula la infección por bacteria de algunas células del cultivo.

Todos los modelos en conjunto pretenden dar a conocer los diferentes mecanismos de mecanotransducción que las células pueden utilizar para percibir su entorno y que podrían desencadenar importantes mecanismos biológicos.

Contents

1	Introduction	1
1.1	Mechanobiological background	2
1.1.1	Main mechanical components of the cell	2
1.1.2	Cell migration	5
1.1.3	Cell mechanosensing	9
1.1.4	Modeling individual and collective cell behavior	12
1.2	Motivation and objectives	15
1.3	Outline	16
2	Passive cell behavior	19
2.1	Introduction	20
2.2	Materials and Methods	22
2.2.1	Geometry and materials	22
2.2.2	Fluid-structure interaction	23
2.2.3	Boundary conditions	25
2.3	Results	27
2.3.1	Cell stretching due to fluid flow	27
2.3.2	Quantification of cell deformability	32
2.3.3	Strains and stresses on the cell nucleus	34
2.3.4	Velocity profile around the cell	36
2.4	Discussion and Conclusions	37

3	Active cell mechanosensing in lobopodium formation	39
3.1	Introduction	40
3.2	Materials and Methods	42
3.2.1	Model description	42
3.2.2	Constitutive law	44
3.2.3	Finite Element approach	46
3.3	Results	47
3.3.1	Cytoplasmic fluid behavior	48
3.3.2	Mechanical state of the ECM and nucleus	49
3.4	Discussion and Conclusions	54
4	Collective cell response under infection conditions	57
4.1	Introduction	58
4.2	Materials and Methods	59
4.2.1	Description of cell model and mechanotransduction mechanism	63
4.2.2	Computational model and boundary conditions	68
4.3	Results	69
4.3.1	Cell contraction and protrusion	70
4.3.2	The role of cell-cell junctions	72
4.3.3	The role of the active/passive part of the cell	78
4.3.4	Cell protrusion law	79
4.4	Discussion and Conclusions	80
5	Discussion and conclusions	83
5.1	General conclusions	84
5.2	Future work	87
5.3	Contributions	88
5.3.1	Publications in peer-review journals	88
5.3.2	Congress and conference contributions	89

6 Conclusiones y líneas futuras	91
6.1 Conclusiones generales	92
6.2 Trabajo futuro	95
6.3 Contribuciones	96
6.3.1 Publicaciones en revistas	96
6.3.2 Congress and conference contributions	97
Bibliography	99

List of Figures

1.1	Simplified cell scheme	3
1.2	Diagram of cell monolayer adhesions	4
1.3	Main steps of cell migration on 2D substrates	6
1.4	Main different migration modes depending on adhesion and contractility	7
1.5	Regulation of cell migration depending on ECM and cell regulators	8
1.6	LINC complex scheme	10
1.7	YAP mechanosensitive transcriptional activator scheme	11
1.8	Continuum mechanics and agent-based models	14
2.1	Setup scheme of the cytometer presented by Otto	21
2.2	Velocity profile in the inlet section that follows the Purday approach	26
2.3	Rigid cell used to stabilize the fluid flow.	26
2.4	Deformed shape of a cell through the channel in the central X-Y plane	28
2.5	Cell longitudinal axis deformed length by channel position	29
2.6	Cell longitudinal axis deformed length by channel position (2)	30
2.7	Experimental cell deformed inside the cytometer	31
2.8	Adimensional inertia along the longitudinal and transversal axis	33
2.9	Nuclear stress distribution across a stabilized deformed cell shape	35
2.10	Velocity profile around a rigid sphere and around a deformed cell	37

3.1	Cell migrating in lamellopodial and lobopodial way and their intracellular pressures	41
3.2	Axisymmetric cell section with a simplified lobopodial geometry	43
3.3	Evolution of the hydrostatic pressure in the front part of the cytoplasm	49
3.4	Sensitivity analysis of the cytoplasmic mechanical properties on the cytoplasmic hydrostatic pressure	50
3.5	Fluid velocity in the cytoplasm	51
3.6	Logarithmic maximum principal strain in the ECM	52
3.7	Final equivalent elastic modulus of the ECM	53
3.8	Maximum principal stresses in the nucleus	53
4.1	Experimental results of L.m. mounding	60
4.2	Monolayer scheme of listeria infection	62
4.3	ECM displacements provoked by uninfected cells migrating towards the infection focus	62
4.4	Cell scheme	63
4.5	Geometrical parts of the cell	65
4.6	Cohesive contacts	66
4.7	Cell mechanotransduction scheme	67
4.8	Computational model of the cell monolayer	68
4.9	Cell displacements and cell stresses during contraction	71
4.10	Cell displacements and ECM displacements during protrusion . .	73
4.11	Mound formation	74
4.12	Displacement and stress of isolated cells	75
4.13	Stresses in cell mixing	76
4.14	Mound formation for cellular mixing	77
4.15	Mound formation when active or passive part is neglected	78
4.16	Protrusion law	80

List of Tables

2.1	Mechanical and geometrical properties of simulated cells	24
2.2	Adimensional inertia tensor of the deformed cell shape along the three axes for different configurations.	34
3.1	Summary of the simulated ECM properties	43
3.2	Mechanical properties of the cytoplasm and nucleus	46
3.3	Number and type of elements used in the model	47
4.1	Summary of cell mechanical properties used in the simulations	64
4.2	Summary of cell-cell junction and cell-ECM adhesion properties	67

Chapter 1

Introduction

Contents

1.1	Mechanobiological background	2
1.1.1	Main mechanical components of the cell	2
1.1.2	Cell migration	5
1.1.3	Cell mechanosensing	9
1.1.4	Modeling individual and collective cell behavior . . .	12
1.2	Motivation and objectives	15
1.3	Outline	16

1.1 Mechanobiological background

In this chapter, we briefly introduce the main cellular components that regulate the mechanical behavior of cells. First, an introduction to the most relevant parts of the cell, with especial focus on mechanics, is given. Then, the main modes of migration described so far are explained, from the migration of single cells to cell assemblies acting collectively or not. In addition, the mechanosensing mechanism of cells is analyzed and how they are able to sense their surroundings. Finally, a brief survey of the state of the art on methods of modeling cell behavior, both individually and collectively, is made.

1.1.1 Main mechanical components of the cell

The cell is the structural unit of the human body, they form all the organs and tissues of the body. There are different types of cells depending on whether they are found in one organ or another and the different functions they perform, but all of them are composed of: nucleus, cytoplasm and membrane.

The nucleus contains the chromosomes, which encodes the genetic material. Its function is to control cellular activity through the genes expression. From a mechanical point of view, it is about ten times stiffer than the cytoplasm (Friedl et al. (2011)) and present a variable compressibility. In fact, experimental works found negative values of Poisson's ratio (Pagliara et al. (2014)). Different authors have linked the mechanical environment in the nucleus to important processes such as cell differentiation, proliferation or apoptosis (Janota et al. (2020); Martins et al. (2012)).

Outside the nucleus and surrounded by the cell membrane is the cytoplasm, which contains different organelles such as the endoplasmic reticulum. From a mechanical point of view, it could be divided into two parts: the cytoskeleton and the cytosol. The cytoskeleton is considered the skeleton of the cell, forming a three-dimensional network and connecting all the structures inside, including the nucleus with the outer membrane. However, this cellular skeleton is dynamic, so that it can change its shape, exert forces, coordinate with or sense the extracellular environment. At the same time, this cytoskeleton has three main

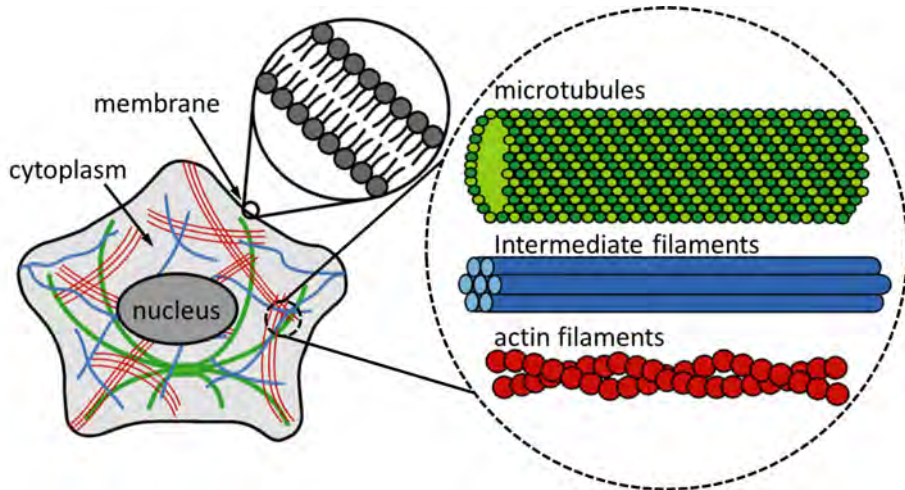


Figure 1.1: Simplified scheme of the principal cell components distinguishing between nucleus, cytoplasm and membrane. Within the cytoplasm we can also distinguish between the cytoskeleton and the cytosol. The main components of the cytoskeleton are microtubules, intermediate filaments and actin filaments. Adapted from Rodriguez et al. (2013)

components: actin filaments, intermediate filaments and microtubules. Actin filaments support tensile loads and together with myosin are responsible for cell contraction, generating tension and allowing the cell to move. Each actin filament is composed of monomers of G-actin, these monomers polymerize forming F-actin and form the filament as a double helix between 5 and 9 nm in diameter. The intermediate filaments also resist tension and hold the nucleus inside the cell, giving mechanical stability. These filaments are composed of combined protofilaments that form filaments of about 10 nm in diameter. Finally, microtubules are the largest diameter structures (24 nm), they work in compression maintaining the shape of the cell. This structure is organized towards the microtubule organization center (MTOC), which is located near the nucleus and it is the place from which the microtubules emerge. In addition, all these structures form the cytoplasm together with an aqueous solution of salts and various organic molecules called the cytosol.

The membrane is a 5 to 10 nm lipid bilayer that contains and separates the interior of the cell from the external environment, although it is selectively permeable, favoring the exchange of ions and organic molecules. It plays a

1.1. Mechanobiological background

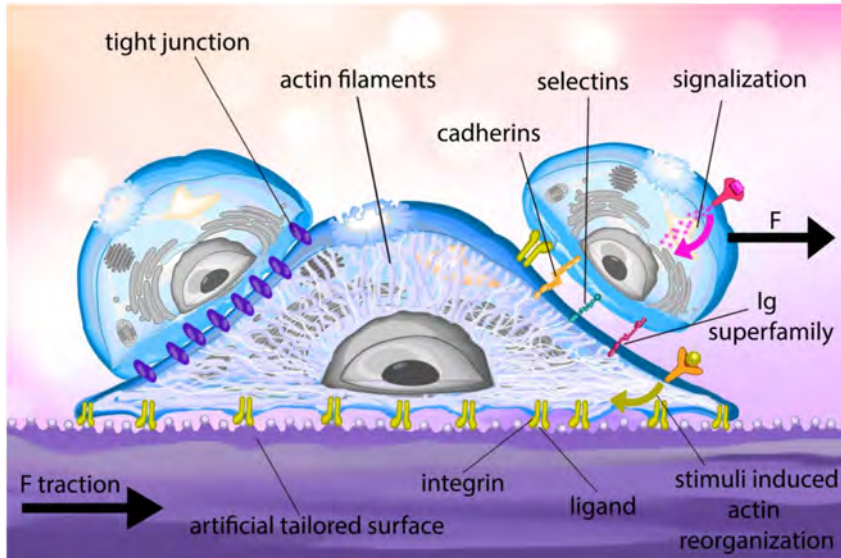


Figure 1.2: Diagram of a cell and its surrounding structure where the cell creates adhesions with extracellular matrix and junctions with contiguous cells. Cell-matrix adhesions are focal adhesions of cytoplasmic protein complexes connecting F-actin with integrins and ligands of the extracellular matrix. Cell-cell adhesions are mainly tight junctions, gap junctions and anchoring junctions. Anchoring junctions are connected to the cytoskeleton and are the most important for force transmission between cells. Diagram including actin filaments distribution (Ungai-Salánki et al. (2019)).

fundamental role in processes such as ion conduction, the exchange of chemical signals between cells or adhesion to the extracellular matrix or other cells.

Adhesions and junctions are essential for cells to be able to migrate and sense the surrounding environment. On the one hand, cells can generate adhesions with the extracellular matrix and junctions with the other cells that are around them. The adhesions they generate with the extracellular matrix are focal adhesions, which are complexes of cytoplasmic proteins (such as vinculin and talin) that connect F-actin with transmembrane receptors (integrins) and finally with the ligands of the extracellular matrix. On the other hand, the way of generating junctions with other cells is mainly by means of tight junctions, gap junctions and anchoring junctions. Tight junctions are composed of proteins that serve to create a seal between cells. Gap junctions are pores com-

posed of connexins, innexins and pannexins that allow the transport of small molecules. Finally, there are the anchoring junctions, which function is mainly structural, transmitting forces and tensions and maintaining the integrity of the cell by connecting the cytoskeletons of the cells. In addition, within the anchoring junctions we can find adherens junctions and desmosomes, which link actin filaments by means of cadherin proteins and intermediate filaments of adjacent cells, respectively. Figure 1.2 shows the adhesion and junction scheme for a monolayer on an extracellular matrix, where cells adhere to each other and to the substrate. In the case of cells embedded in three-dimensional substrates the bonds to the ECM and between cells would be in a combined manner.

Thus, we overview the main components that a cell needs and uses to structure itself internally, generating forces and connecting to the surrounding environment and transmitting and sensing forces.

1.1.2 Cell migration

Cell migration is a key process for establishing and maintaining the correct organization of multicellular organisms. We normally distinguish between two-dimensional (2D) migration and three-dimensional (3D) migration according to how cells move.

Migration in 2D has been widely studied due to its lower complexity to replicate in the laboratory. Normally, this motion is produced by a movement called lamellopodia and involves several consecutive processes: first the cell polarizes, then the front part (in the direction of movement) protrudes and adheres to the matrix, and finally the cell contracts and its rear detaches. The protrusion stage consists of actin polymerization at the front of the cell and depolymerization close to the nucleus. Thus, the cell extends an arm forward on which new adhesions are generated and from which the cell pulls in the contraction stage to produce the movement. Usually, cell migrating in 2D substrate (Figure 1.3) protrudes the front part in the direction of movement, then the rear part of the cell contracts and reacts.

Regarding 3D migration, it is the most common migration in the human body since human tissues are 3D, and it can take place mainly through three

1.1. Mechanobiological background

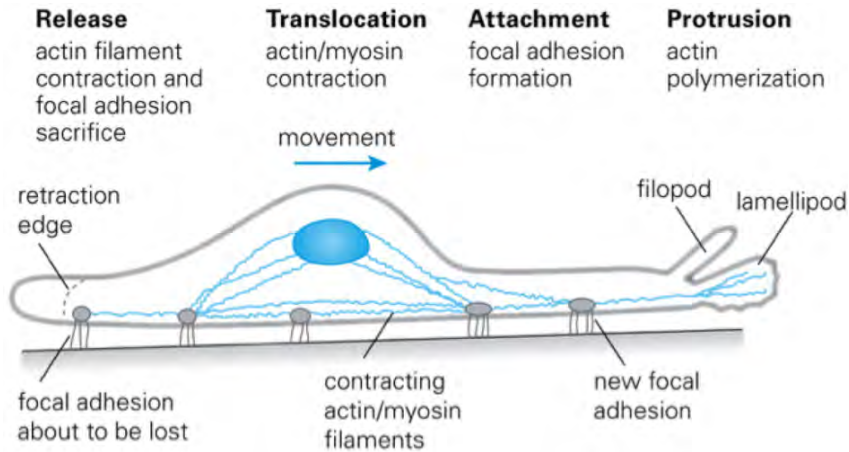


Figure 1.3: The main steps for cell migration on 2D substrates are represented. The first step for lamellipodial migration is protrusion, where the cell extends the front part in the direction of movement and creates new focal adhesions. After that, cell contracts and detaches the rear part pulling from the front part of the cell. Adapted from Introduction to Cell Mechanics and Mechanobiology (Jacobs et al. (2012))

different modes. Lamellopodia (similar to that produced in 2D migration), amoeboid (occurs when cell-matrix adhesion is low) and lobopodia, in which a main protuberance appears at the front of the cell, where the nucleus moves forward and divides the cell in two differentiated parts, (the front and rear of the nucleus). It generates an intracellular hydrostatic pressure producing a high pressure zone (front of the nucleus) and a low pressure zone (rear of the nucleus). In addition to the level of adhesion, the different migration modes also depend on the mechanical properties of the extracellular matrix and, among other factors, each migration mode generates different levels of contraction to migrate. Figure 1.4 shows different migration modes according to the levels of adhesion and contraction that each one presents.

In addition to cell-specific factors, the extracellular matrix is an important regulator of cell migration depending on different properties of the matrix. In 2D migration, matrix composition, stiffness or ligand density are the main regulatory factors.

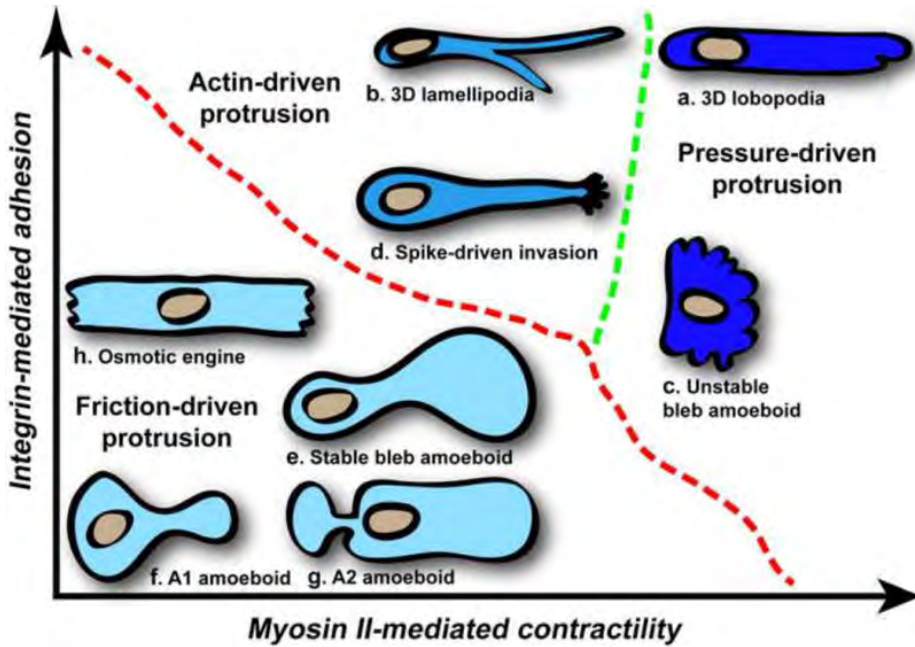


Figure 1.4: Graphical representation of the main different migration modes under different dimensionality conditions of the substrates depending on adhesion and contractility. (a) Lobopodial migration where the nucleus acts as a piston pressurizing the front part of the cell and highly cell-matrix adhesion and actomyosin contractility are required. (b) Lamellopodia in 3D substrates is similar to the described in 2D substrates. The protrusion-contraction mechanism allows the cell's movement pushing the plasma membrane through the matrix. (c) Unstable amoeboid bleb is present in some tumor cells with low cell-matrix adhesion and high contractility. Increased intracellular pressure help the cell to squeeze through the 3D matrix. (d) Spike-drive migration mode is used by breast cancer cells. These cells form distinctive spikes of F-actin at their leading edge and reduce the cell-matrix adhesion to enable the invasive behavior. (e-h) Integrin-mediated adhesion is not always necessary to migrate in 3D. Amoeboids are able to migrate with low contractility and low adhesion to the matrix. Adapted from Petrie and Yamada (2016)

1.1. Mechanobiological background

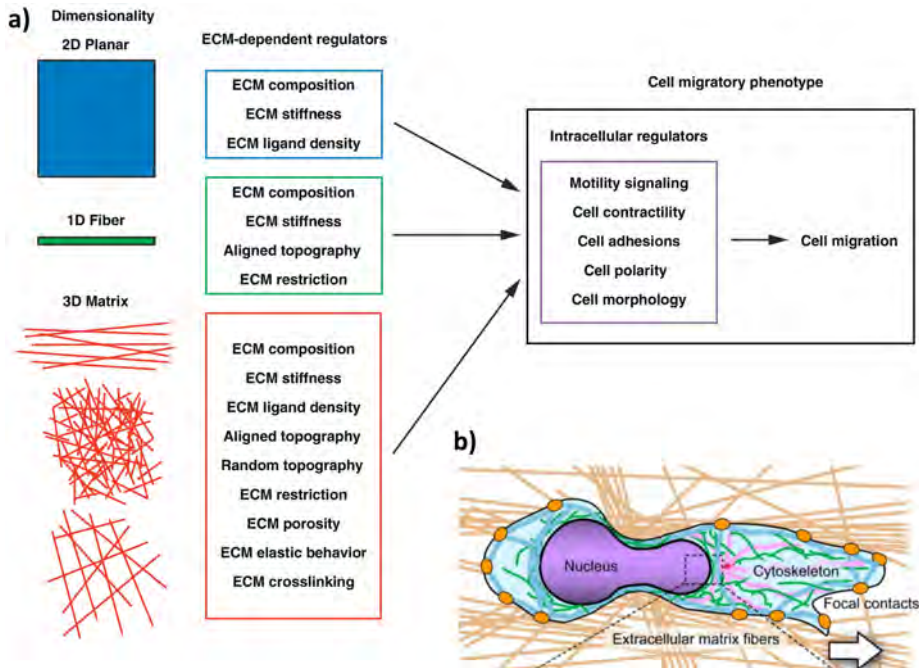


Figure 1.5: Regulation of cell migration depending on ECM and cell regulators. (a) Summary of the main factors that regulate migration modes depending on the extracellular matrix properties and intracellular regulators. (b) Graphical representation of a cell migrating through a 3D matrix where the nucleus is being deformed. Adapted from Doyle et al. (2013) and Friedl et al. (2011)

3D migration is not only influenced by the ECM factors previously discussed in 2D migration, but also by additional factors, such as, topography, porosity, elastic behavior or matrix crosslinking are also important. Figure 1.5a shows the main factors influencing cell migration, both intracellular regulators and extracellular matrix-dependent regulators. An example of how matrix factors affect migration is the work of Pathak and Kumar (2012), where the degree of cell confinement or stiffness of the extracellular matrix is changed and the speed of migration is affected. Another case is the work of Wolf et al. (2013), where the effect of pore size and deformability of the nucleus during migration is studied. A representation of the effect of matrix pore size and stiffness is shown in Figure 1.5b, where the deformed nucleus is pulled by the front part of the cytoplasm.

1.1.3 Cell mechanosensing

Cells are constantly exposed to mechanical stimuli coming from the extracellular matrix or from neighboring cells. The ability of cells to sense these physical stimuli and transform them into biological responses is known as *mechanotransduction*. This involves intracellular molecular processes that cells use to know not only the stiffness of their surroundings, but also the forces, stress, strain, deformation, topography or adhesiveness of their environment.

Compression-induced shape changes in chondrocyte nuclei correlate with changes in cartilage composition and density (Guilak (1995)) and this correlative behavior becomes more striking in pathological states. In addition, changes in nuclear morphology, such as nuclear size or nuclear shape, are often used to identify cancerous tissue (Zink et al. (2004)). Breast cancer cells are known to be affected by their mechanical and structural environment (Paszek et al. (2005)) and Bissell et al. (1999) found a stronger correlation between a cancerous phenotype and nuclear morphology than between cellular morphology and cancer. Furthermore, changes in nuclear stiffness can serve as indicator of increased tumor cell mobility, metastasis potential or bacterial infection (Bastounis et al. (2021); Wolf and Friedl (2006); Wolf et al. (2007)). However, despite the importance of these transduction processes, most of the mechanisms that cells use are unknown.

Focal adhesions (FA) or cell-matrix adhesions are necessary factors for cell migration, as they allow the cell to bind to the substrate (Escribano et al. (2014)). Within focal adhesions there are several types with different molecular composition. To them the cytoskeleton binds, which propagates the forces from the cell to the matrix and vice versa. The different types of focal adhesions preferentially bind to certain parts of the cytoskeleton and finally connect to the nucleus, thus propagating the forces from the outside of the cell to the nucleus. These cell-matrix and FA-nucleus connections (via the cytoskeleton) do not remain constant and are constantly reorganizing, breaking, separating and rejoining. This variation in the organization of the cytoskeleton can lead to changes in gene expression and consequent alteration of the biological response (Dupont et al. (2011); Jaalouk and Lammerding (2009); Tamada et al. (2004)).

1.1. Mechanobiological background

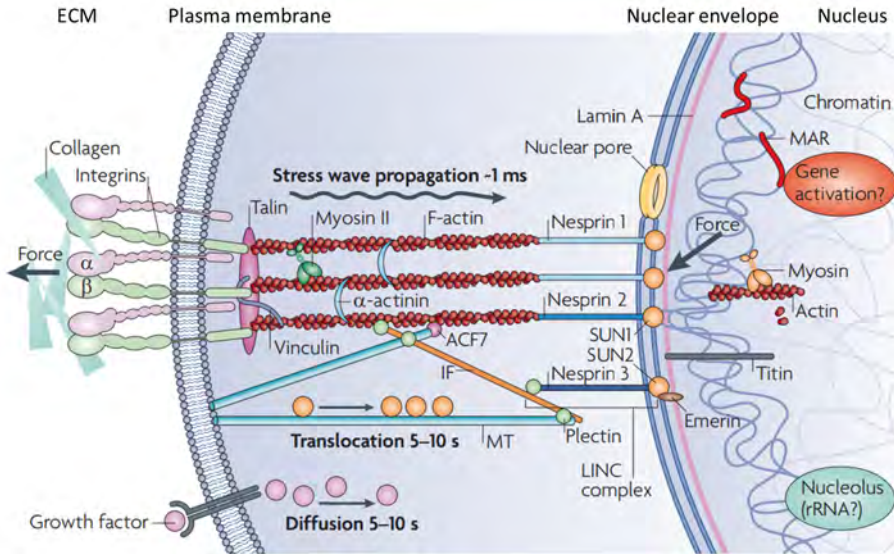


Figure 1.6: Scheme of the LINC complex which links and drives the forces on the cell membrane through the cytoskeleton to the nucleus. Adapted from Wang et al. (2009)

Mechanical information traveling through the cytoskeleton reaches proteins in the membrane of the nucleus or in the cytoplasm, which send the information into the nucleus. One known mechanism is the LINC complex (Figure 1.6) which connects and transmits the exterior forces to the nucleus through transmembrane integrins, associated focal adhesions and junctional complexes, and cytoskeletal filaments that connect to the nucleus (Wang et al. (2009)). Another mechanism is the Hippo pathway, a network of proteins that are important for normal healthy cell behavior and tissue growth, but a switch is often involved in cancer. Yes-associated protein (YAP) is a major pathway in vertebrates and its activity is regulated by extracellular matrix stiffness or cell spreading. There are different conditions under which the balance of YAP is altered (Figure 1.7a), nucleus deformation leads to the alteration of YAP due to changes on the nuclear membrane pores (Figure 1.7b).

Despite the knowledge about some mechanotransduction mechanisms, most of these are unknown and some studies suggest the possibility that the nucleus possesses its own mechanosensing mechanism (Cho et al. (2017)).

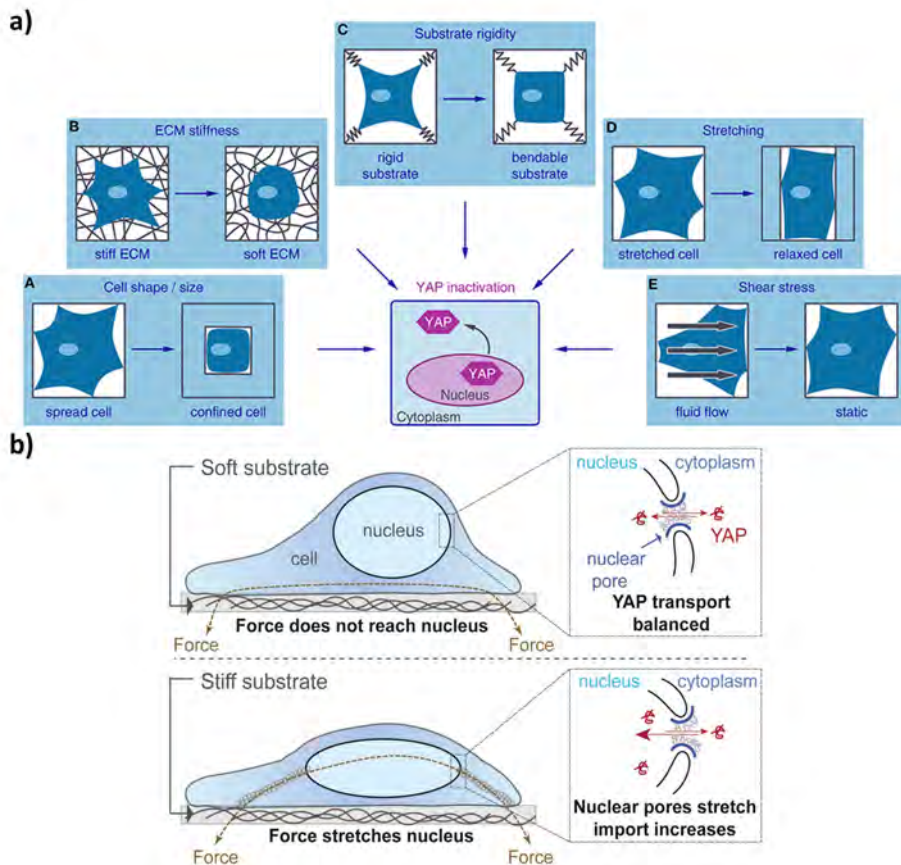


Figure 1.7: YAP mechanosensitive transcriptional activator scheme. (a) Different mechanical inputs regulate YAP activity; (b) Nuclear pores modify the YAP balance when the forces stretch the nucleus. Adapted from Fischer et al. (2016) and Elosegui-Artola et al. (2017)

1.1. *Mechanobiological background*

Nevertheless, there is evidence that sensing mechanisms exist due to the observed biological responses. The mechanism of durotaxis (Lo et al. (2000)), where a cell is able to detect different stiffnesses of the extracellular matrix, haptotaxis (Hsu et al. (2005)), where cells are able to detect areas with increased adhesion or tensotaxis (Lin et al. (2009)), where cells recognize substrate pre-tensions.

1.1.4 **Modeling individual and collective cell behavior**

In this section we summarize the different mechanical methodologies used to simulate both single cells and cell assemblies. We mainly focus on the different continuous models that have been used to replicate, interpret or predict experimental results. Within this category we can distinguish between active or passive models, where cells may or not incorporate biomechanical cellular processes that react to loads or mechanical conditions surrounding them or attempt to replicate cell movements. In addition, we also describe agent-based models in which a discrete approximation of the problem is performed.

Continuum mechanic models

Continuum models have been mainly used to simulate isolated cells under certain conditions, tissues or cell assemblies from a larger scale, where each cell is not simulated separately but together as a continuous material. However, there are also models that use this approach to represent individual cells in a cellular cluster.

Within the continuum models, there are a multitude of sub-models or ways of considering the cells, from liquids surrounded by a membrane, solids, mixtures of solid and liquid or internal structures representing the different parts of the cytoskeleton working under traction and compression. In addition, the constitutive models used are also very different even though the same modeling technique is used, resulting in different cell behavior. Most of these models are solved using the finite element method (De Santis et al. (2011); Kaunas and Hsu (2009); Lim et al. (2006); Mijailovich et al. (2002); Moeendarbary et al. (2013); Müller et al. (2021); Peskin et al. (1993); Rodriguez et al. (2013); Safran and

De (2009); Vernerey and Farsad (2011); Zemel et al. (2006); Zhou et al. (2012, 2005)).

If we divide the models according to the state of the material we have: liquid models, solid models and two-phase models. First, liquid models represent the cell as a fluid enclosed by a thin, solid and prestressed membrane. This type of models can represent the cell homogeneously (only one fluid and one membrane) or as the composition of several fluids enclosed by several membranes (a fluid representing the nucleus and separated by a membrane from an outer fluid representing the cytoplasm and in turn contained by another membrane). In addition, the fluid can be modeled with Newtonian or non-Newtonian behavior which affects the viscous behavior according to the shear rate (Lim et al. (2006)). Secondly, solid models assume the cell as a continuum solid model, although they can simulate different subcellular parts (cytoplasm, nucleus or membrane, among others). There is a great variety of solid models depending on the material constitutive model used and whether they model the cell as a passive component (not being able to generate or react to external stimuli) or active (able of generating or actively reacting to external stimuli). Within the models that consider the cell passively there are different constitutive models of material of different degrees of complexity, linear-elastic model (Mijailovich et al. (2002)), linear-viscoelastic (Zhou et al. (2005)), hyperelastic (Müller et al. (2021)), or power-law rheology (Zhou et al. (2012)). A more complex material needs to adjust more parameters than simple constitutive models. In addition, tensegrity models (De Santis et al. (2011)) are also passive models, where a structure of cables and bars working in tension and compression, respectively, simulates cell cytoskeletal behavior. Regarding active models, there are also several types: dipole polymerization models (Zemel et al. (2006)), Brownian ratchet models (Peskin et al. (1993)), stress-fiber reorganization models (Kaunas and Hsu (2009)), dynamic stochastic models (Safran and De (2009)) or constrained mixture models (Vernerey and Farsad (2011)), among others. These models try to recreate acto-myosin contraction, protrusion forces during polymerization or fiber reorganization (Hervas-Raluy et al. (2019); Ronan et al. (2012)). Furthermore, these models can be combined in such a way that there are passive and active parts in the cell (Moreo et al. (2008)). Finally, biphasic models consider the cell or part of it as a porous solid material that is filled with fluid and can move through pores (Moendarbary et al. (2013)). This type of models are

1.1. Mechanobiological background

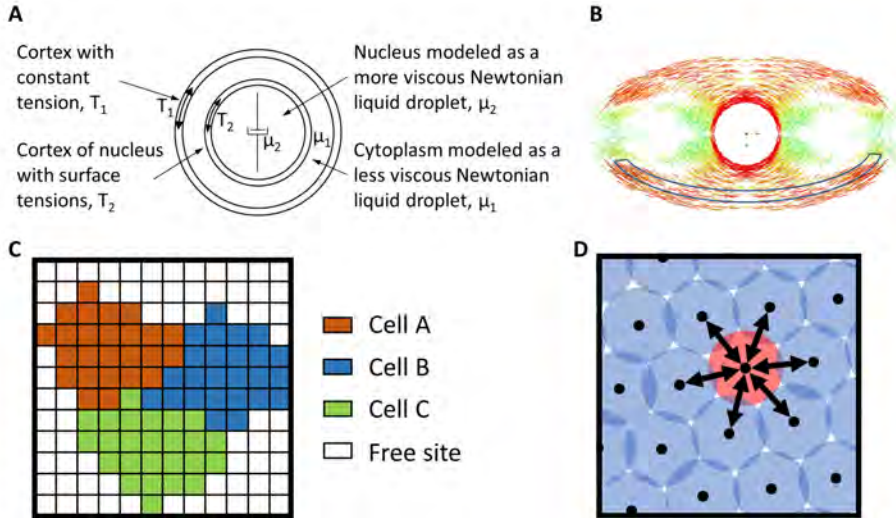


Figure 1.8: Continuum mechanics and agent-based models. (a) Liquid drop model composed by two membranes and two liquids representing the cytoplasm and the nucleus (Lim et al. (2006)). (b) Stress fibers in 3D polarized cell during contraction of a solid mechanics model (Ronan et al. (2012)). (c) Lattice model where each cell is divided in more than one site. (d) Off-lattice model where each cell is represented by one point and cell forces are applied to the centers.

mainly intended and used for the cytoplasm, trying to differentiate between the cytosol and the rest of the solid parts.

Agent-based models

Another widespread way of modeling cellular ensembles by simulating each cell individually is agent-based models. This type of model uses local rules to define the problem in such a way that the interaction between the different agents allows the global behavior of the system to be studied (Van Liedekerke et al. (2015)). Within this type of models we can differentiate between lattice and off-lattice models. In lattice models, the positions of the cells are linked to fixed lattices, as well as their representation. Each site may be occupied by many cells, one site may represent only one cell, or one cell may be the composition of many sites. In contrast, in off-lattice models cells are not fixed to a fixed spatial discretization; we can differentiate between center-based models, where

cells are undeformable geometries, and deformable-based models, in which cells can have more realistic geometries and offer more level of detail, but in contrast, they are much more computationally expensive. Thus, it may be easier to define the problem with an agent-based approach, but it is not possible to obtain the level of detail that continuous models can provide with respect to mechanical environment and they are not used, as far as I know, to model individual cells.

1.2 Motivation and objectives

In this chapter, it has been shown that cells are able to sense the surrounding mechanical environment and respond accordingly in different ways. They can increase their stiffness if they are on very stiff substrates or decrease their stiffness when they are on a substrate with a lower stiffness (Solon et al. (2007)). Cells are also able to choose the migration mode according to the mechanical behavior of the extracellular matrix, changing from lamellipodia to lobopodia, or even a stem cell can differentiate into different cell types depending on the substrate stiffness (Lv et al. (2015)). In addition, there are studies that show the relationship between mechanical stresses in the nucleus with the activation of important cellular processes such as differentiation, proliferation or apoptosis (Martins et al. (2012)). Therefore, it is important to study cell mechanics in order to improve the understanding about the role that different components of the cell play in the transduction of mechanical signals. Cells are able to sense mechanical conditions through active mechanisms, such as contraction, and passive mechanisms, such as, the pre-tension of the tissue or matrix in which they are located, when deformed by the migration of contiguous cells or when subjected to artificial external forces applied in laboratory

In this thesis, we focus on the study of cell mechanics from both a passive point of view, where the cell can be deformed by external forces, and an active point of view, where cells contract to sense the surrounding environment individually or collectively. By means of finite element modeling, we aim to study how cells sense in different situations and how this triggers different responses in the cells.

With this aim in mind, different modeling strategies are combined from the

1.3. Outline

geometrical and material point of view. The material models used to reproduce cell behavior are different in each model, cells are assumed elastic, poroelastic and hyperelastic materials. Furthermore, we consider the cell as a homogeneous material, simulating its different parts (nucleus, membrane, cytoplasm) or a whole that takes into account the active (acto-myosin motors) and passive parts of the cell (microtubules, intermediate filaments and cytoplasm). With this, it is intended to create simplified models that are able to predict and give an explanation of cellular behaviors in different environments.

1.3 Outline

This Thesis is divided into five chapters. The first chapter introduces cell mechanobiology from a mechanistic point of view and gives an overview of the current state of the art. Chapters two, three and four describe different finite element models of cells under different conditions, considering a passive and active part in the cell body and working individually or collectively. Finally, an overview of the work performed and the main conclusions are presented. A more detailed description of the chapters is given below:

- In Chapter 1, a brief introduction to cell mechanics is given. The main parts of the cell that influence cell migration are described, the different migration processes currently known in both two and three dimensions are explained and a short state of the art of how cells sense the mechanical environment that surrounds them is presented. Finally, the motivation and the main objectives of this thesis are explained.
- In Chapter 2, a Coupled Eulerian Lagrangian (CEL) finite element model is proposed in order to simulate the working conditions of a cytometer. Here the cell is studied as a passive part that is deformed by a moving fluid to study the effect of the nucleus and/or the membrane in the global deformation of the cell, as well as to observe the tensional state of the nucleus when passing through this type of channels.
- In Chapter 3, a type of migration that only takes place under certain mechanical conditions (lobopodial migration) is studied. For this purpose, a

finite element model of a migrating cell is developed to study the differences that the cell may sense and proposing possible mechanotransduction mechanisms that make the cells choose one type of migration or another.

- In Chapter 4, it is studied how an infection such as listeria affects the temporal dynamic behavior of a cell monolayer. In this case, a finite element model of the cell cluster on the substrate is constructed to simulate the mechanism by which healthy cells are infected and we propose a possible mechanism by which healthy cells are able to expel and create mounds of infected cells.
- In Chapter 5, the general conclusions of this work are presented and the original contributions of this PhD Thesis are summarized. In addition, some of the possible future lines of research are discussed.

Chapter 2

Passive cell behavior

Contents

2.1	Introduction	20
2.2	Materials and Methods	22
2.2.1	Geometry and materials	22
2.2.2	Fluid-structure interaction	23
2.2.3	Boundary conditions	25
2.3	Results	27
2.3.1	Cell stretching due to fluid flow	27
2.3.2	Quantification of cell deformability	32
2.3.3	Strains and stresses on the cell nucleus	34
2.3.4	Velocity profile around the cell	36
2.4	Discussion and Conclusions	37

This chapter is based on:

F. Serrano-Alcalde, J.M. García-Aznar, M.J. Gómez-Benito, The role of nuclear mechanics in cell deformation under creeping flows, Journal of Theoretical Biology 432 (2017) 25-32.

2.1 Introduction

The mechanical deformation of cells by fluid flow is a fundamental problem with increasing relevance for multiple technological applications in biology and bioengineering, such as experimental quantification of cell mechanical properties (Guillou et al. (2016)), dynamic cell cultures in bioreactors (Massai et al. (2016)), deformability-based cell classification (Hur et al. (2011)), blood filtration (Mach and Di Carlo (2010)), leukocyte endothelial transmigration (Liu et al. (2004); Verdier et al. (2008)), and interstitial cell migration (Schmidt and Friedl (2010)). Under these conditions, it is fundamental to understand the interplay between fluid flow and the mechanical behaviour of a cell, including the nucleus. In this context, simulations and mathematical modelling are the most common and useful tools for quantifying cell deformation under different geometries and fluid flow conditions (Casquero et al. (2017); Giorgi et al. (2016)). Although many different modelling and numerical approaches have been used for this purpose, there are three main types of methods: analytical, particle-based and mesh-based methods.

An important example is the characterization of cell mechanical properties while under deformation due to shear flow (Xavier et al. (2016)). Recently, Otto et al. (2015) performed real-time deformability cytometry (RT-DC) (Figure 2.1). The experimental results were correlated with those of an analytical model (Mietke et al. (2015)) in terms of hydrodynamics and linear elasticity theory, with the assumption that the cell was a homogeneous material. This simple analytical model not only predicted deformed shapes inside the channel but also allowed for the quantification of cell mechanical properties.

The motion of red blood cells (RBCs) or vesicles in the microcirculation (Fedosov et al. (2014); Peng et al. (2015); Ye et al. (2016)) is another example of the many applications of numerical simulations of fluid-solid interactions. In this situation, particle-based techniques are normally used, in which the suspending fluid is modelled by particles representing a small volume of fluid rather than individual atoms or molecules. The RBC membrane is represented by a triangulated network model and coupled with a fluid through friction forces. The cell is represented by a collection of particles connected by springs. Three main approaches are normally used: dissipative particle dynamics, smoothed

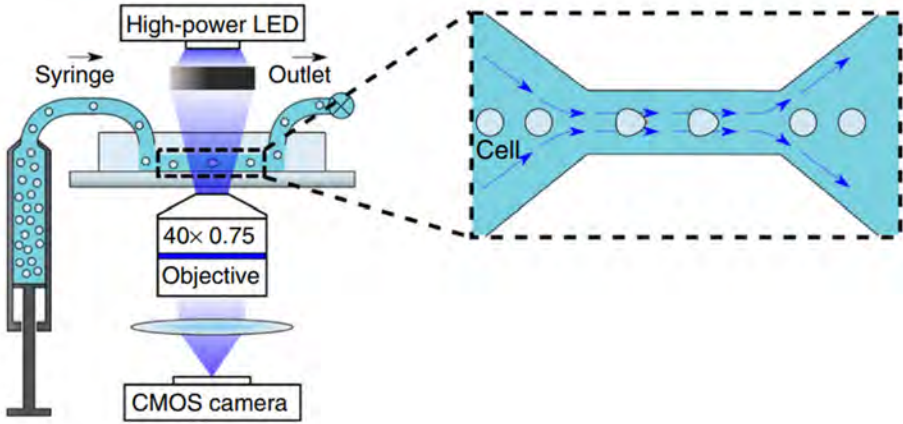


Figure 2.1: Setup scheme of the cytometer presented by Otto et al. (2015). Cells are immersed in a fluid and are forced to pass through a channel narrowing where are deformed by creeping flows.

particle hydrodynamics, and the lattice Boltzmann method. Several reviews with broad descriptions of these methods have recently been published (Imai et al. (2016); Peng et al. (2015); Ye et al. (2016)). In addition, similar numerical techniques have been used to simulate movement in other situations, such as the movements of bacterias (Eisenstecken et al. (2016); Hu et al. (2015)), lipids (Sevink et al. (2017)) and chemotaxis (Avesani et al. (2016); Vermolen and Gefen (2013)).

Mesh-based approaches have also been used to simulate how fluid movement deforms the cell body (Rüberg and Aznar (2016)) in many different tissue engineering applications (Aznar et al. (2016)). In this field, the best dynamic conditions in a bioreactor to achieve specific cell culture conditions must be defined. This level of control can only be realized when the effects of cell culture conditions on the cell microenvironment can be accurately quantified. Specifically, for scaffolds placed inside a perfusion bioreactor, the effects of the bioreactor design, scaffold geometry and flow properties on the physical conditions at the cellular level must be characterized. One of the more relevant aspects for defining these conditions is the fluid velocity at the inlet of the bioreactor, which can result in disrupted or damaged cells that fail to proliferate and differentiate

2.2. Materials and Methods

during cell culture (Vaughan et al. (2015); Zhao et al. (2016)). Therefore, it is very relevant to accurately quantify the stress and deformation levels that a cell nucleus can support during culture in a bioreactor.

However, despite the crucial role of nuclear deformation in all these cases, most of these works do not consider the existence of the cell nucleus during cell deformation under flow. Therefore, the present study investigates the role that the cell nucleus plays in the dynamics of cell deformation under different geometrical and fluid flow conditions, but without adhesions to the channel walls. Fluid flow imposes shear stresses on cells and causes nuclear deformation, which may result in localized deformation of the nuclear envelope and DNA, thereby regulating cell responses.

2.2 Materials and Methods

We performed three-dimensional (3D) simulations of single cells flowing inside a channel. The dimensions of the channel are large enough to allow cells to move due to fluid flow without adhesion to the channel walls. The simulations are based on cells immersed in a physiological serum that flows through a microfluidic channel. This channel has a variable cross section, in which cells are deformed by a creeping flow.

2.2.1 Geometry and materials

The simulated channel has a square section of $20 \mu m$ per side in the central region and $40 \mu m$ per side in the entrance section. The flow rate through the channel is on the order of $0.02 \mu l/s$ to $0.04 \mu l/s$; thus, a laminar flow regime is assumed. The simulated fluid in which the cells are embedded is a physiological saline solution with a density of $1000 kg/m^3$ and a kinematic viscosity of $15 mPa \cdot s$ (Mietke et al. (2015)). The fluid is considered Newtonian.

Four different cell configurations were analyzed (Table 2.1): (I) a cell considered a homogeneous material; (II) a cell considered a homogeneous solid with a membrane; (III) a cell with a spherical nucleus; and (IV) a cell with cytoplasm,

a nucleus and a membrane. In all cases, the nucleus was assumed to be ten-fold stiffer than the cytoplasm, in accordance with the work of Friedl et al. (2011).

The initial geometry of the cell was assumed to be spherical with a diameter of $15 \mu m$. To analyse the impact of the cell nucleus and its size on the average mechanical behaviour of the cell, the following nucleus diameters were analysed: one-third, one-half (medium nucleus) and two-thirds (large nucleus) of the cell diameter. Neo-Hookean hyperelastic behaviour was assumed for the nucleus and cytoplasm under large cell deformations, which is following the strain energy function:

$$U = C \cdot (\hat{I}_1 - 3) + \frac{1}{D} \cdot (J^{el} - 1)^2 \quad (2.1)$$

where \hat{I}_1 is the first invariant of the right Cauchy-Green deformation tensor, C and D are material parameters, and J^{el} is the elastic volume ratio. The role of the cell membrane was also analysed, and the membrane thickness was estimated to be $5 nm$ (Nelson et al. (2008)). The mechanical behaviour of the cell membrane was assumed to be linearly elastic, and shear and bending stiffness were neglected (Jacobs et al. (2012)). The Poisson's ratio of the cell nucleus was also modified from 0.49 to -0.16, in accordance with the work of Vaziri et al. (2006) and Pagliara et al. (2014). All geometrical characteristics and material properties are summarized in Table 2.1.

2.2.2 Fluid-structure interaction

Cells deform when they are flowing inside the channel. This deformation modifies fluid flow, which subsequently alters cell deformation. Thus, a fluid-structure interaction calculation scheme was adopted using the commercial finite element program ABAQUS (Hibbit, Karlsson and Sorensen, Inc. (2006)) and a coupled Eulerian-Lagrangian analysis. Thus, a Eulerian mesh was used to simulate the fluid, and a Lagrangian mesh was used to simulate the cell (solid). The nodes in the Eulerian mesh remain fixed on its spatial configuration, allowing the material to flow through the elements. Therefore, the Eulerian mesh was not deformed. Each Eulerian element can contain fluid in a range from 0 to 1. This range defines the occupancy rate of each Eulerian element by fluid. Mesh zones without cellular material take the value 0, representing a material "void". Mesh elements in contact with the cell contour take values between 0 and 1, and mesh

2.2. Materials and Methods










	Description	Cytoplasm	Nucleus	Membrane
	Homogeneous cell	C = 503 Pa D = $4 \cdot 10^4$ GPa ⁻¹	- -	- -
	Cell with cytoplasm and a membrane	C = 503 Pa D = $4 \cdot 10^4$ GPa ⁻¹	- -	E = 1285 kPa ν = 0.49
	Cell with cytoplasm and a nucleus	C = 503 Pa D = $4 \cdot 10^4$ GPa ⁻¹	C = 5.03 kPa D = $4 \cdot 10^3$ GPa ⁻¹	- -
	Cell with cytoplasm and a medium nucleus	C = 503 Pa D = $4 \cdot 10^4$ GPa ⁻¹	C = 5.03 kPa D = $4 \cdot 10^3$ GPa ⁻¹	- -
	Cell with cytoplasm and a large nucleus	C = 503 Pa D = $4 \cdot 10^4$ GPa ⁻¹	C = 5.03 kPa D = $4 \cdot 10^3$ GPa ⁻¹	- -
	Cell with cytoplasm, a nucleus and a membrane	C = 503 Pa D = $4 \cdot 10^4$ GPa ⁻¹	C = 5.03 kPa D = $4 \cdot 10^3$ GPa ⁻¹	E = 1285 kPa ν = 0.49
	Cell with cytoplasm, a nucleus and a membrane	C = 503 Pa D = $4 \cdot 10^4$ GPa ⁻¹	C = 8.93 kPa D = $2.64 \cdot 10^5$ GPa ⁻¹	E = 1285 kPa ν = 0.49
	Cell with cytoplasm, a medium nucleus and a membrane	C = 503 Pa D = $4 \cdot 10^4$ GPa ⁻¹	C = 5.03 kPa D = $4 \cdot 10^3$ GPa ⁻¹	E = 1285 kPa ν = 0.49
	Cell with cytoplasm, a large nucleus and a membrane	C = 503 Pa D = $4 \cdot 10^4$ GPa ⁻¹	C = 5.03 kPa D = $4 \cdot 10^3$ GPa ⁻¹	E = 1285 kPa ν = 0.49

Table 2.1: Mechanical and geometrical properties of simulated cells (Friedl et al. (2011); Nelson et al. (2008); Pagliara et al. (2014); Trepap et al. (2008); Vaziri et al. (2006)).

elements completely occupied by cellular material take the value 1. The fluid distribution depends on the cell geometry that is computed in each increment.

Regarding the number of elements used in the simulations, 17.052 reduced integration brick elements (type EC3D8R) were used for the Eulerian mesh, 16.551 tetrahedral solid mechanics elements (type C3D4) were used for the cytoplasm and nucleus, 1.570 membrane triangular elements (type M3D3) were used for the membrane, and 888 brick solid mechanics elements (type C3D8) were used for the channel.

2.2.3 Boundary conditions

As a first approach, the channel was simulated as a rigid solid. To reproduce flow into the channel, a Hagen-Poiseuille law was applied to the inlet section using a Purday approximation for the square sections (Berthier and Silberzan (2010)). The velocity profile at the inlet section was fixed (Figure 2.2), and the rigid tangential behaviour between the fluid and solid was assumed to be zero. A Purday velocity profile exhibits a maximum value at the centre of a channel and a value of zero near the wall, according to equation (2):

$$v(y, z) = u_{max} \cdot \left[1 - \left(\frac{y}{b/2} \right)^{2.2} \right] \cdot \left[1 - \left(\frac{z}{b/2} \right)^{2.2} \right] \quad (2.2)$$

where u_{max} is the maximum velocity ($0.053 \mu m/\mu s$ for $0.04 \mu l/s$ and $0.026 \mu m/\mu s$ for $0.02 \mu l/s$), y and z are the coordinates of the channel cross-section, and b is the dimension of the side of the square channel cross-section.

To stabilize fluid flow in the simulations, we first simulated the cell as a rigid sphere inside the large channel. Once the fluid velocity stabilized, a deformable cell replaced the rigid sphere.

2.2. Materials and Methods

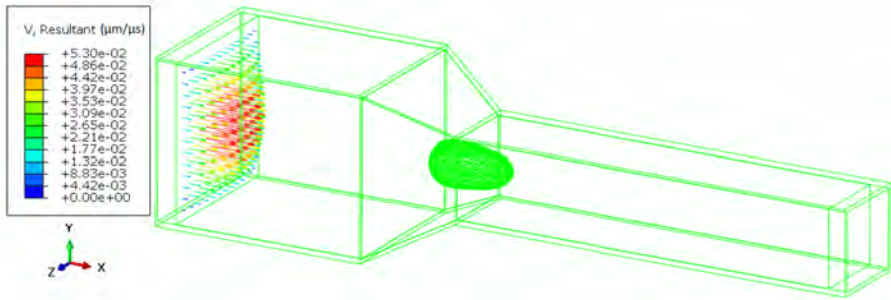


Figure 2.2: Velocity profile in the inlet section that follows the Purday approach (Berthier and Silberzan (2010)).

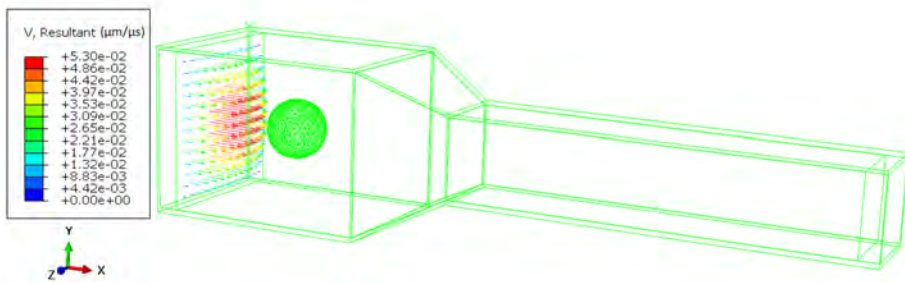


Figure 2.3: Rigid cell used to stabilize the fluid flow.

2.3 Results

2.3.1 Cell stretching due to fluid flow

First, we analyzed the deformed shape of the cell passing through microfluidic channels of different sizes (Figure 2.4), and we compared the different shapes of the deformed cells. In all cases, the cell deformed from a spherical shape into a bullet-like shape, in agreement with the experimental measurements from a cytometer obtained by Otto et al. (2015) (see experimental deformation in Figure 2.7). This deformation was greater in the region of the channel where the cross-sectional area changed and was stable in the central region of the channel. To quantify the change in cell shape, the longitudinal axis of the cell length was computed (Figure 2.4a). Figures 2.5 and 2.6 show the variation in this length as a function of cell position in the channel.

As a reference case for comparative purposes, we defined a cell model in which a homogeneous material was assumed (Table 2.1). In all simulations, fluid velocity changed in the region of the channel where the cross-section changed, thereby deforming the cell. First, the longitudinal length of the cell increased due to the increase in fluid velocity. Once the cell was inside the smallest section of the channel, its longitudinal length decreased and its deformed shape became stable (Figure 2.4).

Figure 2.5 compares the deformed shapes of cells modelled as heterogeneous with those of the cell modelled as homogeneous. The model corresponding to the cell with homogeneous properties and a membrane exhibited less deformation along the longitudinal axis than the reference cell model (Figure 2.5a). Compared with the reference model, the model of a cell with a spherical nucleus one third of the cell radius exhibited faster longitudinal axis stabilization (Figure 2.5b), and the model of a cell with cytoplasm, a nucleus and a membrane exhibited even faster stabilization and less deformation along the longitudinal axis (Figure 2.5). Nevertheless, in all simulations, the deformed shape was similar to that of a bullet. These deformations are qualitatively similar to that shown in a previous work in which a cell was deformed while flowing inside a cytometer (Otto et al. (2015)).

2.3. Results

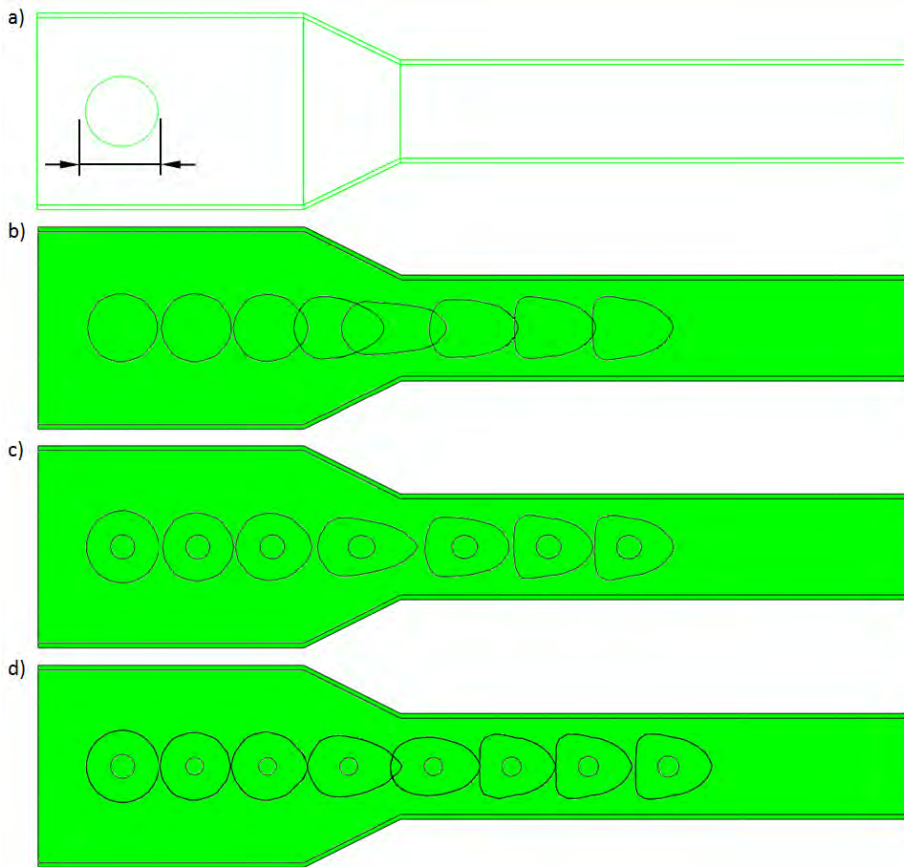


Figure 2.4: Deformed shape of a cell through the channel in the central X-Y plane (see Figure 2.2): (a) cell longitudinal axis length; (b) homogeneous cell model; (c) model of a cell with cytoplasm and a nucleus; (d) model of a cell with cytoplasm, a membrane and a nucleus with a negative Poisson's ratio (Pagliara et al. (2014)).

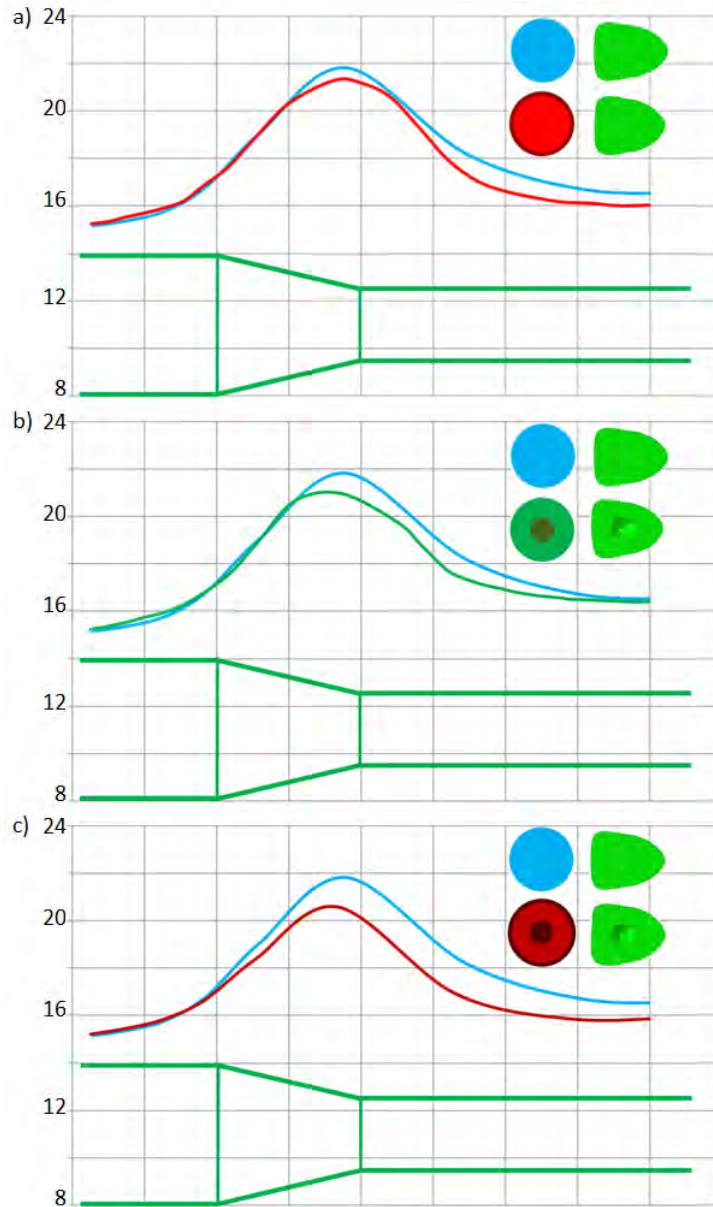


Figure 2.5: Cell longitudinal axis deformed length by channel position: (a) homogeneous cell and a homogeneous cell with a membrane; (b) a homogeneous cell and cell with a small nucleus; (c) a homogeneous cell and a cell with a nucleus and a membrane (units, μm). The channel is represented in the figures as a reference for the position of the cell center.

2.3. Results

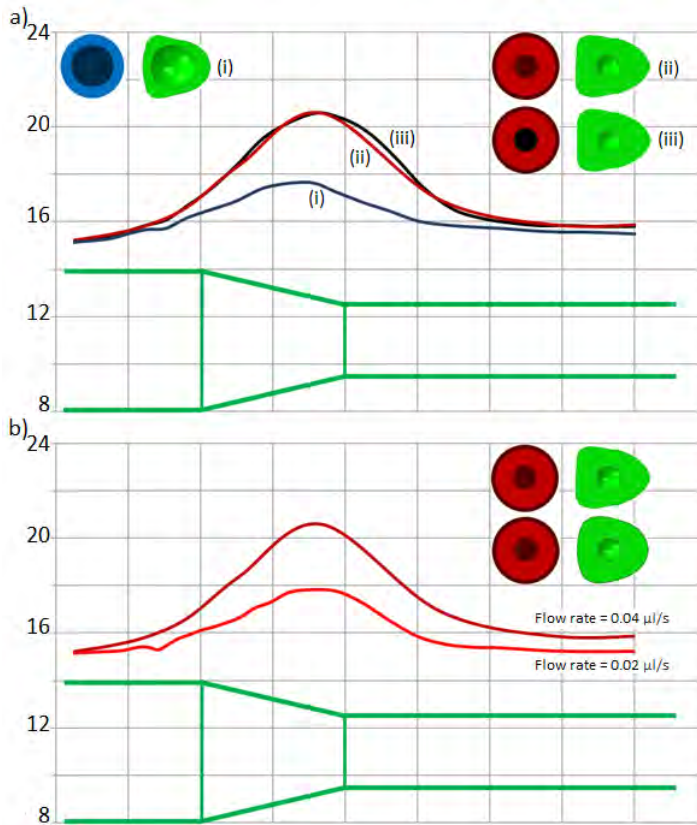


Figure 2.6: Cell longitudinal axis deformed length by channel position: (a) cell with a large nucleus (i), cell with a nucleus and a membrane (ii), and cell with a nucleus (negative Poisson's ratio) and a membrane (iii); (b) cells with a nucleus (positive Poisson's ratio) and a membrane under flow rates of $0.04 \mu l/s$ and $0.02 \mu l/s$ (units, μm). The channel is represented in the figures as a reference of the position of the cell center.

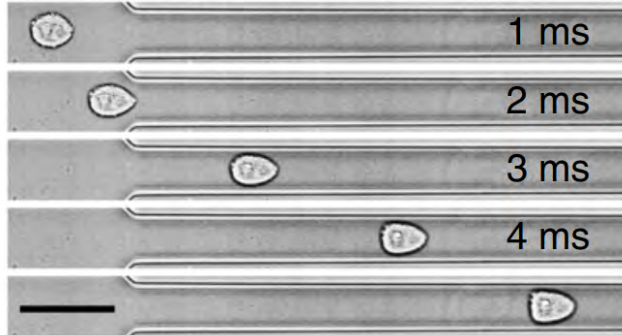


Figure 2.7: Experimental cell deformed inside the cytometer at different times. Image taken from Otto et al. (2015).

To analyze the impact of the nucleus on cell deformation, we changed the nucleus size and the nucleus mechanical properties independently (Table 2.1). We compared these models with the cell model that considers the cytoplasm, nucleus and membrane. When the nucleus size was increased, the variation of the cell longitudinal axis was decreased, and the deformed shape differed from the previous deformed shapes (Figure 2.6a). Thus, the nucleus size was fixed at one third of the cell body diameter.

When the nucleus Poisson's ratio was modified from a positive (0.49) (Vaziri et al. (2006)) to a negative value (-0.16) (Pagliara et al. (2014)), there were no variations in the cell longitudinal axis and deformed shape. However, the final nucleus volume was approximately 40% lower with the negative Poisson's ratio than with the positive Poisson's ratio (Figure 2.6a).

In addition, we computed a cell with cytoplasm, a membrane and a nucleus with an elastic modulus of 45 kPa (50% higher elastic modulus following Zhang et al. (2016)). We compared this cell with the same case but with a low elastic modulus to study the influence of nuclear stiffness. However, we did not observe significant changes in the results for cell deformation and fluid velocities.

Simulations of a cell with cytoplasm, a nucleus and a membrane were also analysed under different fluid flow conditions: $0.02 \mu\text{l}/\text{s}$ and $0.04 \mu\text{l}/\text{s}$. While the variation in the cell longitudinal axis length exhibited the same overall form in both cases, the maximum and final length values were lower under a flow rate

2.3. Results

of $0.02 \mu\text{l}/s$ than $0.04 \mu\text{l}/s$. Furthermore, the deformed cell shape was more spherical in the former case than the latter (Figure 2.6b).

2.3.2 Quantification of cell deformability

To quantify the 3D deformed configuration of the cells and detect when the nucleus caused a relevant effect on the mechanical behavior of the cells, we computed the inertia tensor of the deformed cells.

To render the value independent of cell size, we normalized the inertia tensor by dividing each component by the trace of the inertia tensor (I_{kk}) to obtain the adimensional inertia (\hat{I}), as shown by equations 2.3 and 2.4:

$$\hat{I} = \begin{pmatrix} \hat{I}_{xx} & 0 & 0 \\ 0 & \hat{I}_{yy} & 0 \\ 0 & 0 & \hat{I}_{zz} \end{pmatrix} \quad (2.3)$$

$$\hat{I}_{ij} = \frac{I_{ij}}{I_{kk}} \quad (2.4)$$

where the x axis is the longitudinal axis along which cells exhibit the maximum deformation due to fluid flow. Due to the axisymmetric geometry of the cell while flowing inside the channel, the product of inertia is zero ($\hat{I}_{ij} = 0$ when $i \neq j$). For a spherical cell, the adimensional inertia value for all three axes would be 0.33 if the cell remains a sphere. Therefore, this tensor permits the quantitative measurement of how one cell deforms when passing through the channel.

The normalized inertia along the longitudinal axis differed for the different cell configurations (Figure 2.8a). When the cell was assumed to be a homogeneous solid, the normalized longitudinal inertia was 28.5%. This value increased with increasing cell nucleus size, reaching a value of approximately 31% when considering the large nucleus; this value is very close to that of the normalized inertia for a spherical cell (33%). The cell membrane slightly stiffens the cell, thereby increasing the normalized inertia along the longitudinal axis by approximately 0.5-1%, and the largest effect was observed for the cell with the smallest

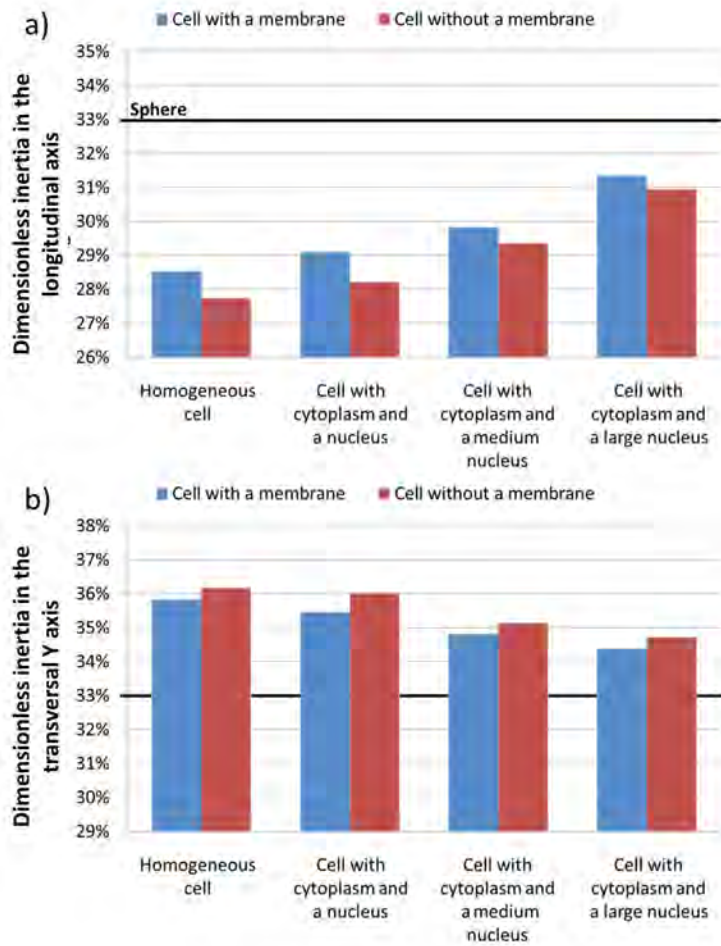


Figure 2.8: Dimensionless inertia along the longitudinal axis (a) and on the y transversal axis (b) for different cell models to reveal the effect of considering the cell membrane in the model.

2.3. Results

nucleus. In the transverse section, the deformations along both axes were similar, and the largest normalized inertia values were observed for the homogeneous cell; these values decreased with increasing nucleus size approaching the value obtained for a sphere.

Although, the nucleus size affected global cell deformation, the trends were similar in all simulated cases. To investigate global cell deformation, homogeneous mechanical properties could be considered. However, to investigate active cell behaviors (e.g., differentiation, proliferation, death), it would be necessary to include the nucleus with its geometry and corresponding mechanical properties (Figure 2.9).

	\hat{I}	Cell with a membrane	Cell without a membrane
Homogeneous	x	0.285	0.277
	y	0.358	0.362
	z	0.356	0.361
Cell with cytoplasm and a nucleus	x	0.291	0.282
	y	0.355	0.360
	z	0.354	0.358
Cell with cytoplasm and a medium nucleus	x	0.298	0.293
	y	0.348	0.351
	z	0.353	0.355
Cell with cytoplasm and a large nucleus	x	0.314	0.309
	y	0.344	0.347
	z	0.342	0.343

Table 2.2: Adimensional inertia tensor of the deformed cell shape along the three axes for different configurations.

2.3.3 Strains and stresses on the cell nucleus

The mechanical state of the cell nucleus was analyzed under different fluid flow conditions. We obtained the maximum tensile stress (Figure 2.9a) and the maximum compressive stress (Figure 2.9b) of the cell nucleus using different cell modeling approaches. All numerical results represent stable cells in the small channel section.

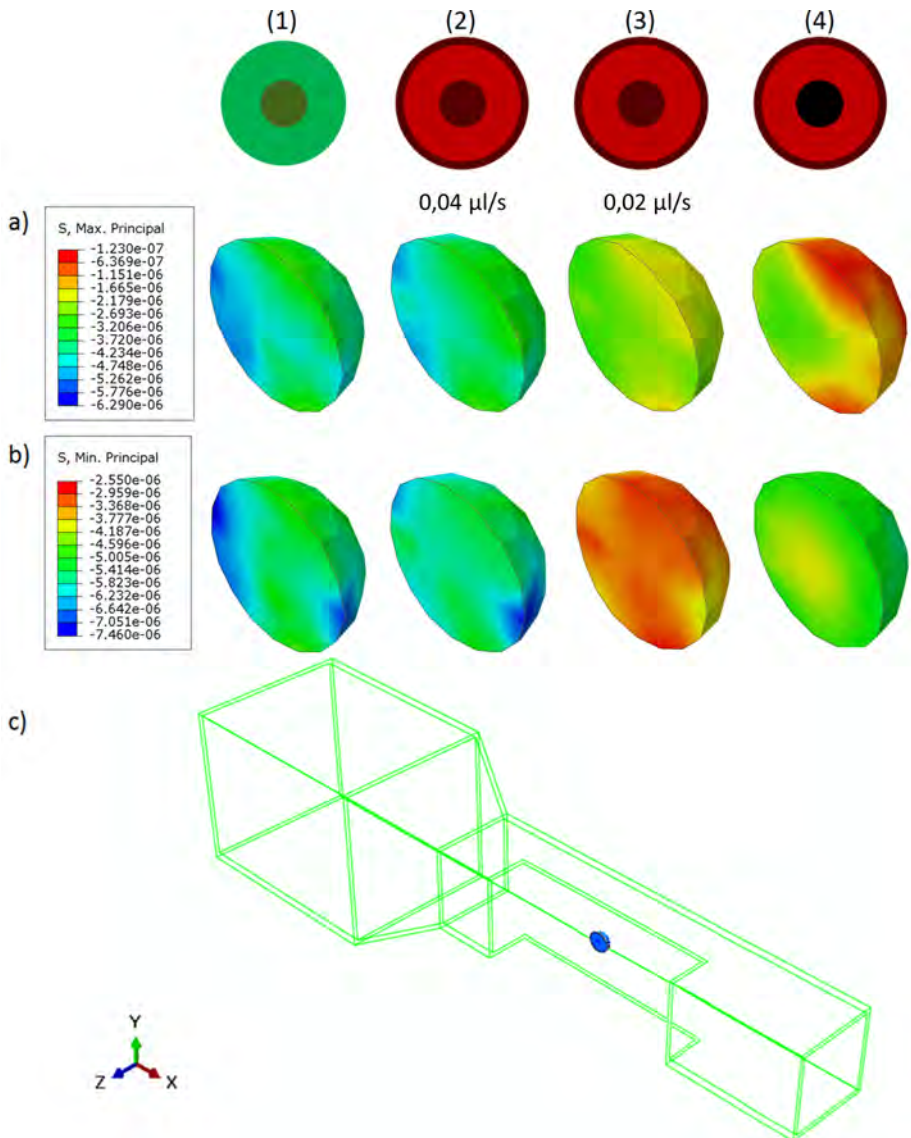


Figure 2.9: Nuclear stress distribution across a stabilized deformed cell shape: (a) maximum tensile stress; (b) maximum compressive stress; (c) nucleus status in the channel during measurement. The first column shows the results for the cell with cytoplasm and a nucleus (1), and the second (2) and third (3) columns show the results for the cell with cytoplasm, a nucleus and a membrane at flow rates of $0,04 \mu\text{l/s}$ and $0,02 \mu\text{l/s}$, respectively. The last column (4) shows the results for the cell with cytoplasm, a nucleus (with a negative Poisson's ratio) and a membrane (see Table 2.1) (units, GPa).

2.3. Results

In all simulations, the cell nucleus is under compression. The front and back parts of the nucleus are the zones with the greatest compression (7 kPa for a cell without a membrane). The middle part is also compressed but to a lesser extent (5 kPa for a cell without a membrane).

When considering a cell membrane and a cell nucleus, the maximum tensile stress (Figure 2.9a) and maximum compressive stress (Figure 2.9b) decreased compared with the reference case (a cell comprising cytoplasm and a nucleus).

While the maximum tensile stress distribution for a cell nucleus with a negative Poisson's ratio was similar to that of a cell nucleus with a positive Poisson's ratio, the former values were the lowest among all simulations (Figure 2.9a). By contrast, the distribution of maximum compressive stress values showed higher values on the surface and lower values in the core, a special distribution obtained only for this cell nucleus model (Figure 2.9b).

Analyzing the same cell under two different flow rates (0.04 and $0.02\ \mu\text{l/s}$) revealed identical value distributions of the maximum tensile stress and maximum compressive stress for the nucleus (Figure 2.9). However, both the tensile and compressive stresses values were approximately 40% lower than those found using the reference flow rate.

2.3.4 Velocity profile around the cell

In contrast to a previous study (Mietke et al. (2015)) that analyzed the fluid and the solid as independent parts and did not consider their interaction, we used a coupled fluid-solid analysis that considered both the effects of the fluid phase on the cell and the effects of the solid phase (cell) on the fluid. Although we observed a difference between the velocity profiles of a rigid sphere and a deformed cell inside the channel (Figure 2.10) the magnitudes of the velocities were similar.

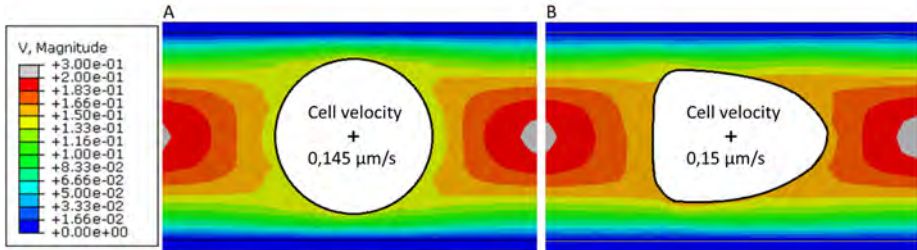


Figure 2.10: Velocity profile around a rigid sphere (a) and around a deformed cell (b) in the X-Y plane. Cell velocity is also indicated (units, $\mu\text{m}/\mu\text{s}$).

2.4 Discussion and Conclusions

Using computer simulations, we demonstrated that a small cell nucleus does not play a crucial role in cell deformability-based experiments guided by fluid flow. In this work, we found that an externally deformed cell shape induced by a creeping flow is largely unaffected by the mechanical properties of the nucleus and is much more affected by the size of the nucleus. Thus, we should keep in mind the deformed shape and the 3D deformation of the cell when deciding whether to consider the nucleus. Therefore, if we attempt to estimate cell properties from cell deformability experiments, we will obtain an average representation of cell properties, which is valid for comparative purposes but not for quantitative measurements. We found that subtle changes in the geometrical or fluid flow conditions produced relevant alterations in the stress levels of the nuclear body, which may be crucial for different biomedical applications, such as bioreactors. Although RT-DC can classify cells according to their homogenized mechanical properties, combining this technique with finite elements might provide more information on the analyzed cells.

In this work, we developed a fluid-solid interaction numerical model to understand how fluid flow modifies cell nucleus deformation. However, some simplifications were made. First, the complexity of the cell mechanical behavior (Maloney and Van Vliet (2014); Trepap et al. (2008)) was simplified by including three cellular components, i.e., the membrane (considered a linearly elastic material), the cytoplasm and the nucleus (both considered Neo-Hookean hyperelastic materials). However, considering more complex behaviors and different

2.4. Discussion and Conclusions

factors, such as viscoelastic liquids or other material models, would result in similar behaviors because we are mainly interested in short-term deformation on the order of 10^{-3} seconds, which is the time required for a cell to pass through the channel of a cytometer. A mesh sensitivity study performed by increasing the number of Eulerian elements up to 147.175 obtained comparable results, but the calculation time significantly increased. The active components of the cytoskeleton may also play roles in cell deformation. However, we posit that these contributions would be more relevant under fully confined conditions (Giverso et al. (2017)). The elastic modulus of living cells has been established to be on the order of 1 kPa (Treat et al. (2008)). The mechanical properties of cells have been characterized based on stiffness (Mietke et al. (2015)) and fluidity (Maloney and Van Vliet (2014)). Other works have estimated the elastic modulus of the cell membrane to be 10 kPa (Hochmuth et al. (1973)); however, the cell membrane has also been reported to be unable to support strains greater than 4%-6%, and for a membrane thickness of 5 nm , the axial elastic modulus has been found to be on the order of 10^3 kPa (Nelson et al. (2008)).

Previous works have attempted to elucidate whether a single elastic modulus is sufficient to characterize the complexity of cell mechanical behaviors (Guz et al. (2014)). Our simulations provide evidence that the nucleus size plays a key role in global cell deformation induced by a fluid flow. This effect was previously noted during an investigation of cell migration in confined environments (Giverso et al. (2014); Scianna and Preziosi (2013); Scianna et al. (2013)). In addition, consideration of the cell membrane is an important factor for determining the mechanical properties of cells, and previous studies have considered the membrane stiffness in terms of membrane pre-stress (Mietke et al. (2015)). The model presented here allowed quantification of the spatio-temporal distribution of the stress and strain levels of the cell nucleus, which exert strong effects on cell responses by regulating fundamental events, such as differentiation, proliferation or apoptosis (Martins et al. (2012)). To the best of our knowledge, this is the first numerical study to consider cell nucleus deformation induced by creeping flow. We expect that our work will inspire other studies that will provide further insight on the link between the nucleus and intracellular deformation induced by fluid flow.

Chapter 3

Active cell mechanosensing in lobopodium formation

Contents

3.1	Introduction	40
3.2	Materials and Methods	42
3.2.1	Model description	42
3.2.2	Constitutive law	44
3.2.3	Finite Element approach	46
3.3	Results	47
3.3.1	Cytoplasmic fluid behavior	48
3.3.2	Mechanical state of the ECM and nucleus	49
3.4	Discussion and Conclusions	54

This chapter is based on:

F. Serrano-Alcalde, J.M. García-Aznar, M.J. Gómez-Benito, Cell biophysical stimuli in lobopodium formation: a computer based approach, Computer Methods in Biomechanics and Biomedical Engineering (2020) 1-10.

3.1 Introduction

Cell migration is essential for many processes, such as embryogenesis, morphogenesis, and cancer cell progression, and to maintain tissue regeneration. In recent years, several studies have investigated the relationship between the mechanical properties of the extracellular matrix (ECM) and the mechanisms of cellular migration (Friedl and Wolf (2010); Luque et al. (2013); Zaman et al. (2006)). Understanding how and why cells are able to sense the ECM stiffness and select the best migration strategy have become crucial for progress in these areas of research.

Cell migration in two dimensions (2D) has been extensively described in previous experimental works (Lauffenburger and Horwitz (1996)). These studies have revealed some basic migration mechanisms, such as lamellipodia protrusion, adhesion-mediated traction (Oria et al. (2017)) and actomyosin contractility (Ridley et al. (2003); Sunyer et al. (2016)). In addition, there are different studies in 2D and in three dimensions (3D) relating the mode of cell migration with the mechanical properties of the ECM (DeSimone and Horwitz (2014); Friedl and Wolf (2010); Petrie et al. (2012, 2014); Petrie and Yamada (2016)). These mechanisms depend on the cell type and their physical environments. To better understand the cellular behavior, several authors studied the influence of the ECM molecular composition (Moreno-Arotzena et al. (2015)), the density and orientation of fibers, the fiber-cell interaction (Escribano et al. (2015); Fralley et al. (2015); Sturm (2011)), the bulk and local stiffness of the ECM (Kubow et al. (2013)), the dynamic of actin filaments (Hervas-Raluy et al. (2019); Inoue et al. (2010)) and the mechanical response of the ECM (Petrie et al. (2012)).

However, cell movement mainly occurs in 3D, where cells normally adopt two modes of migration, based on lamellipodia or blebs, depending on the degree of adhesion (Te Boekhorst et al. (2016)). Recently, Petrie et al. (2012) proposed a new mode of single cell migration, lobopodia-based migration, which takes place only in 3D matrices. In this migration mode, the nucleus has a relevant role. The effect of the nucleus has been studied in previous works for different situations (Allena et al. (2015); Serrano-Alcalde et al. (2017)). In this case, the nucleus acts as a piston dividing the cell into two parts with different pressures. The internal pressure in the leading edge is three times larger in lobopodia-based

3. Active cell mechanosensing in lobopodium formation

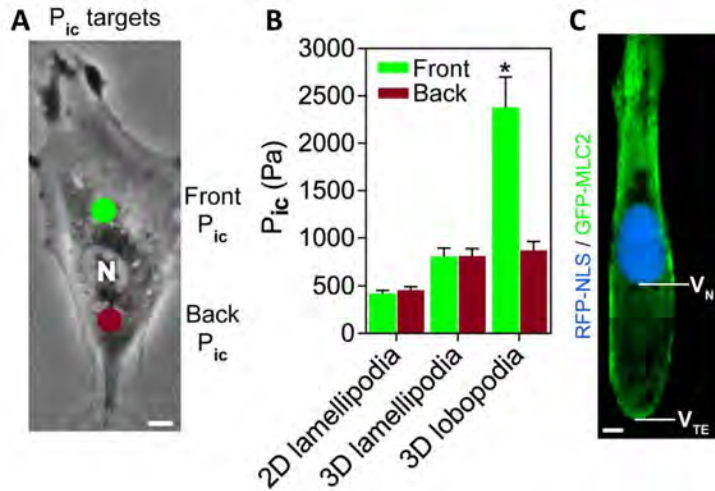


Figure 3.1: Experimental images of a cell migrating in lamellopodial way (A) and a cell migrating in lobopodial way (C). (B) Intraellular pressure measured in the front and back part of the nucleus. Adapted from Petrie et al. (2014)

migration than in lamellipodia-based migration (Petrie et al. (2014)) (Figure 3.1). In lamellipodia-based migration, the cell uses different lamellae to move instead of a single large cylindrical protrusion (lobopodium). The possibility of measuring the internal pressure of cells (Petrie and Koo (2014)) addresses one of the largest differences found between these two migration modes.

Petrie et al. (Petrie et al. (2012, 2014)) showed that a single fibroblast may switch from actin-driven lamellipodial protrusion to a nuclear piston lobopodia-driven mode of migration. This migration mode depends on the mechanical properties of the ECM, primarily the deformation of the matrix. In fact, whether the ECM is linearly elastic or non-linearly elastic is an essential factor. To elucidate when and where the cell adopts this lobopodial migration mode, the authors carried out experiments with different ECMs (Petrie et al. (2012)). Fibroblasts were embedded in three linearly elastic and non-linearly elastic matrices with different stiffnesses, ranging from 8 to 647 Pa. The ECM was treated to maintain its architecture and change its stiffness and behavior from linearly elastic or non-linearly elastic. An additional ECM with a higher elastic modulus was also analyzed (10 kPa). The authors found no correlation between the migration mode and stiffness of the ECM. However, they found a strong corre-

3.2. Materials and Methods

lation between the ECM non-linear or linear elasticity and the migration mode. Their main conclusion was that the mechanical properties of the ECM are related to the mode of cell migration. For non-linearly elastic matrices, migration occurs via the lamellipodia; however, for linearly elastic matrices, lobopodia predominate in migration. It is known that RhoA, ROCK and myosin II govern intrinsically large protrusions, but why a combination of these signals does not appear in non-linearly elastic ECMs is still unclear. Furthermore, no correlation between the ECM stiffness and the mode of migration was found (Petrie et al. (2012)).

Thus, the aim of this work is to elucidate how the mechanical properties and behavior of the ECM may influence the cell migration mode and why cells adopt a lamellipodial migration mode in non-linearly elastic matrices and a lobopodial mode in linearly elastic matrices. In fact, we hypothesize about the role of the poroelastic behavior of the cell as a possible mechanotransduction mechanism that could distinguish the impact of different regulatory effects of the surrounding matrix.

3.2 Materials and Methods

3.2.1 Model description

We simulate the experiment developed by Petrie et al. (2012) in which a single cell is embedded in different ECMs. A sufficiently large ECM is simulated to avoid border effects. The cell is in the center of the ECM, and its geometry is a simplified lobopodial geometry (Figure 3.2). This geometry is approximated from typical lobopodia-based migration behavior, as shown by Petrie et al. (2014). The model is implemented in commercial finite element (FE) software (ABAQUS).

We simulate four different extracellular matrices (Table 3.1). Two of them have a constant Young's modulus: a cell-derived matrix (CDM) (Petrie et al. (2012)) and a trypsinized CDM, both without strain-dependent behavior and with an elastic modulus of 627 and 8 Pa, respectively. The other two ECMs

3. Active cell mechanosensing in lobopodium formation

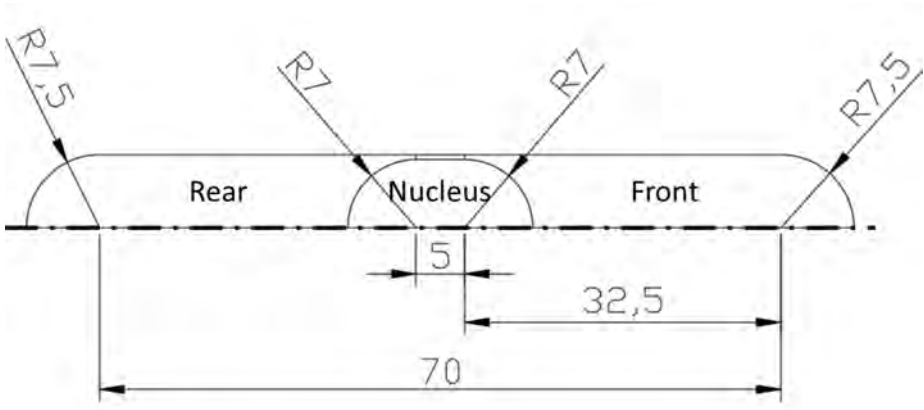


Figure 3.2: Axisymmetric cell section with a simplified lobopodial geometry (units: μm).

Matrix	Initial Young's modulus (Pa)	Strain-dependent?
Low stiffness, linearly elastic	8	No
Low stiffness, non-linearly elastic	8	Yes
High stiffness, linearly elastic	627	No
High stiffness, non-linearly elastic	627	Yes

Table 3.1: Summary of the simulated ECM properties (Petrie et al. (2012)).

initially have the same mechanical properties but with a strain-dependent behaviour when the cell starts to deform. Herein, the non-trypsinized CDM matrix is considered the high-stiffness linearly elastic matrix, and the non-trypsinized matrix with strain-dependent behavior is considered the high-stiffness non-linearly elastic matrix. The trypsinized CDM matrices with an elastic modulus of 8 Pa are considered the low-stiffness linearly and non-linearly elastic matrices.

We fix the Poisson's ratio of the ECM as 0.48 following Petrie et al. (2012). As a first approach, we assume finite strains in all simulations. All linearly elastic

3.2. Materials and Methods

matrices are modeled as an elastic material defined by a Young's modulus and Poisson's ratio. We assume a fibrous hyperelastic material in the non-linearly elastic ECMs (Elsdale and Bard (1972); Gelman et al. (1979)). The fibers are assumed to be randomly distributed in the ECM, thus an isotropic behavior can be considered (Gasser et al. (2006)). This model captures the major features of the material properties of collagen gels, including non-linear elasticity.

3.2.2 Constitutive law

For collagen hydrogels, we use the strain energy function for fibrous hyperelastic materials from Holzapfel-Gasser-Ogden (Holzapfel et al. (2000)):

$$U = C \left(\hat{I}_1 - 3 \right) + \frac{1}{D} \left(\frac{(J^{el})^2 - 1}{2} - \ln J^{el} \right) + \frac{k_1}{2k_2} \sum_{\alpha=1}^N \left\{ \exp \left[k_2 \langle \bar{E}_\alpha \rangle^2 \right] - 1 \right\} \quad (3.1)$$

with

$$\bar{E}_\alpha = \kappa \left(\hat{I}_1 - 1 \right) + (1 - 3\kappa) \left(\hat{I}_{4(\alpha\alpha)} - 1 \right) \quad (3.2)$$

where C, D, k_1, k_2 and κ are material parameters, N is the number of families of fibers ($N \leq 3$), \hat{I}_1 is the first invariant of the right Cauchy-Green deformation tensor, J^{el} is the elastic volume ratio and $\hat{I}_{4(\alpha\alpha)}$ are pseudo-invariants of the right Cauchy-Green deformation tensor. In our simulations, the parameter κ is fixed to 0.33 assuming a random distribution of fibers, thus resulting in an isotropic material. The values of k_1 and k_2 are 40,000 Pa and 85, respectively, for the stiff matrix and 1,000 Pa and 20 for the compliant matrix.

To simplify the cell complexity, we simulate only the cytoplasm and the nucleus. The cell nucleus is considered a neo-Hookean hyperelastic material with an initial Young's modulus ten times larger than the stiffness of the cytoplasm following Friedl et al. (2011) and Dahl et al. (2008) (Table 3.2) and a Poisson's ratio of 0.49, in accordance with the work of Vaziri et al. (2006). The strain energy function presents the following form:

3. Active cell mechanosensing in lobopodium formation

$$U = C \left(\hat{I}_1 - 3 \right) + \frac{1}{D} (J^{el} - 1)^2 \quad (3.3)$$

According to the work of Moeendarbary et al. (2013), the cytoplasm is simulated as a poroelastic material. Thus, it is composed of two distinct phases, the solid matrix (which is modeled as a linearly elastic material) and the fluid flowing through the solid matrix pores. We consider poroelasticity following the constitutive equation introduced by (Biot (1941)). This equation relates the total stress tensor $\boldsymbol{\sigma}$ to the strain energy density (a function of the shear G_s and Poisson's ratio ν_s of the drained network) W_s of the solid phase and the pore fluid pressure p following Malandrino and Moeendarbary (2019):

$$\boldsymbol{\sigma} = \frac{2}{J} \frac{\partial W_s}{\partial \mathbf{b}} \mathbf{b} - p \mathbf{I} \quad (3.4)$$

where J and \mathbf{b} are the determinant and the Left Cauchy-Green tensor both derived from the deformation gradient in the large strain theory. In the solid phase, we assume different Young's modulus depending on the initial stiffness of the ECM following Solon et al. (2007). Cells are able to adjust their internal stiffness to the stiffness of the ECM, clearly indicating mechanical feedback between the cell and its environment. To define the fluid phase, we use the permeability of the solid phase (wherein is implicit the viscosity of the fluid (Moeendarbary et al. (2013))), the volume fraction of the fluid and the specific weight of water. The permeability value is taken from Moeendarbary et al. (2013); however, the volume fraction is chosen as an intermediate value between the previous works of Taber et al. (2011), in which the volume fraction was fixed at 0.5, and Moeendarbary et al. (2013), in which the volume fraction was fixed at 0.75 of the fluid. All cytoplasmic properties are shown in Table 3.2.

Finally, following other previous work (Petrie et al. (2014)), we assume that all the organelles of the cell (Golgi apparatus, endoplasmic reticulum, and so on) are compacted and do not allow fluid flow between the front and the rear part of the cell. Thus, an elastic cytoplasm is simulated surrounding the nucleus and separating the front part of the cytoplasm from the rear part. We assume a linearly elastic material model in this volume, with material properties equal to those of the solid phase of the cytoplasm.

3.2. Materials and Methods

	Cell in a compliant ECM	Cell in a stiff ECM
Young's modulus of the cytoplasmic solid phase (Discher et al. (2005))	100 Pa	2500 Pa
Poisson's ratio of the cytoplasmic solid phase	0.4	0.4
Permeability of the cytoplasmic solid phase (Moeendarbary et al. (2013))	$4 \cdot 10^{-15} \frac{m^4}{N \cdot s}$	$4 \cdot 10^{-15} \frac{m^4}{N \cdot s}$
Volume fraction of fluid in the cytoplasm (Moeendarbary et al. (2013); Taber et al. (2011))	0.6	0.6
Young's modulus of the cell nucleus (Dahl et al. (2008); Friedl et al. (2011))	1 kPa	10 kPa
Poisson's ratio of the cell nucleus (Vaziri et al. (2006))	0.49	0.49

Table 3.2: Mechanical properties of the cytoplasm and nucleus.

3.2.3 Finite Element approach

Regarding the FE discretization, the model is simulated using coincident node conditions in the cell and ECM, thus assuming full adhesion between the cell and ECM. We discretize the nucleus, the elastic cytoplasm, the poroelastic cytoplasm and the extracellular matrix with tetrahedral elements (C3D4) (Table 3.3). The total number of nodes in the final model is 36,990. Furthermore, a mesh sensitivity analysis is performed by increasing the total number of nodes up to 369,132, and the results are equivalent except for a significantly increased calculation time.

As boundary conditions, we fix all normal displacements of the ECM external surface, and we also fix the flow rate through the cell-matrix interface to zero to avoid the loss of fluid in the cytoplasm, simulating the effect of the cell membrane.

In the simulation, we first apply a predefined stress in the cytoplasm assuming an initial pressure inside the cell (Petrie et al. (2014)). Previous work

3. Active cell mechanosensing in lobopodium formation

Part	Number of elements	Element geometry type	Element material type
ECM	164.224	Tetrahedral C3D4	Solid mechanics
Cytoplasm	44.850	Tetrahedral C3D4P	Solid mechanics and pore pressure
Elastic cytoplasm	3.591	Tetrahedral C3D4	Solid mechanics
Nucleus	6.869	Tetrahedral C3D4H	Hybrid elements

Table 3.3: Number and type of elements used in the model.

(Discher et al. (2005)) established an initial pre-stress in the cell that is related to the ECM stiffness. Petrie et al. (2014) also measured the hydrostatic pressure of a cell with a lamellipodial migration mode. Thus, we use this pressure to calibrate the initial pressure of the cell. In addition, we simulate 3 seconds to make the internal pressure along the cell homogeneous after the initial pre-stress and to establish the initial equilibrium state.

Finally, for lobopodia-based migration, the cell is not polarized in the same way as lamellipodia-based, and the movement depends on the RhoA, ROCK and myosin II contractility (Petrie et al. (2012)). Furthermore, the myosin II distribution inside the cell for lamellipodia-based migration is homogeneous, while for lobopodia-based migration, the distribution is concentrated forward of the nucleus. Thus, a different polarization is present and is apparently necessary to maintain cell migration. Accordingly, we apply a constant linear contraction for 20 seconds at the front of the cell to simulate the cell contractility. Due to the behavior of the poroelastic material, we are modeling a dense solid network connecting the nucleus with the trailing edge and we apply the contraction on this solid phase of the cytoplasm. Furthermore, we assume anisotropic contraction of the cell and we only allow cell contractility in the longitudinal direction.

3.3 Results

We focus our analysis on the pressure in the front part of the cell (where contraction occurs), the ECM strains, the stresses on the cell nucleus and the fluid flow inside the cell. All measurements are taken during cell contraction.

3.3. Results

3.3.1 Cytoplasmic fluid behavior

First, we analyze the evolution of pressure in the front part of the cytoplasm. Figures 3.3a and 3.3b show the evolution of hydrostatic pressure in the front part of the cytoplasm for the stiff and compliant ECMs, respectively, while the cell contracts. Cell contraction provokes the volume variation of the cell in the longitudinal direction. This added to the coupled effect of the solid phase (compressibility) and the cell-matrix adhesion are the main effects causing the pressure variation. The initial pressure of cells in the stiff matrix is higher than that of cells in the compliant matrix since we apply more pre-stress in the stiffer cytoplasm following the work of Discher et al. (2005). Then, the difference between linearly elastic and non-linearly elastic ECMs can be observed. For the high-stiffness linearly elastic matrix, the pressure increases linearly from the initial 600 *Pa* to 2000 *Pa* at the end of the contraction. Nevertheless, for the high-stiffness non-linearly elastic matrix, the pressure starts increasing; however, it subsequently reaches saturation at approximately 1500 *Pa*. The same tendency is found for the cell in the compliant ECM: in the linearly elastic case, the increase in pressure is maintained; however, in the non-linearly elastic case, the pressure first increases and then reaches saturation.

We also carry out a sensitivity study of the cytoplasmic mechanical properties. We vary the fluid content, elastic modulus and Poisson's ratio for the cell in the stiffer ECM. We choose a higher and a lower value for each parameter. All the results show the same behavior of cell pressure, but the values are property dependent. There is a sustained increase in the cytoplasmic pressure when the cell contracts in the linearly elastic ECM and an initial increase and subsequent asymptotic decrease in pressure in the non-linearly elastic ECM (Figure 3.4). The effects of the elastic modulus and Poisson's ratio of the cytoplasm on the cytoplasmic pressure are higher than those of the fluid volume fraction. Nevertheless, there are slight differences in the pressure for the linearly elastic and non-linearly elastic ECMs.

Second, we analyze the fluid velocity in the cytoplasm during contraction. We find a change in the direction of the fluid flow in the non-linearly elastic case. In the first seconds of contraction, the fluid shifts from the front part to the rear part of the cytoplasm, which undergoes contraction in both the linearly

3. Active cell mechanosensing in lobopodium formation

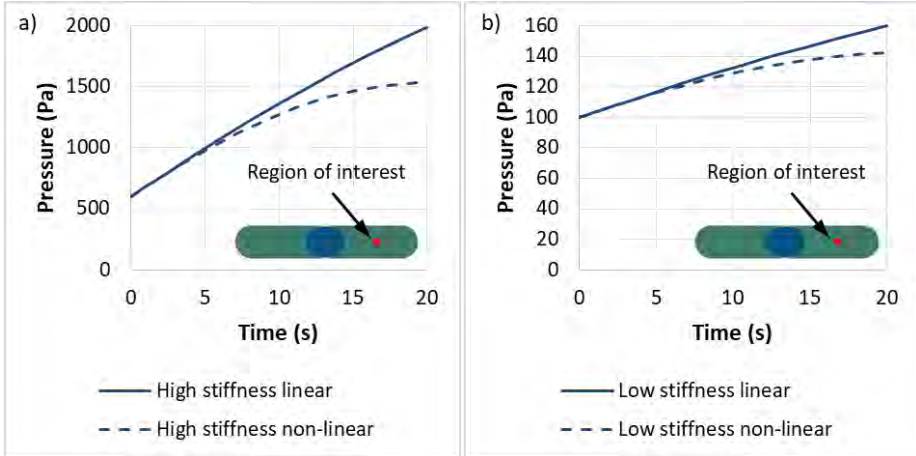


Figure 3.3: Evolution of the hydrostatic pressure in the front part of the cytoplasm while the cell contracts for high-stiffness (a) and low-stiffness (b) linearly elastic and non-linearly elastic ECMs. The variable is represented in the point indicated in red, in the front part of the cytoplasm (region of interest).

elastic and the non-linearly elastic ECMs. Nevertheless, when the pressure starts to increase in the non-linearly elastic matrices (Figure 3.3a and 3.3b), the fluid in the cytoplasm changes direction and flows from the nucleus to the front part (Figure 3.5). This response could activate some mechanotransduction mechanism in the cell to change from a lobopodia-based to a lamellipodia-based migration mode.

3.3.2 Mechanical state of the ECM and nucleus

We also analyze the role of the mechanical characteristics of the ECM. We focus on the maximum tensile strains in the ECM for both the linearly elastic and the non-linearly elastic ECMs with high and low elastic modulus (Figure 3.6). In general, the maximum principal strains are lower in the non-linearly elastic matrices than in the linearly elastic matrices for both high- and low-stiffness matrices. In addition, the strains around the cell are more homogeneously distributed (with values close to 17 %) in the non-linearly elastic ECM. For the linearly elastic ECMs, the distribution is less uniform, and the strain values close to the cell are between 30 and 60 % in the linearly elastic case. The maximum

3.3. Results

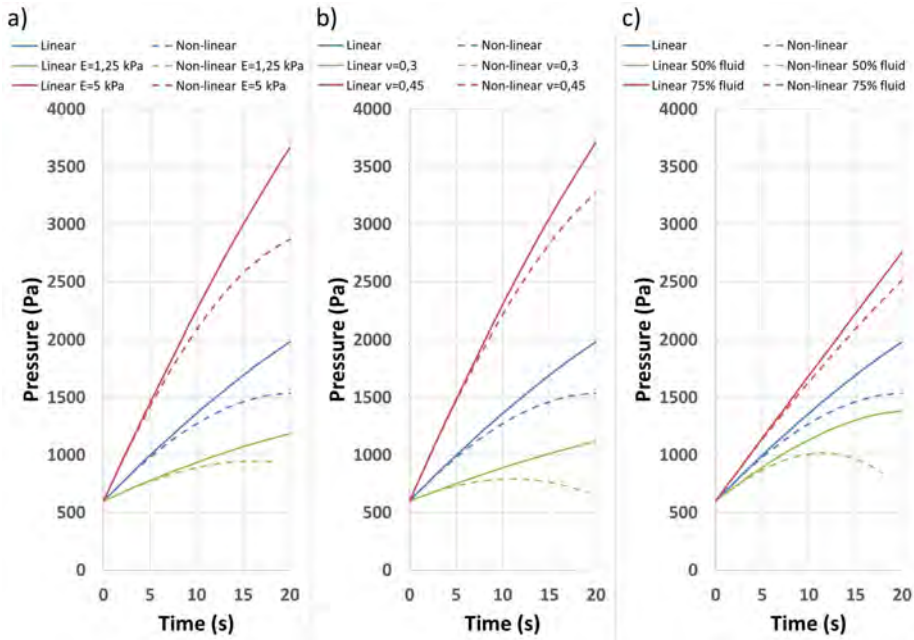


Figure 3.4: Sensitivity analysis of the cytoplasmic mechanical properties on the cytoplasmic hydrostatic pressure while the cell contracts within high-stiffness linearly elastic and non-linearly elastic ECMs. a) Influence of the elastic modulus of the cytoplasm solid phase; b) influence of Poisson's ratio of the cytoplasm solid phase; c) influence of the fluid volume in the cytoplasm. The variable is represented in the point indicated in red in Figure 3.3, in the front part of the cytoplasm (region of interest).

3. Active cell mechanosensing in lobopodium formation

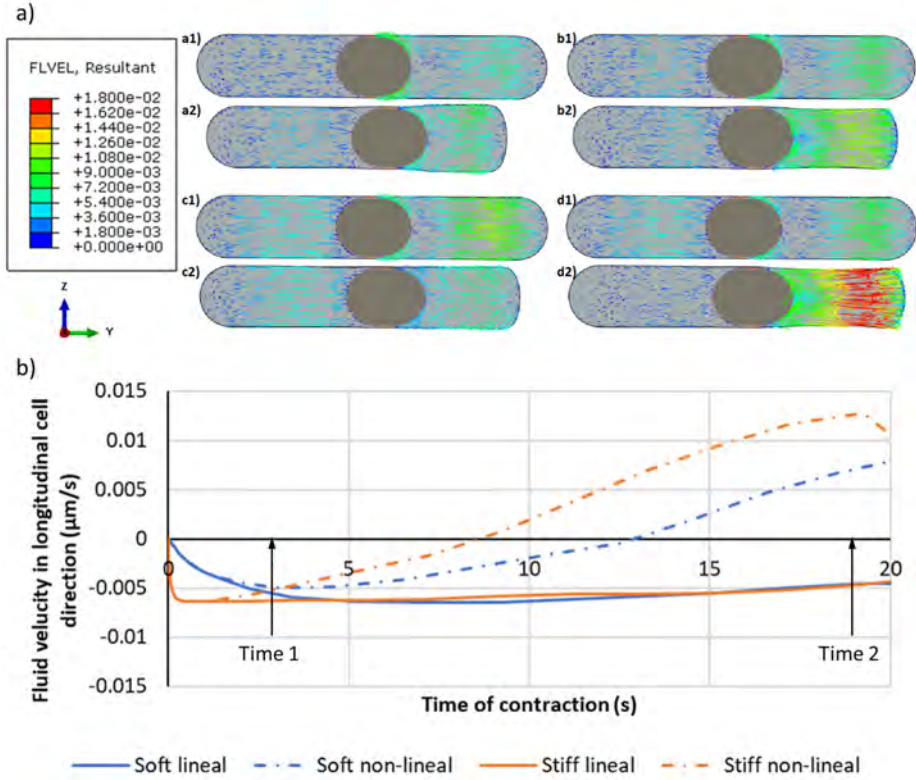


Figure 3.5: Fluid velocity in the cytoplasm for the a) low-stiffness linearly elastic ECM, b) low-stiffness non-linearly elastic ECM, c) high-stiffness linearly elastic ECM and d) high-stiffness non-linearly elastic ECM at the beginning of the contraction (1) and the end of the contraction (2) (units: $\mu\text{m/s}$).

3.3. Results

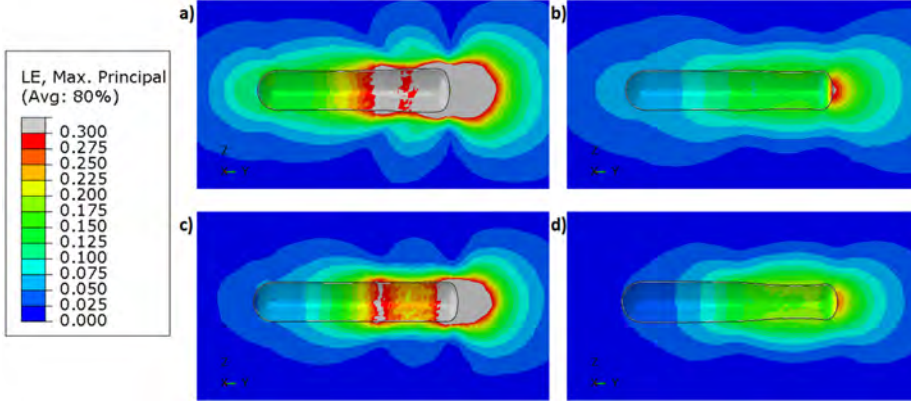


Figure 3.6: Logarithmic maximum principal strain in the ECM: a) low-stiffness linearly elastic ECM, b) low-stiffness non-linearly elastic ECM, c) high-stiffness linearly elastic ECM and d) high-stiffness non-linearly elastic ECM.

value is at the front of the cell, but the strain distribution away from the cell is very similar for both the linearly elastic and the non-linearly elastic ECMs.

These differences can be attributed to the non-linear or linear elasticity of the ECM. In the case of the linearly elastic matrices, the stiffness remains constant, but for the non-linearly elastic matrices, the elastic modulus of the ECM increases in the areas with high strains, mainly in the front part of the cell (Figure 3.7).

Finally, we analyze the mechanical state of the cell nucleus related to different cell processes, such as differentiation (Dahl et al. (2008)). To study how ECM behavior could affect the nucleus, if cells migrate in the lobopodia-based mode, we obtain the maximum tensile stress in the cell nucleus (Figure 3.8). Although the value of the maximum principal stress depends on the ECMs in which cells migrate, we find the same distribution of stresses depending on the mechanical behavior of the ECM. For the linearly elastic matrices, all the nuclei bear the same tensile stress, while for the non-linearly elastic matrices, the range of values is higher, with a higher tensile stress in the front part of the nucleus and a lower stress in the rear part of the nucleus.

3. Active cell mechanosensing in lobopodium formation

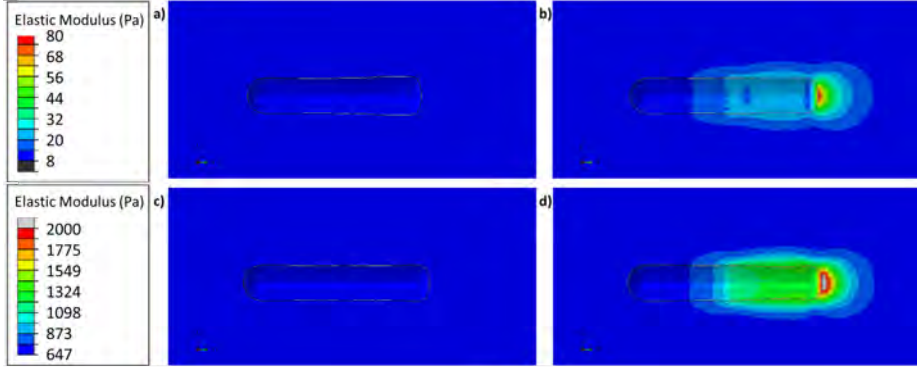


Figure 3.7: Final equivalent elastic modulus (Pa) of the ECM: a) low-stiffness linearly elastic ECM, b) low-stiffness non-linearly elastic ECM, c) high-stiffness linearly elastic ECM and d) high-stiffness non-linearly elastic ECM.

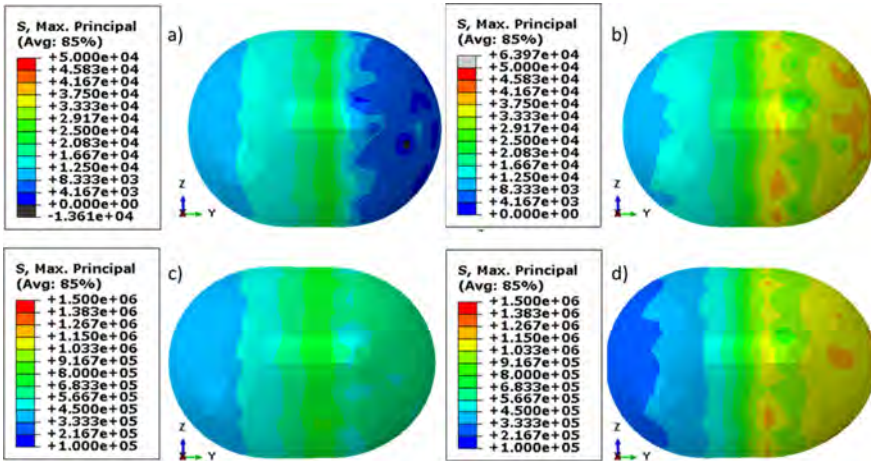


Figure 3.8: Maximum principal stresses in the nucleus for the a) low-stiffness linearly elastic ECM, b) low-stiffness non-linearly elastic ECM, c) high-stiffness linearly elastic ECM and d) high-stiffness non-linearly elastic ECM (units mPa).

3.4 Discussion and Conclusions

Different mechanotransduction mechanisms could regulate the cell to change from a lobopodial to a lamellipodial migration mode or vice versa. From our simulation, we hypothesize that the cell capacity to deform the ECM regulates the pressure differences across the cell body. Pressure variation is actively caused by cell contraction, but how easy or not the matrix allows the movement of the cell influences passively the pressure. Somehow, there is a competition between the cell and the extracellular matrix. Therefore, depending on the mechanical response to the cell forces, the pressure differs inside the cell. In fact, these pressure differences could also reorganize the cytoskeleton and consequently define the migratory path (Jiang and Sun (2013)). In particular, in our work, we estimate that the first increase in pressure at the beginning of cell contraction and the subsequent decrease could be one factor leading a mechanotransduction mechanism. Additionally, the change in fluid flow inside the cytoplasm when the cell contracts could act as a stimulus that prompts the cell to change to a lamellipodial migration mode. Other authors have hypothesized that cells can select different migration mechanisms depending on the external coefficient of hydraulic resistance associated with the ECM (Li and Sun (2018)). Under this framework, the mechanism that regulates cell migration is the capacity of the cell to displace the external water in the ECM. Both theories—i.e., that are based on the effect that the cytoskeleton exerts on the movement of the fluid inside the cell body or that are based on a related effect outside the cell body—can provide new perspectives on how cells regulate their movement.

One of the challenges of computational models of single cells is the mechanical properties of cells and the ECM. It is difficult to obtain an accurate measure of such properties due to the scale and the complexity of testing each single component of the cell separately from the other components. In addition, most works assume different Poisson ratios when measuring the elastic modulus of the cell. For example, Moeendarbary et al. (2013), who presented (to our knowledge) the first work in which the cytoplasm is assumed to be a poroelastic material, fixed the Poisson's ratio of the solid phase as 0.3, and Mahaffy et al. (2004) studied the effect of different values. This problem is even more important if we are assuming a two-phase material (poroelastic cytoplasm). Thus, in our opinion, it is important to develop and implement computational models

3. Active cell mechanosensing in lobopodium formation

because they provide us with information that allows us to qualitatively compare the cell behavior under different assumptions. In our parametric study, as shown in Figure 3.4, we can see the different behavior of the intracellular pressure varying the cytoplasmic properties. For an increasing elastic modulus or Poisson's ratio, the increase in pressure is very similar, but we observe more differences between the linearly elastic and non-linearly elastic ECMs in terms of the increasing elastic modulus of the cytoplasm. In contrast, by decreasing Young's modulus or Poisson's ratio of the cytoplasm, the pressure decreases in both cases, but the differences between the linearly elastic and non-linearly elastic ECMs are higher as Poisson's ratio decreases. Furthermore, the effect of the fluid volume ratio on the cytoplasm is quite similar to that of Poisson's ratio, but the former parameter has a lower impact on the intracellular pressure.

To carry out this work, we make several simplifications in the model due to the absence of available experimental data. First, the role of the membrane is taken into account only to avoid fluid flow between the cell and the ECM; it is not simulated as an active part of the cell. Second, we assume that the cell changes its properties depending on the ECM in which it is embedded. In fact, Solon et al. (2007) demonstrated that the elastic modulus of the cytoplasm changes depending on the substrate properties. However, we decided to simulate these particular ECMs since they are the only ones for which Petrie et al. (2014) measured the hydrostatic pressure inside the cell. Finally, the geometry is a simplification of a real cell because of the variability in cell geometry while migrating. This geometry captures the main geometrical features of the cell in its lobopodial migration mode.

In this work, we simulate the experimental work of Petrie et al. (2014). Our aim is to elucidate whether the differences observed in their experiments could be at least partially explained by the water movement through the solid phase of the cytoplasm (featuring a cytoskeleton and macromolecular crowding) (Moeendarbary et al. (2013)). We observe different behavior in the internal pressure of the cytoplasm, and we also show the effect of the cytoplasmic properties. Another important result is the internal fluid flow of the cell. This flow changes direction depending on the ECM response. The final elastic modulus of the ECM (Figure 3.7) results in higher stresses in the nucleus for the non-linearly elastic ECM.

3.4. Discussion and Conclusions

Despite all these simplifications, we obtain similar results to those obtained in the experimental work (Petrie et al. (2014)). We use the results of the intracellular pressure in the front part of a lobopodial cell in the CDM matrix (high stiffness, linearly elastic) to validate our results. The experimental value of the pressure is on the order of 2 kPa , which is approximately the value estimated from our numerical predictions in Figure 3.3. Thus, the model could help to better understand why cells do not use lobopodia-based migration in non-linearly elastic matrices. We identify two possible mechanosensory variables that could regulate the cell changes from the lobopodial to the lamellipodial migration mode, which are the fluid flow and the hydrostatic pressure inside the cytoplasm. Our results show that relevant differences can be found in the fluid flow and the hydrostatic pressure for different behaviors of the extracellular matrix, although we do not analyze how these variables can control cell migration. Certainly, this aspect would require additional study and further simulations.

Chapter 4

Collective cell response under infection conditions

Contents

4.1	Introduction	58
4.2	Materials and Methods	59
4.2.1	Description of cell model and mechanotransduction mechanism	63
4.2.2	Computational model and boundary conditions	68
4.3	Results	69
4.3.1	Cell contraction and protrusion	70
4.3.2	The role of cell-cell junctions	72
4.3.3	The role of the active/passive part of the cell	78
4.3.4	Cell protrusion law	79
4.4	Discussion and Conclusions	80

This chapter is based on:

*Bastounis, E., Serrano-Alcalde, F., Radhakrishnan, P., Engström, P., Gómez-Benito, M.J., Oswald, M., Yeh, Y.T., Smith, J.G., Welch, M.D., García-Aznar, J.M. & Theriot, J. (2021). Mechanical competition triggered by innate immune signaling drives the collective extrusion of bacterially infected epithelial cells. *Developmental Cell*, 56(4), 443-460.*

4.1 Introduction

Mechanosensing is an important mechanism that describes the way that cells sense their mechanical surroundings. It is known that cells tend to adapt their stiffness to the properties of the surrounding extracellular matrix (ECM), becoming stiffer or softer when they are in a high or low stiffness ECM, respectively (Solon et al. (2007)). But, they are also able to work collectively sensing stiffness gradients in the ECM and moving from the lower stiffness region to the stiffer part of the substrate (called durotaxis) (Sunyer et al. (2016)). In addition, there are other processes, such as wound healing, in which mechanotransduction have a relevant role and there is extensive evidence that contractility and integrin engagement to ECM via focal adhesions (FAs) are required for mechanical sensing (Hoffman et al. (2011)).

Mechanotransduction mechanisms are also relevant in bacterial infection. During this process, cells and pathogens communicate through chemical signals, but there is also mechanical interaction and regulation. It has been previously shown that intracellular pathogens are able to modify host cell functions, in order to spread more efficiently (Faralla et al. (2018); Lamason et al. (2016); Rajabian et al. (2009)). *Listeria monocytogenes* (L.m.) and *Rickettsia parkeri* (R.p.) are two bacterial pathogens that are able to reduce the cell-cell junctions tension, in order to make easier for them the spread from one cell to another (Lamason et al. (2016)). Moreover, intestinal epithelial cells infected with *Salmonella enterica* seovar Typhimurium (S.Tm) has shown responses to extrude the infected cells and reduce bacterial spread (Knodler et al. (2010)). Similar extrusion response has also been observed in human intestinal enteroids infected with L.m. or S.Tm (Co et al. (2019)).

This extrusion mechanism is similar to the one used by normal epithelial to extrude dying or excess cells in the context of overpopulation (Gudipaty and Rosenblatt (2017)). The extruded cell begins to contract and the surrounding cells create a contractile purse-string, lamellipodial protrusion and crawling (Kocgozlu et al. (2016); Kuipers et al. (2014); Rosenblatt et al. (2001); Tamada et al. (2007)). Nevertheless, some bacteria, such as L.m, are able to spread efficiently and infect large domains in a short period of time (Ortega et al. (2019)).

4. Collective cell response under infection conditions

Bastounis et al. (2021) showed the effect of L.m. on epithelial monolayers. They observed the collective response of cells surrounding the infection (surrounders) to avoid the spread of the bacteria. Surrounders cells squeeze the infected cells (mounders) and create mounds of cells (Figure 4.1). Other results observed in this work are the role of contraction and the level of movement. When cell contraction is blocked by drugs, the surrounders can not create mounds and bacterial spread increases. In addition, when there is a focus of infection, all cells tend to move more, while for the uninfected and stable case the cell displacement of cells is much more lower. Furthermore, from the mechanical point of view, the stiffness of cells decreases when bacterial pathogens are inside.

All these results suggest the mechanical properties and mechanotransduction mechanisms of cells as a key role to limit and control bacterial spread. Without forgetting all the existing chemical factors that influence the contractility, level of adhesion of the cell to the ECM, intercellular junctions or cellular stiffness.

Thus, the aim of this work is to create a model to simulate the experiments developed by Bastounis et al. (2021) in the lab of Julie Theriot. With this simulation, we are able to hypothesize what uninfected cells are sensing and the mechanisms that could regulate infected cell extrusion and mound formation. For this aim, we simulate different conditions and make different assumptions in order to analyze the mechanobiological mechanisms under bacterial spreading and mound formation.

4.2 Materials and Methods

We develop a three-dimensional (3D) model of cells simulating a monolayer on collagen I-coated polyacrylamide hydrogels. Although the problem is a cell monolayer and there are previous computational works for cell monolayers in 2D (Brodland et al. (2006); Escribano et al. (2018); Farhadifar et al. (2007); González-Valverde and García-Aznar (2018)), this problem is highly three-dimensional. We consider the axial and the vertical directions as the more important ones, because it is the direction in which the mound formation occurs (Figure 4.2). It is also important the collective cell-cell interaction, the

4.2. Materials and Methods

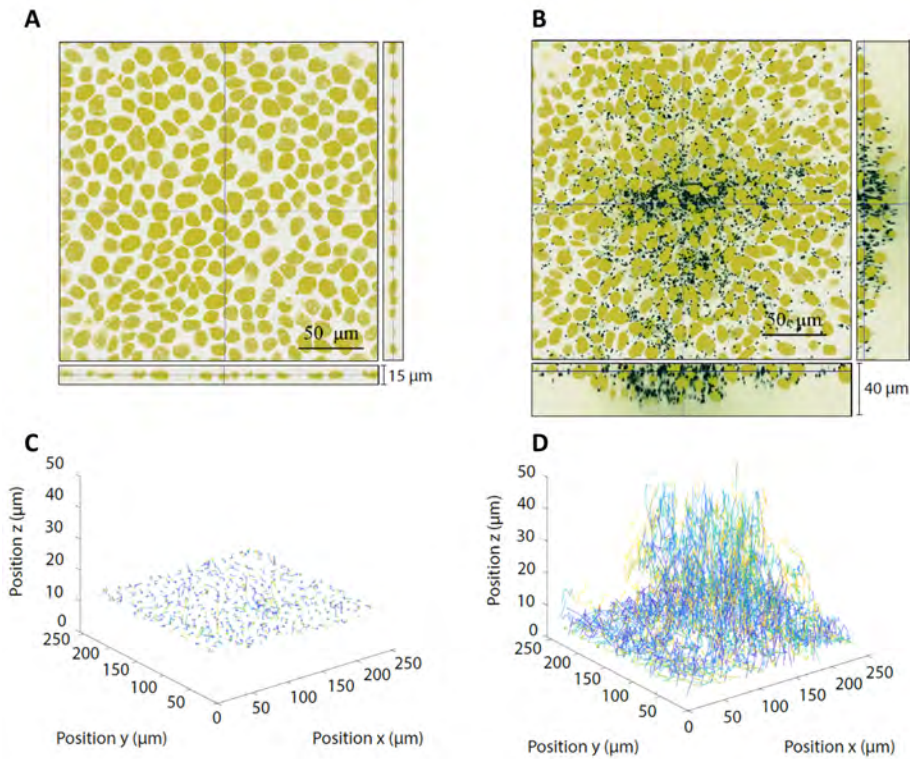


Figure 4.1: Experimental results showing the effect of the infection in the monolayer and the mound formation. Images (a) and (b) show the position of the nucleus of the cell culture (yellow) after a period of time for the uninfected and infected monolayer, respectively (black dots are bacteria infection). (c) and (d) show the tracking of the nucleus over the time for the uninfected and infected culture, respectively. The results of the infected culture show clearly the mound formed in the center of the bacterial infection, while the cells of the uninfected culture form a constant thickness of the monolayer. Adapted from Bastounis et al. (2021).

4. Collective cell response under infection conditions

stress distribution and the closure of the infection focus in the axial-radial plane. Thus, three dimensional modeling is required to replicate most of the relevant biophysical aspects of this experiment.

The experimental work of Bastounis et al. (2021) consists of a human epithelial cell monolayer, where some cells in the center of the domain are infected. To test the effect of cell behavior in mound formation, they supply different drugs to avoid the cell contractility or to avoid the cell-cell junctions or ablate groups of cells close to the infection. Initially, a cell monolayer is cultured and its behavior is quantified (cell displacements, tractions on the surface of the extracellular matrix, elastic modulus of the cells) and then a cell in the center of the culture is infected. The infection spreads from cell to cell and after 24 hours a focus of infected cells is obtained in the center, surrounded by uninfected cells. At this time, the cells surrounding the infection move towards them, causing an extrusion of infected cells subsequently forming a mound of infected cells. It should be noted that the number of cells at the beginning and at the end is the same (the level of cell death and proliferation is negligible), so it could not be attributed to an increase in uninfected cells. Several measurements performed (with different experimental techniques) showed higher cell motility, lower elastic modulus of infected cells and the appearance of a ring surrounding the focus of infection on the displacements map in the ECM (Figure 4.3). In addition, when drugs are delivered to the cells and contraction or cell-cell junctions are inhibited, no mound is observed, so that both contraction and cell-cell junctions must be present for the mound to appear.

Following experimental observations (Bastounis et al. (2021)) and previous computational works (Escribano et al. (2019); O’Dea and King (2012); Schmedt et al. (2012)), we assume that cells can be simulated as regular hexagons with side length and thickness of $7\mu m$. The ECM hydrogel is large enough to avoid border effects and we model it as a linear elastic material with elastic modulus (E) of $3kPa$ and Poisson’s ratio (ν) of 0.3 (Bastounis et al. (2021)).

4.2. Materials and Methods

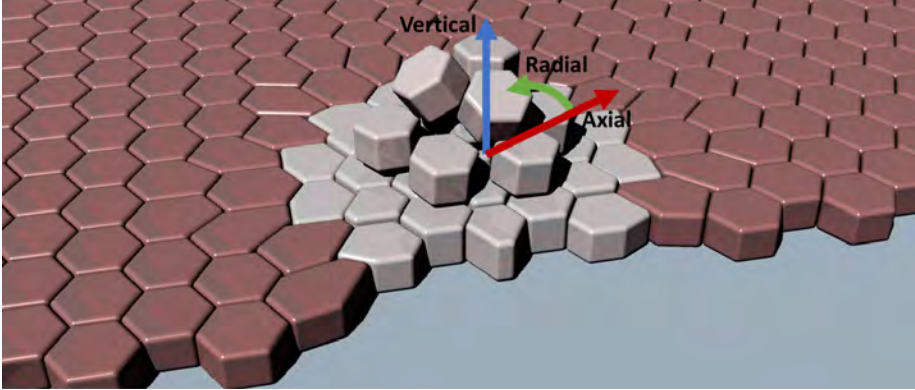


Figure 4.2: Monolayer scheme with uninfected surround cells (dark color) and infected mounder cells (light color). The cylindrical system is placed in the center of the infection and axial-radial axis are in the plane of the monolayer. Uninfected cells protrude in the axial direction to extrude the infected cells.

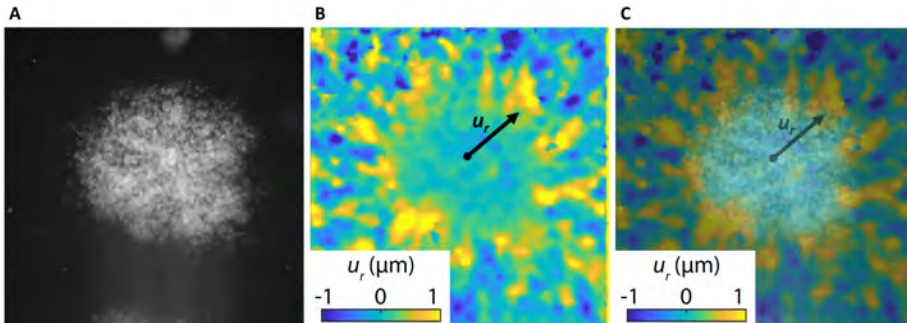


Figure 4.3: ECM displacements provoked by uninfected cells migrating towards the infection focus. (a) Phase contrast image of the culture showing the bacteria in white. (b) Radial component of the ECM's displacements in a cylindrical coordinate system from the center of the infection. (c) Superposition of images *a* and *b* showing the main direction of the displacements towards the exterior of the infection and placed on the first row of uninfected cells. Adapted from Bastounis et al. (2021).

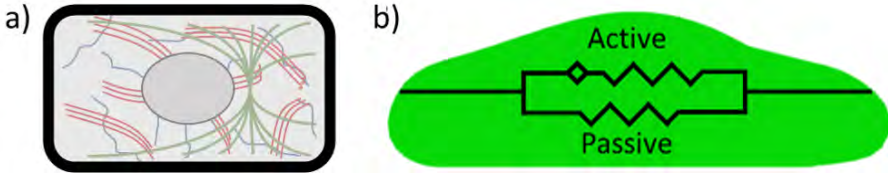


Figure 4.4: Cell scheme: (a) illustrative cell with nucleus, cytosol, cytoskeleton and membrane; (b) simplified model of the cell representing the active cytoskeleton mechanisms (contractile motors) and the rest passive components.

4.2.1 Description of cell model and mechanotransduction mechanism

We model the cell distinguishing a passive and active component (Figure 4.4). The passive part represents the passive strength of the cytoskeleton and the active one the actomyosin contractility system (Borau et al. (2011); Moreo et al. (2008)). Both parts work in parallel assuming a linear elastic material, where the total stresses of the cell are the sum of the passive and the active ones:

$$\sigma_{cell} = \sigma_{passive} + \sigma_{active} \quad (4.1)$$

as we assume both passive and active parts deform the same:

$$\epsilon_{cell} = \epsilon_{passive} = \epsilon_{active} \quad (4.2)$$

where σ_{cell} are the total stresses of the cell, $\sigma_{passive}$ are the stresses of the passive part of the cell, σ_{active} are the stresses of the active part of the cell and ϵ_{cell} are the total strains of the cell, $\epsilon_{passive}$ are the strains of the passive part of the cell and ϵ_{active} are the strains of the active part of the cell.

Following the experimental AFM measurements (Bastounis et al. (2021)), we vary the cell stiffness depending on the infection degree. We set the total elastic modulus (E_{cell}) in $1000Pa$ for uninfected cells and $250Pa$ for infected cells, respectively. As a first approach, we assume that both, passive ($E_{passive}$)

4.2. Materials and Methods

	Uninfected		Infected	
	$E(Pa)$	ν	$E(Pa)$	ν
Passive	500	0.48	125	0.48
Active	500	0	125	0
Cell	1000	-	250	-

Table 4.1: Summary of cell properties used in the simulations for the uninfected and infected cells distinguishing the contribution of the passive and active parts.

and active (E_{active}) elastic modulus, are $500Pa$ for uninfected cells and $125Pa$ for infected cells, respectively.

The Poisson ratio for the passive part is set to 0.48, thus we assume it is nearly incompressible (Moreo et al. (2008)). Nevertheless, the active part mainly represents the actomyosin contraction and we assume this contraction is not isotropic but it just occurs in the plane of the monolayer. Thereby, the Poisson ratio is assumed 0 to uncouple the vertical direction of the active part of the cell and the monolayer plane effects. Hence, we assume cytoskeleton is organized to induce maximum contraction in the plane of the monolayer. Table 4.1 summarizes the mechanical properties of cells.

We also divide the cell body in three differentiated zones: contractile, adhesive and protrusive zone (Figure 4.5). This division is carried out to condense in one geometrical continuum cell model the two main processes we simulate: contraction and protrusion. At this point, as a first approach, we do not simulate the nucleus, neither the membrane because they do not add important value to the simulated process.

Regarding the cell interactions, we consider both cell-cell and cell-matrix ones. On the one hand, cell-cell junctions are modeled as a linear elastic continuum material with $1000Pa$ and $500Pa$ for elastic and shear modulus, respectively. Following the experimental work of Bastounis et al. (2021), we simulate the inhibition of cell-cell junctions decreasing these values close to zero. Thus, when cell-cell junctions are inhibited, cells do not interact anymore with each other. On the other hand, cell-ECM adhesions are simulated as cohesive contacts. The cohesive joints used in the model follow the uncoupled traction-separation law, where they have a linear behavior that is defined by the stiffness

4. Collective cell response under infection conditions

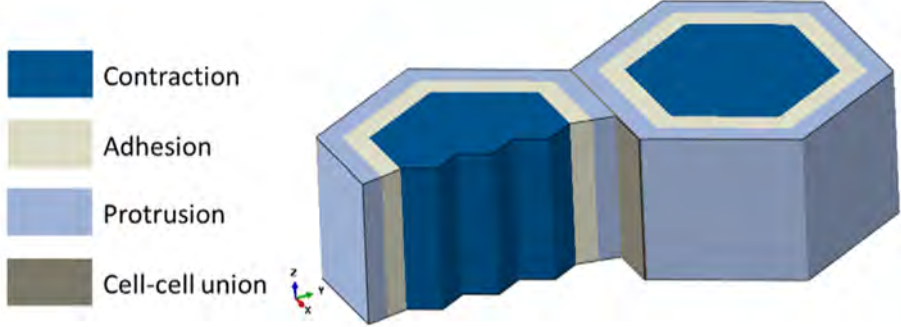


Figure 4.5: Geometrical parts of the cell. The contraction of the cell is simulated in the cell center, where we assume the acto-myosin is located (dark blue). At the exterior part of the cell we assume G-actin polymerize forming the F-actin complexes regulating cell protrusion (light blue). Between the contractive and protrusive zones, we set the adhesive zone, where the cell adheres to the substrate (light gray). Finally, we add the cell-cell junctions assuming that all the face is joined (dark gray).

in three directions: normal direction to the contact surface and the two in-plane shear directions. Thus, the elastic behavior can be written as follows:

$$\mathbf{t} = \begin{Bmatrix} t_n \\ t_s \\ t_t \end{Bmatrix} = \begin{bmatrix} K_{nn} & 0 & 0 \\ 0 & K_{ss} & 0 \\ 0 & 0 & K_{tt} \end{bmatrix} \begin{Bmatrix} \delta_n \\ \delta_s \\ \delta_t \end{Bmatrix} = \mathbf{K}\boldsymbol{\delta} \quad (4.3)$$

where \mathbf{t} , \mathbf{K} and $\boldsymbol{\delta}$ are the stress vector, stiffness and separation of the cohesive contact, respectively. And the subscripts n , s and t denote the normal and shear directions to the surface (see Figure 4.6). It should be noted that the cohesive behavior is not introduced as elements, but as cohesive contact. Therefore, the units of stiffness will be $N/\mu m^3$.

This type of contact allows the bonding of two different meshes and control the stiffness in normal and shear direction of this cell-ECM adhesion. In this case, we have also assumed two possible behaviors depending if cell-cell junctions are working or not. If cell-cell junctions are simulated (it means that cells behave collectively), cell-ECM adhesion is weaker than when cell-cell junctions are inhibited (in this other case cells behave individually). When we assume

4.2. Materials and Methods

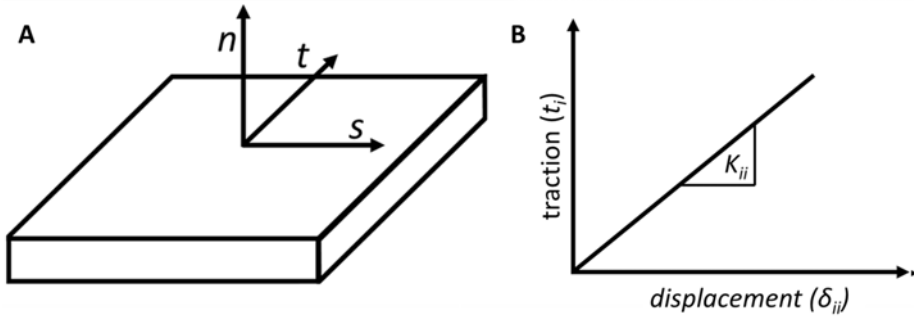


Figure 4.6: Cohesive contacts: (a) principal directions of the cohesive contacts; (b) stress-displacement curve for a given stiffness \mathbf{K}_{ij} for i equal to normal (n), tangential one (t) and tangential two (s) directions.

the weaker adhesion, the stiffness in normal direction is $10nN/\mu m^3$ per area of contact and negligible in shear direction. Meanwhile, when we assume the rigid one, the stiffness in normal and shear direction is $1000nN/\mu m^3$ per area of contact. Each cell has a total area of contact of $31.61\mu m^2$ (six zones of $5.268\mu m^2$), thus, the total adhesion of each cell to the ECM is $31.61nN/\mu m$ and $31608nN/\mu m$ for the weak and the rigid adhesion, respectively. This behavior has been observed experimentally in previous works measuring the force exerted on the ECM when migrating on a gradient stiffness substrate. In this case, cells work collectively and allow them to detect different substrate stiffness and to move towards the highest stiffness side (durotaxis) (Sunyer et al. (2016)). This assumption has been successfully implemented in a previous computational work (Escribano et al. (2018)). The adhesion properties are summarized in Table 4.2.

We hypothesize a mechanotransduction theory based on the experimental observations (Bastounis et al. (2021)). First of all, each single cell contracts to sense the mechanical microenvironment. If cell-cell junctions are working properly, the cell-ECM adhesions initially are soft, so the cell can move relative to the matrix. If these displacements are large (cell relative to the matrix), the cell creates stiffer cell-ECM adhesions (we assume the same values as when cell-cell contact is inhibited, see Table 4.2). Once the cellular displacements relative to the ECM are small enough (with or without stiff cell-ECM adhesions), the cell senses the stresses. At this point, if the cell detects a tensional asymmetry, it protrudes in the direction of lower stress (this is summarized in Figure 4.7).

4. Collective cell response under infection conditions

		Base case	Cell-cell contact inhibition	New cell-ECM adhesion
Cell-cell junction	Elastic modulus (Pa)	1000	~ 0	1000
	Shear modulus (Pa)	500	~ 0	500
Cell-ECM adhesion	Normal direction ($nN/\mu m^3$)	10	1000	1000
	Shear direction ($nN/\mu m^3$)	~ 0	1000	1000

Table 4.2: Summary of cell-cell junction and cell-ECM adhesion properties. We consider two scenarios: the base case when all cells are uninfected and the culture is homogeneous and the cell-cell contact inhibition when cells are not able to form cell-cell junctions and increase their cell-ECM adhesion. Additionally, we also consider the creation of new cell-ECM adhesions following the mechanotransduction mechanism. The new cell-ECM adhesion only increases the stiffness of the adhesion.

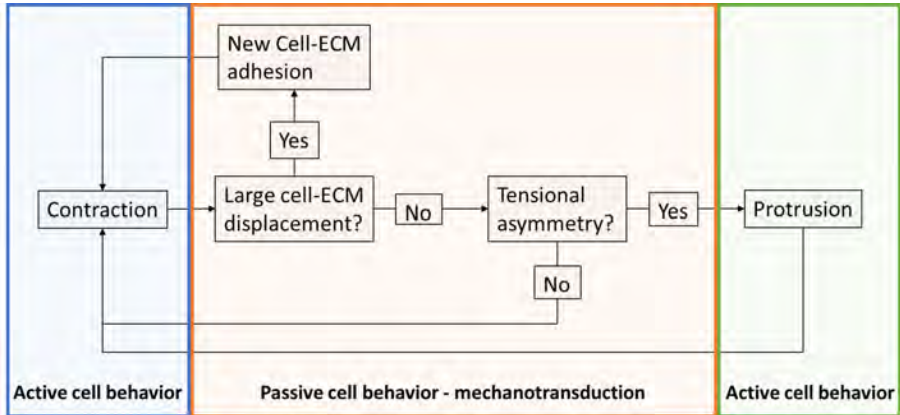


Figure 4.7: Cell mechanotransduction scheme. We propose two active phases (contraction and protrusion) and one passive phase, where the cell decides depending on the mechanical stimulus that is sensing. Cell protrudes only after two conditions: cellular displacements relative to the ECM are small and there is tensional asymmetry.

4.2. Materials and Methods

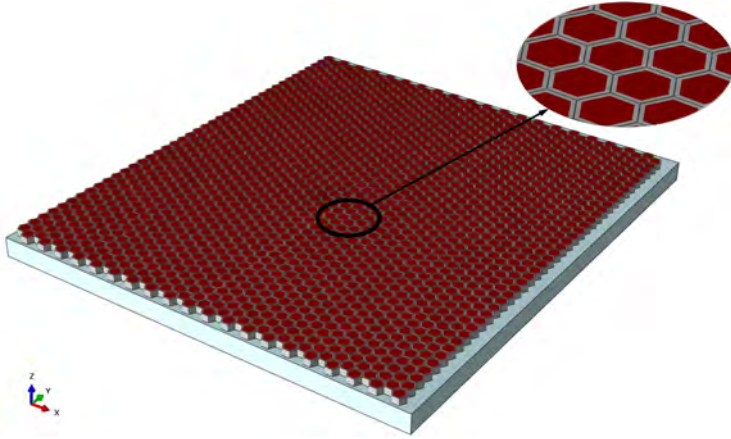


Figure 4.8: Computational model of the cell monolayer, a total of 1 600 cells are included in the model. Cells are in red and gray (gray color for the protrusion zone of each cell to make easier cells visualization) and ECM in light blue.

4.2.2 Computational model and boundary conditions

We simulate a cell monolayer formed by 1 600 cells. It is simulated into the commercial finite element software (FE-based) ABAQUS (Hibbit, Karlsson and Sorensen, Inc. (2006)) (Figure 4.8). To simulate the passive and active behavior of the cell, we have created two overlapping meshes sharing the nodes for the cells. This mesh is discretized with linear wedge elements of average size $2\mu\text{m}$ and 270 elements each part of the cell, active and passive (540 total elements for each cell). The cell-cell junctions are modeled with nine linear hexahedral elements per contact face and the ECM is modeled with 117 600 linear hexahedral elements. The total number of elements in the model is 1 024 800 and 606 232 nodes.

To simulate the infection of the monolayer, initially we consider that seven cells in the center are infected, thus, we avoid boundary effects in the region of interest. In addition, we apply a non-displacement boundary condition on the exterior cells of our simulation domain, because we assume that displacements far of the infection are negligible. Moreover, when a cell is infected, we decrease the stiffness. Thereby, we do not take into account different levels of infection.

4. Collective cell response under infection conditions

We only analyze a short period of time in which only one mechanotransduction cycle is simulated. This cycle could be repeated several times and the displacements would be more prominent. Nevertheless, from the mechanical point of view, one cycle is enough to analyze the behavior.

4.3 Results

Due to the mechanotransduction mechanism here proposed, we distinguish two main phases: contraction and (if it occurs) protrusion.

First, we analyze three cases to understand how cells sense and the relevance of the new adhesions created by the uninfected cells close to the infection zone: **(Case 1)** All cells are uninfected and the base case of cell-cell junctions and cell-ECM adhesions; **(Case 2)** Seven cells are infected (lower cellular stiffness of the infected cells) and the base case of cell-cell junctions and cell-ECM adhesions; and **(Case 3)** Seven cells are infected (lower cellular stiffness of the infected cells), base case of the cell-cell junctions and cell-ECM adhesions and new cell-ECM adhesions only in the uninfected cells close to the infection. The base case of junctions and adhesions is summarized in Table 4.2, where we assume stiff cell-cell junction and soft cell-ECM adhesion.

When the stiffness of the infected cells decrease, we observe higher displacements in the first uninfected cells close to the infection (case 2). Thus, we consider these cells with high displacements as the new border of the uninfected cellular cluster and increase the cell-ECM adhesion stiffness creating the new adhesions of case 3. In other words, these cells are detecting large cell-ECM displacements and we are creating new adhesions in order to avoid the frictional behavior (Figure 4.7).

Thus, the difference between cases 2 and 3 are the cell-ECM adhesions of uninfected cells in contact with infected cells. We observe large displacements in uninfected cells relative to the ECM when we decrease the stiffness of the infected cells (case 2). Therefore, the proposed mechanotransduction mechanism suggests creating new cell-ECM adhesions in the first ring of uninfected cells (case 3).

4.3. Results

4.3.1 Cell contraction and protrusion

The first phase of the mechanosensing mechanism is the contraction. Figures 4.9 and 4.10 show the displacement and the total stress status of two non-infected cells in the different cases analyzed. In order to represent what is happening in the monolayer, one of these cells is placed at a medium distance between the infection and the exterior border of the model (cell α) and the other is next to the infection (cell β) (see Figure 4.9A and 4.10A). Where the infected cells are placed in the center of the model, when the infection is simulated (Figures 4.9A and 4.10A).

When all simulated cells are uninfected (case 1), so we have a homogeneous cell culture, we can observe the low level of displacement and a symmetrical stress distribution along the cell, no matter where the cell is in the monolayer (Figure 4.9 B1 and C1).

In the second case of study, we change the mechanical properties of seven cells in the center of the monolayer to simulate the infection (see 4.1). Looking to the displacements, the cell closest to the infection (cell β) shows the highest values (see Figure 4.9B2). The cell moves from the infection towards the exterior and this movement is induced just by the collective contraction when we have a non-homogeneous cell culture (infected and non-infected cells). If we study the stress state, we can observe how the infection affects to the uninfected cells. While the stress distribution of a cell placed at a medium distance (cell α) is not influenced, the uninfected cell next to the infection (cell β) is highly influenced (Figure 4.9C2).

The third case simulated is a variation of the second one, where we add cell-ECM adhesion for β cells. For this situation, we obtain a similar behavior both in displacements and stresses than in the second one, but cell displacements are lower due to the new adhesions to the matrix.

After the contraction phase, we simulate protrusion of cells adjacent to the infection if there is stress asymmetry (β cells). Figure 4.10B shows the displacements during the protrusion. The stress distribution of cells in the first case is symmetrical, hence, we assume that the protrusion does not occur in this situation. Nevertheless, the cell protrudes for the second and third case and we

4. Collective cell response under infection conditions

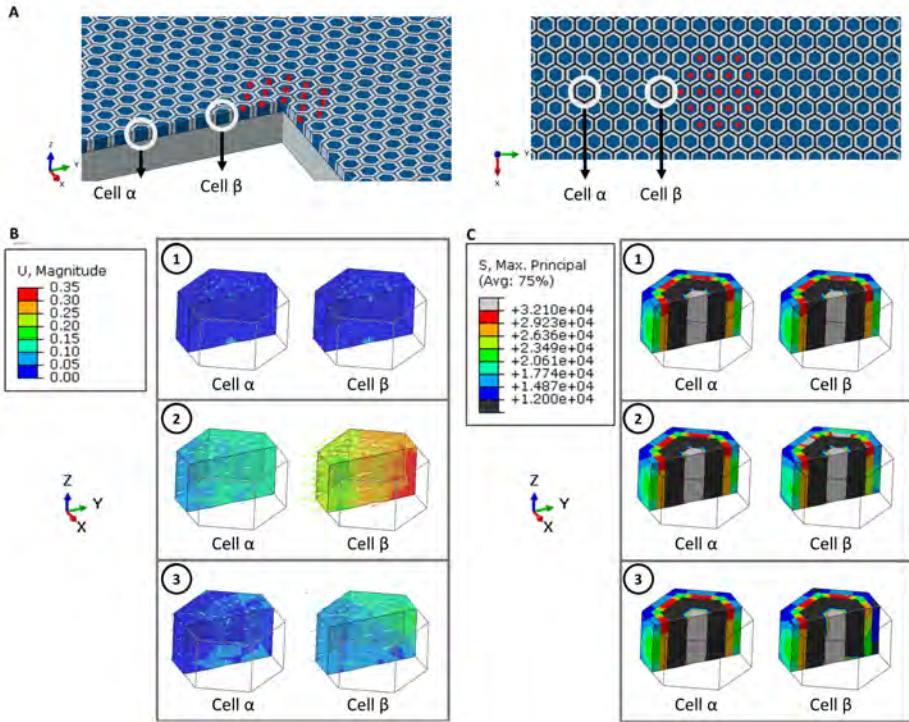


Figure 4.9: Cell displacements (μm) and cell stresses (mPa). We analyze the results in two uninfected cells to observe how the infection affects and what the cell is sensing. (A) Position of the cells analyzed and asterisks denote the infected cells. (B) and (C) Displacement and stresses results during the contraction phase, respectively. (1) all cells simulated are uninfected, (2) infected and uninfected cells are simulated just changing the mechanical properties of the infected cells and (3) same as case 2 but additionally changing mechanical properties of cell-cell junctions of surroundings close to the infection. Results of displacement in B2 justify the creation of new adhesions following the mechanotransduction mechanism (Figure 4.7). Results of stresses in C2 and C3 justify cell protrusion following the mechanotransduction mechanism.

4.3. Results

can appreciate the effect of the new cell-ECM adhesion. While for the second case (without new cell-ECM adhesion) the major displacements are towards the exterior, when we allow cells to create new cell-ECM adhesion to the cells that are protruding, we observe more displacement in the protrusion direction.

In the third case, cells are using the matrix to push the infected cells. Thus, the formation of new adhesions not only reduce the "passive" displacement of cells during contraction, but also helps the cell to advance in the direction of the protrusion.

Another result where we can observe and compare the effect of new adhesions is in the displacements of the ECM. Figure 4.10C shows the radial displacement of the matrix. The center of the cylindrical system is placed in the center of the infection, thus, we can see how cells are pushing the ECM towards the exterior to get an efficient movement. The displacements in the second case are negligible in comparison to the third one. If we look to the experimental results of Bastounis et al. (2021) (see Figure 4.3), we can notice the similarities with the case number three, were the ECM's displacements are toward the exterior while cells move to the interior, to the infection.

Finally, we analyze the size of the infection mound. Figure 4.11 shows vertical displacement of the cells after protrusion. As we have seen in the previous results, the highest cell movement to the infection cells is observed when the protrusion is supported by new cell-ECM adhesions. Nevertheless, we also observe a little mound without the presence of new cell-ECM adhesions. Finally, the results of mounding for the case one are zero. Since all the cells are uninfected and there is not tensional asymmetry, following the mechanotransduction mechanism the protrusion does not occur.

4.3.2 The role of cell-cell junctions

The fourth case analyzed is the inhibition of cell-cell junctions. The stiffness of cell-cell interface properties were reduced to a negligible value and the stiffness of cell-ECM adhesions were increased to $1000nN/\mu m^3$, both in normal and shear directions (Table 4.2). Thus, when we inhibit the junctions between cells, the adhesion of each cell to the substrate is increased.

4. Collective cell response under infection conditions

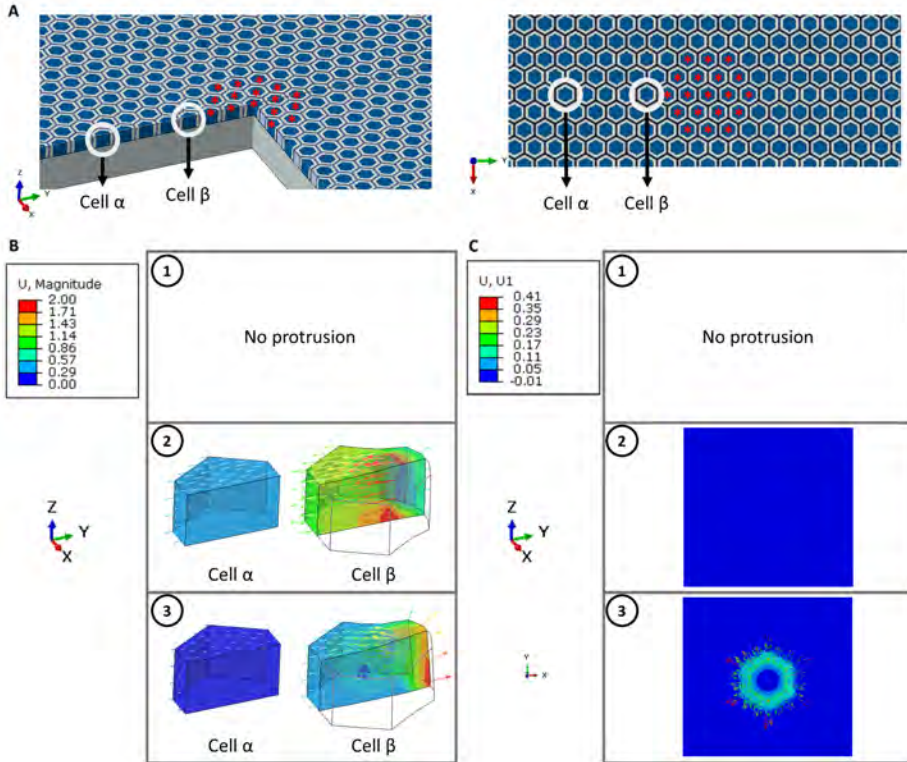


Figure 4.10: Cell displacements (μm) and ECM displacements (μm). We analyze the results in two uninfected cells to observe how affect the infection and what the cell is sensing. (A) Position of the cells analyzed and asterisks denote the infected cells. (B) Displacement during the protrusion (if cell protrude). (C) Displacements provoked for the cells on the ECM's surface during the protrusion (if cells protrudes). (1) all cells simulated are uninfected, (2) infected and uninfected cells are simulated just changing the mechanical properties of the infected cells and (3) same as case 2 but additionally changing mechanical properties of cell-cell junctions of surroundings close to the infection. Results of displacement in B2 justify the creation of new adhesions following the mechanotransduction mechanism (Figure 4.7). Results in B and C show the effect of the new adhesions during protrusion (C3 ECM displacements are in line with the experimental results).

4.3. Results

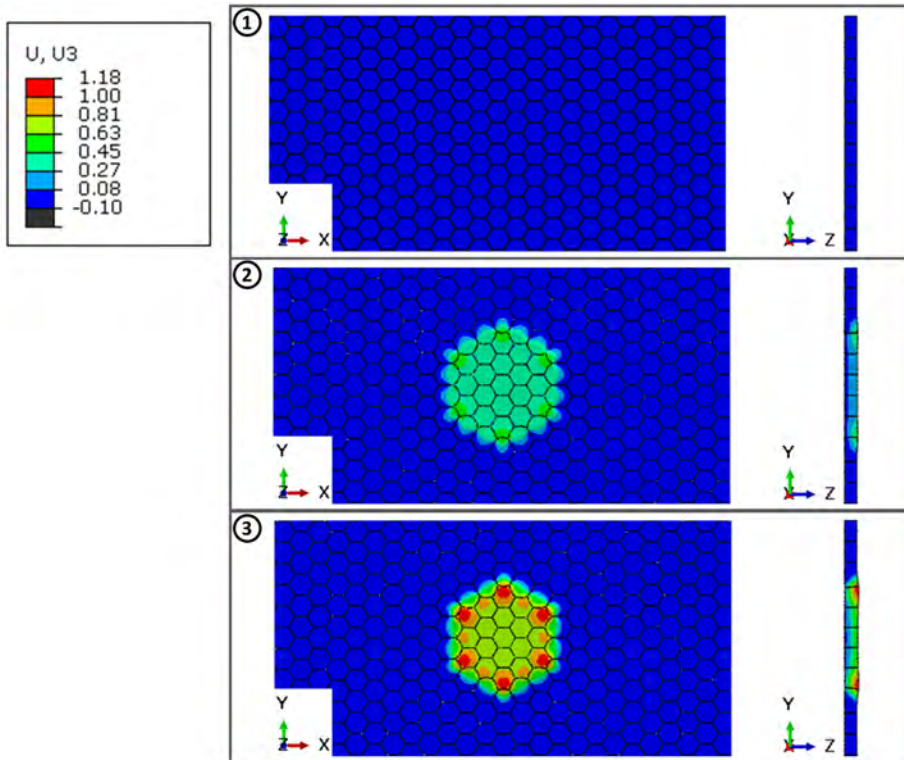


Figure 4.11: Displacement (μm) in vertical direction of the culture during the protrusion phase (mound formation). It can be observed the initiation of mound formation and the importance of the new adhesion to obtain higher displacement.

4. Collective cell response under infection conditions

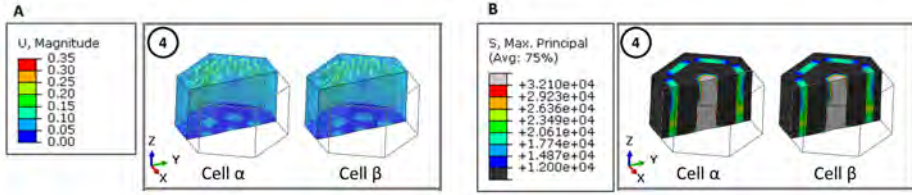


Figure 4.12: Displacement (μm) and stress (Pa) of isolated cells. In this case cell-cell-junctions are inhibited and cell-ECM adhesion are strengthened.

The displacement and stress distribution of both cell types (α and β cells described in Figure 4.9A) is similar to the ones of case 1 (Figure 4.12), when all the cells are uninfected (Figure 4.9B1). Nevertheless, the values of displacements and stresses are higher because the contraction force applied is the same. The stress values are again different than the ones in case 1 (Figure 4.9C1), but the stress distribution is homogeneous (there is not asymmetry). Thus, there is no protrusion phase and therefore, no mound formation.

Experimentally, it has been observed that mixing a population of cells able to create cell-cell junctions with others that are not able, the cells with the capacity to join with others tend to concentrate close to the infected cells joining together and surrounding the focus of infection, thus creating the mound of infected cells (Bastounis et al. (2021)). To study this case, two simulations have been performed.

In the first of these cases (case study number 5), the cell-cell junctions of the uninfected cells that are far from the infection are eliminated (Figure 4.13A). Although asymmetry is also observed in the last cell able to form cell-cell junctions, this is because at one end it is attached to the ECM and not to the adjoining cell. This is an expected result but in the above cases it is not observed due to the boundary conditions, since the cell culture is assumed to be large enough to avoid this effect. In the uninfected cells surrounding the infection, where there are cell-cell junctions, stress asymmetry is also observed. Therefore, protrusion and consequent mounding appears (Figure 4.14A).

In the second simulation mixing cells with the capacity to generate cell-cell junctions (case study number 6), the conditions are changed, where we assume cells able to create cell-cell junctions tend to concentrate far from the infection

4.3. Results

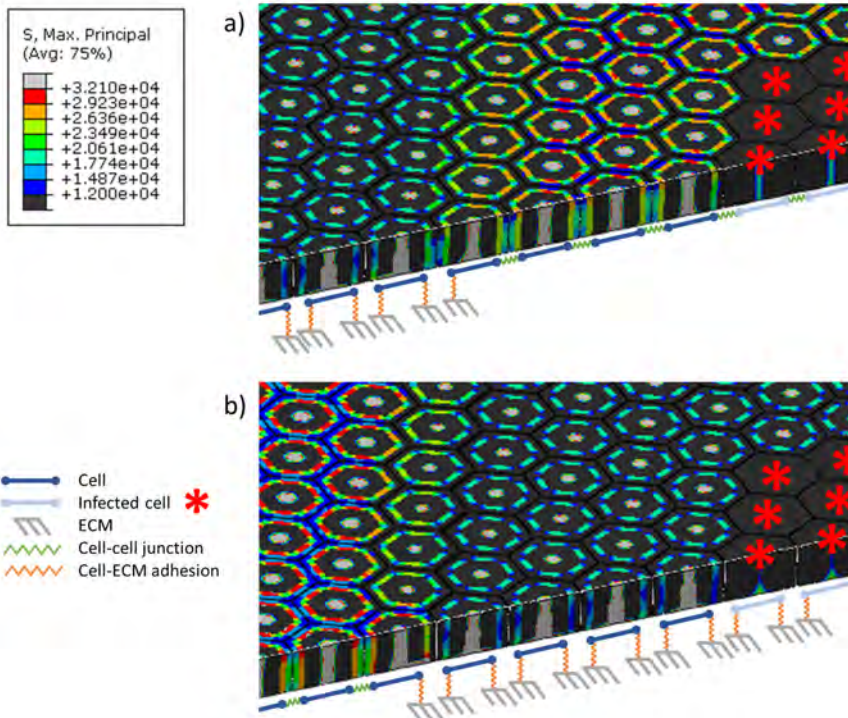


Figure 4.13: Stresses in cell mixing (mPa): (a) cells far of the infection cannot create cell-cell junctions; (b) cells close to the infection and infected cells cannot create cell-cell junctions.

focus (Figure 4.13B). In this case, stress asymmetry also appears in the cells bordering the central cells without the capacity to join other cells. This is due to two factors, the first one is that it has no junction to another cell and it is bound to the ECM. As we have seen in the previous case this produces a slight asymmetry. The second reason is that there is a hole/wound effect in the center of the substrate and as seen in previous studies, cells tend to close that wound. Since there is stress asymmetry, it also simulates the protrusion of uninfected cells against uninfected cells (with a focus of infection in the center). The mound formation is much smaller than when protruding against infected cells and it is totally localized in the cells that protrude and the first cells that do not create cell-cell junctions (Figure 4.14B).

4. Collective cell response under infection conditions

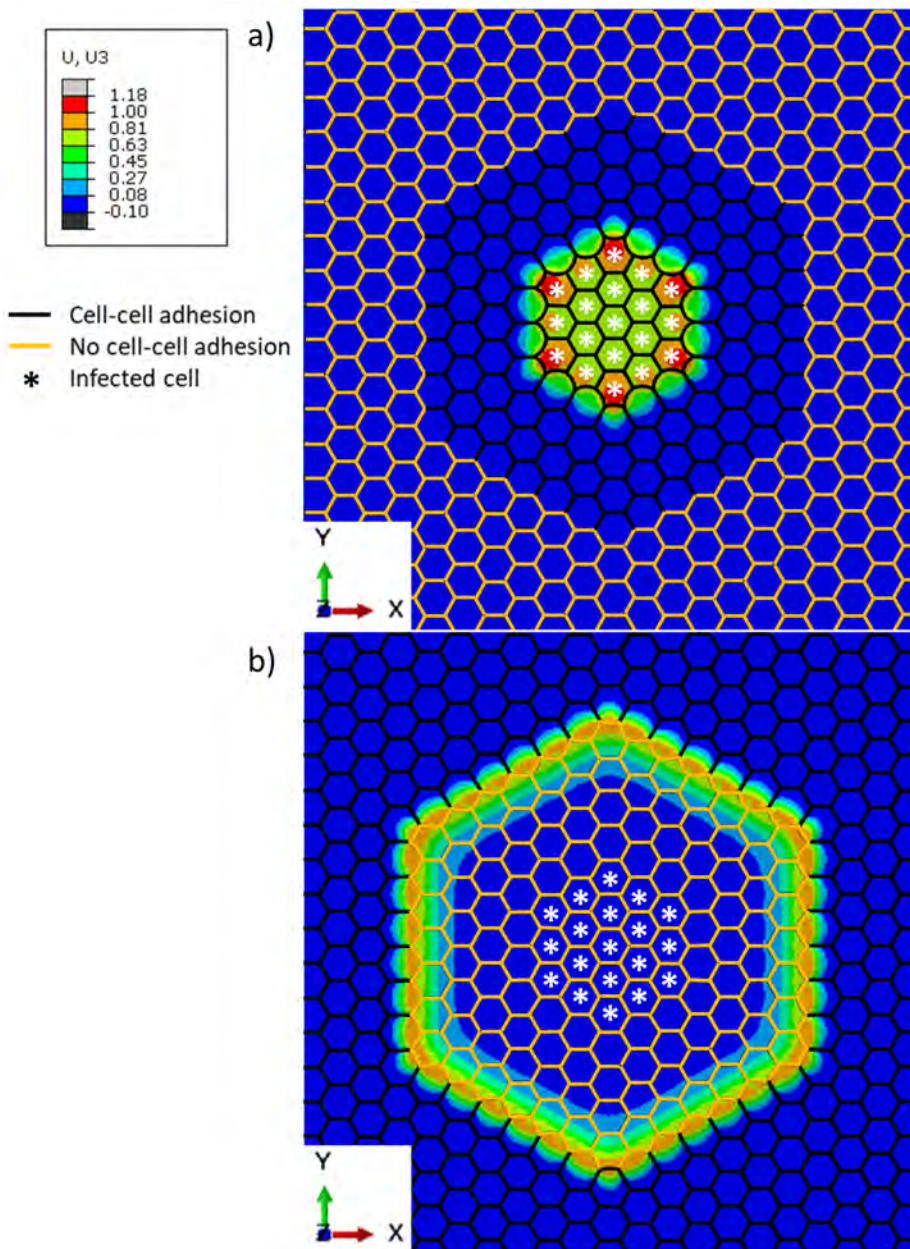


Figure 4.14: Vertical displacements (μm) for cell mixing: (a) cells far of the infection cannot create cell-cell junctions; (b) and when cells close to the infection and infected cells cannot create cell-cell junctions.

4.3. Results

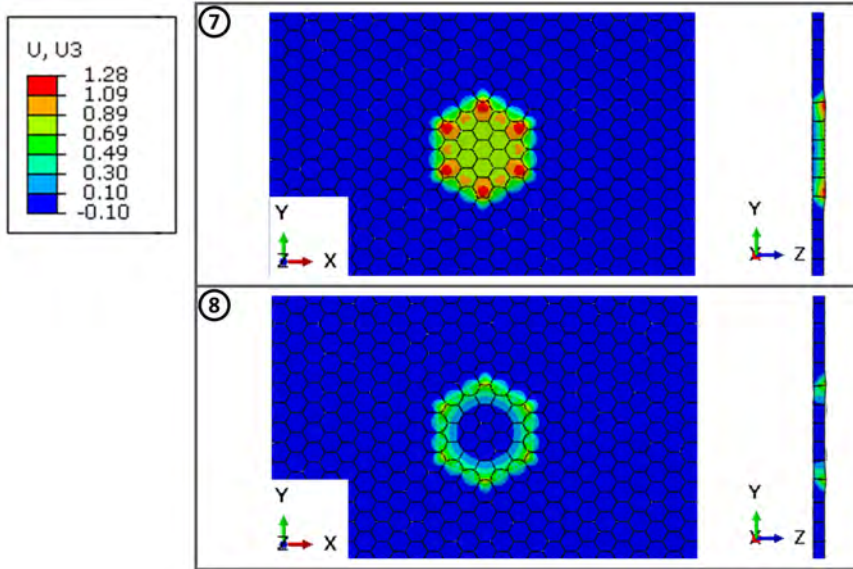


Figure 4.15: Vertical displacement (μm) during protrusion when active part is neglected (7) and when passive part is neglected (8).

4.3.3 The role of the active/passive part of the cell

Another hypothesis analyzed is whether the bacterium could be affecting only the active or passive part of the infected cells. To do this, case number 3 (infected cells and new cell-ECM adhesion) is used as a starting point and the stiffness of the passive or active part of the cell is made negligible, keeping the other part with the same value as the uninfected cells. To see the effect of eliminating the active part of the cell, the stiffness of the infected cell is left as the stiffness of the passive part, which for a uninfected cell is $500Pa$ (see Table 4.1). In the case in which the passive part of the cell is negligible, the total stiffness of the cell is the stiffness of the active part of a uninfected cell ($500Pa$). This causes the elastic modulus of the infected cells to be reduced from $1000Pa$ to $500Pa$. Removing the active part produces much more mound than removing the passive part (Figure 4.15).

The size of the mound is not comparable with the previous cases, since the stiffness of the infected cells remains as half of the stiffness of uninfected cells,

4. Collective cell response under infection conditions

while for the previous cases the stiffness drops to a quarter of the uninfected cells. However, these cases allow us to understand how each component of the cell contribute to the mound effect, with a clear difference and higher mound when the active part is removed.

4.3.4 Cell protrusion law

Within the mechanotransduction mechanism, the active response of the cell to sudden changes in tension within the cell is to generate a protrusion in the area where the tensions change and asymmetry occurs. In the way it has been developed, the protrusion in the model is implemented as all or nothing, i.e., if asymmetry exists the cell always protrudes the same, no matter how small or large the difference in stresses is. Nevertheless, here we hypothesize the cell protrudes proportionally to the stimulus it is sensing. When the asymmetry of the cell is higher, the protrusion response of the cell is also higher than when the level of asymmetry is lower. Therefore, a linear protrusion law is proposed as a function of the difference in stresses (equation 4.4). We assume the cell is polarized towards the infection, thus, the front part is the one close to infection and the rear one is the farthest from infection. Thus, the protrusion occurs in the front part of the cell resulting in a directional (from the center towards the exterior) change in volume of this part:

$$p = c \cdot (\sigma_{max}^{front} - \sigma_{max}^{rear}) \quad (4.4)$$

where p is the level of protrusion, c is a constant and σ_{max}^{front} and σ_{max}^{rear} are the maximum principal stress of the front and rear part, respectively.

For this, we look at the maximum principal stress in the adhesion zones and compare it with the same zone on the opposite side and extract the percentage of variation. Figure 4.16A shows the percentage of tension asymmetry in four of the cases studied in this section; there is infection but no new cell-ECM adhesions are produced (case 2), there is infection and new cell-ECM adhesions (case 3), there is infection and only uninfected cells close to the infection are able to produce cell-cell junctions (case 5) and there is infection and only uninfected

4.4. Discussion and Conclusions

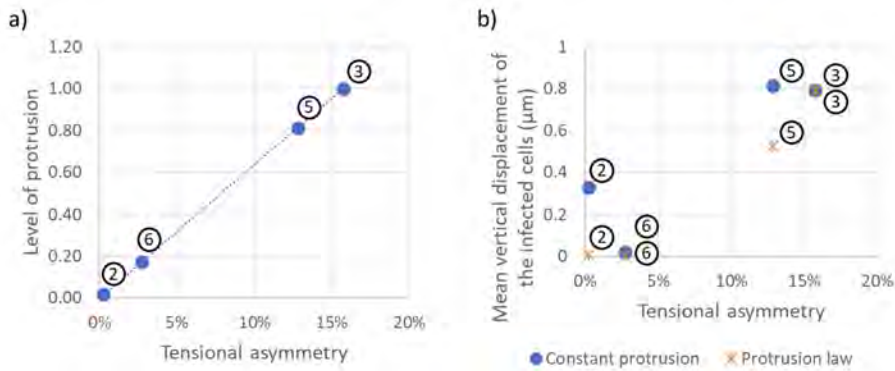


Figure 4.16: Protrusion law: (a) linear protrusion law proposed based on cases two, three, five and six; (b) height of the mound (μm) of the infected cells applying the protrusion law.

cells far from the infection are able to produce cell-cell junctions (case 6). A level of protrusion is applied to each case according to the percentage of asymmetry, with the case with the highest asymmetry having the highest protrusion. Thus, the mound result for case 3 will be the same with and without this law since it corresponds to the same protrusion level, while for the other three cases the result changes (Figure 4.16B). The protrusion levels decrease substantially when applying the protrusion law and the new displacement values are not proportional to the applied protrusion. These changes make more remarkable some of the results previously observed, such as, the importance of the new cell-ECM adhesion in the cells close to the infection (case 2 vs case 3), the lower ability of uninfected cells of protruding against uninfected cells (case 6) and the lower mound formation when only few uninfected cells are able to create cell-cell connections (case 5 vs case 3).

4.4 Discussion and Conclusions

In this chapter, a continuous model of a cell culture infected with listeria has been created. The aim of this chapter is to find a possible mechanotransduction mechanism that explains why LM-infected cells are ejected from the monolayer, creating mounds of extruded cells. In the model, the stress difference that occurs

4. Collective cell response under infection conditions

in uninfected cells close to the infection is proposed as the main trigger for a protrusion process, which eventually results in the mound of infected cells. This implies that the cells are constantly contracting, thus sensing their surroundings, and are thus able to detect the infection. However, this is not enough to create the mound and it is necessary that the cells also protrude, extruding the infected cells.

When the cells contract, it is observed in case two (where the only change with the uninfected cell culture is that the infected cells decrease their stiffness) that the cells adjacent to the infection have a displacement relative to the ECM. Therefore, and favoring protrusion, the new adhesions are added (case three). In protrusion, these adhesions are shown to be necessary to obtain both the mound and the displacements observed experimentally in the ECM. The cells rely on the ECM to protrude in order to push the infected cells. Thus, the ECM displaces outward, in the opposite direction to that in which the cell tries to advance. Therefore, cases one, two and three are the base cases with which the mechanotransduction mechanism is justified.

Another mechanism whose relevance has been shown to be crucial is cell-cell junctions. The work done by Bastounis et al. (2021) shows how cell-cell junctions play a fundamental role. Not only they are necessary for the mound to appear, but when cultures with cells capable of binding to each other and cells that are not capable are mixed, the cells that are able to form cell-cell adhesions tend to surround the infection and they generate the mound. In the case where none of the cells in the model is attached to any other cell (case four), it is observed that when the cell contracts it is not able to detect differences around it, so it does not protrude and no mound will appear. However, when simulating mixed cells, where cells able of generating junctions are placed surrounding the infection (as observed experimentally, case five) or surrounding the infection and some uninfected cells (case six), the cells able to generate junctions sense tension asymmetry and therefore protrude. Here a larger mound appears in case five than in case three, possibly because the adhesion with the ECM of the outer ring is very close to the infection and the cells are also using this as a foothold to exert force on the infection. Still, it should also be noted that the protrusion of the cells is being taken as constant. By introducing the linear protrusion law, case five considerably decreases the protrusion of the uninfected cells and the displacement of the mound. This phenomenological law has been

4.4. Discussion and Conclusions

proposed considering that the level of protrusion is proportional to the level of asymmetry in tensions between opposite parts of the cell, therefore the cell is able to sense differences of tension in its cytoskeleton and respond by generating a protrusion proportionally to it. However, it is difficult to know if the cell always protrudes in the same way, if it is a protrusion proportional to what it is sensing mechanically or if it is a more complex mechanism.

Finally, we study how the active or passive part of the cell affects the behavior of the monolayer, thus we simulate the cell without active or passive part, since the effect that the bacterium has on the cell is still unknown. This gives us a qualitative idea, since due to the way the model is created, it is not possible to lower the stiffness of the infected cell to the experimentally measured values (about $250Pa$) by lowering only the active or passive part. However, the results shown give us a clear idea that for mounding to occur, it is the active part that would have to be removed and not the passive part. This would imply that the infected cells also have much lower contractile capacity, generating greater tension asymmetry in the uninfected cells close to the infection.

Chapter 5

Discussion and conclusions

Contents

5.1	General conclusions	84
5.2	Future work	87
5.3	Contributions	88
5.3.1	Publications in peer-review journals	88
5.3.2	Congress and conference contributions	89

5.1 General conclusions

This chapter summarizes the main conclusions obtained during the development of this PhD Thesis and sets out the future lines that would continue the work carried out during the Thesis.

The main objective of this Thesis has been to study how cells are able to sense both passively and actively the mechanical environment. For this purpose, three models have been developed under different conditions and in all of them it has been shown that the mechanical environment in which cells are found is highly linked to their behavior and regulates the cellular response. In addition, we have used different constitutive material models to mimics cell behavior. Since depending on what we are analyzing the viscoelastic, hyperelastic or poroelastic components dominates cell behavior.

In our opinion, cell behavior is really complex, but depending on the exact problem that we are studying, mechanical behavior can be simplified being adequate for the case under study.

In addition to this main conclusion, additional interesting conclusions have been obtained, which are grouped in the same way as the PhD Thesis by chapters and can be summarized as follows:

- **Chapter 2.** Cell deformation due to accelerated fluid flow through a channel narrowing:
 1. The nucleus size plays a significant role in the overall deformation of the cell when nucleus size is large enough. Moreover, mechanical properties of the nucleus are lower relevant than nucleus size in total cell deformation.
 2. The mechanical properties of the cell obtained from the cytometers are valid for a qualitative comparison between cells, but not as quantitative data because they make an average estimation that does not take into account the variability of the different components of the cell.

3. Small changes in geometry or flow rate produce relevant changes in the stresses supported by the nucleus. A good estimation of this level of stresses can be important for setting optimal conditions in different biomedical applications, such as bioreactors.
4. The combination of real-time deformability cytometry with finite element fluid-structure interaction models can give us more information about the process than fluid or solid deformation separately.

• **Chapter 3.** Lobopodial migration on three-dimensional substrate:

1. Intracellular pressure at the front of the lobopodium is actively caused by the contraction of the cell itself. However, the mechanical properties of the extracellular matrix and the behavior of the extracellular matrix when deformed by the cell, influence the intracellular pressure passively. Somehow, this intracellular pressure is determined by the cell force contraction and the extracellular matrix deformation.
2. The pressure differences that occur inside the cell, as well as the difference in stresses in the solid part, could lead to a reorganization of the cytoskeleton or one of its parts and be a first trigger for the migration process that the cell uses.
3. Two possible mechanotransduction mechanisms have been detected that cells could be using to discern the mode of migration, or at least, when they do not use lobopodia. The first one of these is the change in pressure. When the cell contracts to migrate, there is a rise in pressure in the front part of the cell, but in cases where the matrix has nonlinear behavior (and experimentally no lobopodial migration appears) the pressure stops increasing, although the cell continues contracting. The second mechanism could be the change in direction of the fluid flow in the cytoplasm. During contraction, in addition to the rise in intracellular pressure, there is a fluid flow from the nucleus to the front part of the cell. However, again for nonlinear matrices, there comes a point at which the direction of this flow changes to go from the front toward the nucleus.
4. The elastic modulus and Poisson's ratio of the solid phase have a similar effect on the absolute value of pressure generated during cell

5.1. General conclusions

contraction, but the differences between linear and non-linear matrices change. Larger differences are generated with increasing elastic modulus and decreasing Poisson's ratio.

5. The fluid volume ratio in the cytoplasm has a smaller effect on the absolute value of intracellular pressure than the properties of the solid phase, but the differences between linear and non-linear matrices are larger when decreasing the fluid volume ratio.
6. Finally, the stresses in the nucleus are highly dependent on the stiffness of the extracellular matrix, although higher tensile stresses are also observed at the front of the nucleus for non-linear matrices.

- **Chapter 4.** Mound formation of listeria-infected cells in epithelial monolayer:

1. The difference in stresses during contraction in healthy cells close to the infection is the trigger for the protrusion mechanism that results in extrusion of infected cells.
2. Cellular contraction is required to sense the surrounding environment and thus detect infection.
3. Cell-cell junctions are crucial for the transmission of forces between cells as they contract and for the appearance of stress asymmetry, which probably is one of the mechanisms that cells use to detect the infection.
4. Cell-matrix adhesions are necessary for the appearance of infected cell mounds. As healthy cells protrude, they need to adhere to the matrix to have a foothold on which to exert force for extrusion of the infection. In addition, it has been shown experimentally that matrix displacements in areas close to the infection (protruding healthy cells) go in the opposite direction to that of protrusion. These displacements in the matrix are only achieved by cell-matrix adhesions.
5. The proposed phenomenological law of protrusion as a function of the level of stress asymmetry, results in a better correlation of the height of the mounds, but remains difficult to calibrate.
6. The qualitative study on whether the infection affects more to the active or to the passive part of the cell, results in higher strain asym-

metry in healthy cells and lower contraction of infected cells when the infection affects the active part.

5.2 Future work

In general, as future work, further research is needed on mechanosensor mechanisms and how they trigger different cellular processes (Ladoux and Mège (2017); Mofrad and Kamm (2009); Wang (2017)). It is also important to further study in the selection and adjustment of material models and especially in the effects when measuring properties because cells are a constantly changing living organism.

In particular, if we focus on each of the models proposed in this Thesis, it would be interesting to present the future lines of each chapter separately:

- **Chapter 2.** Cell deformation due to accelerated fluid flow through a channel narrowing:
 - Generate batches of simulations for different channel geometries, flow rates, cell geometries or mechanical properties of the cell components, with the objective of creating a digital twin capable of running in real time and combining it with experimental work to have more information on the cells being studied in the laboratory.

- **Chapter 3.** Lobopodial migration on three-dimensional substrate:
 - Consider cell-matrix adhesions, so that not all of the cell is totally attached to the matrix and can also generate new adhesions or detach existing ones by adding, for example, existing models of cohesive materials or clutch models from literature (Swaminathan and Waterman (2016)).
 - Include cytoskeleton remodeling as a function of stresses or other variable and couple contraction with remodeling, thus, generating inhomogeneous contractions throughout the cell.

5.3. Contributions

- **Chapter 4.** Mound formation of listeria-infected cells in epithelial monolayer:
 - Implement a fully dynamic model to generate random initial geometries (by means of Voronoi cells), automatic meshing, automatic generation of new adhesions and protrusions. Thus, a whole flow of contraction, mechanosensing decision-making, protrusion should be implemented for each cell individually. The mounds obtained repeating the loop could be comparable to the experimental ones.
 - Model the spread of the bacteria is not a big issue, but it is to incorporate the spread to the dynamic model, and to be able to simulate the time-dependent whole problem.

5.3 Contributions

As a result of the research work carried out in this Thesis, three journal publications are already published and one more is in preparation. This work have also resulted in five contributions in international congresses.

5.3.1 Publications in peer-review journals

Published work:

- **Serrano-Alcalde, F.**, Gómez-Benito, M.J. & García-Aznar, J.M. (2017). The role of nuclear mechanics in cell deformation under creeping flows. *Journal of Theoretical Biology*, 432, 25-32. DOI: 10.1016/j.jtbi.2017.07.028
- **Serrano-Alcalde, F.**, Gómez-Benito, M.J. & García-Aznar, J.M. (2020). Cell biophysical stimuli in lobopodium formation: a computer based approach. *Computer Methods in Biomechanics and Biomedical Engineering*, 1-10. DOI: 10.1080/10255842.2020.1836622
- Bastounis, E., **Serrano-Alcalde, F.**, Radhakrishnan, P., Engström, P., Gómez-Benito, M.J., Oswald, M., Yeh, Y.T., Smith, J.G., Welch, M.D.,

García-Aznar, J.M. & Theriot, J. (2021). Mechanical competition triggered by innate immune signaling drives the collective extrusion of bacterially infected epithelial cells. *Developmental Cell*, 56(4), 443-460. DOI: 10.1016/j.devcel.2021.01.012

In preparation:

- **Serrano-Alcalde, F.**, Bastounis, E., García-Aznar, J.M., Theriot, J. & Gómez-Benito, M.J. Collective sensing and extrusion of listeria-infected cells.

5.3.2 Congress and conference contributions

- **Serrano-Alcalde, F.**, García-Aznar, J.M. & Gómez-Benito, M.J. The role of matrix stiffness on 3D cell migration. *6th European Conference on Computational Mechanics (ECCM 6)*, Glasgow, June 2018
- **Serrano-Alcalde, F.**, Gómez-Benito, M.J. & García-Aznar, J.M. Influence of the mechanical properties of cell nucleus on overall deformation of the cell: a computational study. *Virtual Physiological Human conference (VPH)*, Zaragoza, September 2018.
- **Serrano-Alcalde, F.**, Gómez-Benito, M.J. & García-Aznar, J.M. Influence of the mechanical properties of cell nucleus in different 3D conditions. *Virtual Physiological Human conference (VPH)*, París, August 2020.
- **Serrano-Alcalde, F.**, Gómez-Benito, M.J., Radhakrishnan, P., Theriot, J.A., Bastounis, E.E. & García-Aznar, J.M. Collective mechanosensing in infected cell cultures. *26th Congress of the European Society of Biomechanics*, Milan, July 2021.

Chapter 6

Conclusiones y líneas futuras

Contents

6.1	Conclusiones generales	92
6.2	Trabajo futuro	95
6.3	Contribuciones	96
6.3.1	Publicaciones en revistas	96
6.3.2	Congress and conference contributions	97

6.1 Conclusiones generales

En este capítulo se resumen las principales conclusiones obtenidas durante el desarrollo de la Tesis y se plantean las líneas futuras que darían continuación a los trabajos realizados durante la Tesis.

El objetivo principal ha sido estudiar cómo afecta el ambiente mecánico en el que se encuentran las células y cómo estas son capaces de sentirlo de forma tanto pasiva, como activa. Para ello, se han desarrollado tres modelos bajo diferentes condiciones y en todos ellos se ha mostrado que el ambiente mecánico en el que las células se encuentren está altamente relacionado con su comportamiento y regula la respuesta celular. Además, se han usado diferentes modelos constitutivos de material para recrear el comportamiento celular, debido a que dependiendo de lo que estemos analizando los componentes viscoelásticos, hiperelásticos o poroelásticos dominan el comportamiento celular.

En nuestra opinión, el comportamiento celular es realmente complejo, pero dependiendo del problema concreto que estemos estudiando, se puede simplificar este comportamiento mecánico de modo que se adecúe al fenómeno estudiado.

Además de estas conclusiones principales, se han obtenido interesantes conclusiones adicionales que están agrupadas por capítulos y pueden resumirse como sigue:

- **Capítulo 2.** Deformación celular producida por la aceleración de un flujo fluido al atravesar un estrechamiento de canal:
 1. El tamaño del núcleo juega un papel importante en la deformación global de la célula cuando el núcleo es lo suficientemente grande. Además, las propiedades mecánicas del núcleo son menos relevantes que su tamaño.
 2. Las propiedades mecánicas de la célula que se obtienen de los citómetros son válidas para una comparación cualitativa entre células, pero no como dato cuantitativo debido a que hacen una estimación promedio en la que no se considera la variabilidad de las diferentes partes de la misma.

3. Pequeños cambios en la geometría o en el caudal producen cambios relevantes en las tensiones que soporta el núcleo. Conocer este nivel de tensiones puede ser importante para configurar las condiciones óptimas en diferentes aplicaciones biomédicas, como los biorreactores.
4. La combinación de citometría de deformación en tiempo real con modelos de simulación fluido-estructura de elementos finitos puede darnos una mayor información sobre el proceso que el análisis del fluido o sólido por separado.

• **Capítulo 3.** Migración lobopodial en matriz tridimensional:

1. La presión intracelular en la parte frontal del lobopodio está causada de forma activa por la contracción de la propia célula. Sin embargo, las propiedades mecánicas de la matriz extracelular y el comportamiento de ésta cuando es deformada por la célula, influyen en la presión intracelular de manera pasiva. De alguna manera, se produce una competición entre la célula y la matriz extracelular de la cual depende la presión que se genera.
2. Las diferencias de presión que se producen en el interior de la célula, así como la diferencia de tensiones en la parte sólida, podrían dar lugar a una reorganización del citoesqueleto o de alguna de sus partes y ser un primer desencadenante del proceso de migración que la célula use.
3. Además, se han detectado dos posibles mecanismos de mecanotransducción que las células podrían estar usando para discernir el modo de migración, o al menos, cuando no forman un lobopodio. El primero de ellos es el cambio en la presión. Cuando la célula contrae la parte frontal para migrar, se produce una subida de la presión en esa zona, pero en los casos en que la matriz tiene comportamiento no lineal (y experimentalmente no aparece migración lobopodial) la presión deja de aumentar, aunque la célula continúa contrayéndose. El segundo es cuando la dirección del flujo en el citoplasma cambia. En la contracción, además de subir la presión intracelular, se produce un flujo del fluido que va desde el núcleo hacia la parte delantera. Sin embargo, de nuevo para las matrices no lineales, llega un punto en

6.1. Conclusiones generales

el que la dirección de este flujo cambia para ir de la parte delantera hacia el núcleo.

4. El módulo elástico y coeficiente de Poisson de la fase sólida tienen similar efecto en el valor absoluto de presión que se genera durante la contracción, pero cambian las diferencias entre matriz lineal y no lineal. Se generan mayores diferencias al aumentar el módulo elástico y al disminuir el coeficiente de Poisson.
5. El ratio de volumen de fluido en el citoplasma tiene menor efecto en el valor absoluto de presión intracelular que las propiedades de la parte sólida, pero las diferencias entre la matriz lineal y no lineal son mayores al disminuir el volumen de fluido.
6. Por último, las tensiones en el núcleo dependen altamente de la rigidez de la matriz extracelular, aunque también se observan mayores tensiones de tracción en la parte frontal del núcleo para las matrices no lineales.

- **Capítulo 4.** Formación de montículos de células infectadas por listeria en un cultivo celular en monocapa:

1. La diferencia de tensiones durante la contracción en las células sanas próximas a la infección es el detonante del mecanismo de protrusión que produce la extrusión de las células infectadas.
2. Las células necesitan estar constantemente contrayéndose para de esta manera sentir el ambiente que las rodea y así detectar la infección.
3. Las uniones célula-célula son cruciales para la transmisión de fuerzas entre células mientras se contraen y de esta forma aparece la asimetría de tensiones que probablemente es uno de los mecanismos usados por las células para detectar a las células infectadas adyacentes.
4. Las adhesiones célula-matriz son necesarias para que aparezcan los montículos de células infectadas. Al protrusionar las células sanas, necesitan adherirse a la matriz para tener un punto de apoyo sobre el que hacer fuerza para la extrusión de la infección. Además, experimentalmente, se ha visto que los desplazamientos de la matriz en las zonas cercanas a la infección (células sanas que protrusionan)

van en dirección opuesta a la de protrusión. Sólo con las adhesiones célula-matriz se consiguen estos desplazamientos en la matriz.

5. La ley fenomenológica de protrusión propuesta en función del nivel de asimetría resulta en una mejor correlación de la altura de los montículos, pero sigue siendo difícil ajustarla.
6. El estudio cualitativo sobre si la infección afecta más a la parte activa o pasiva de la célula da como resultado una mayor asimetría de tensiones en las células sanas y menor contracción de las infectadas cuando la infección afecta a la parte activa.

6.2 Trabajo futuro

En general, como trabajo futuro, es necesario seguir investigando en los mecanismos mecanosensores y cómo estos desencadenan diferentes procesos celulares (Ladoux and Mège (2017); Mofrad and Kamm (2009); Wang (2017)). También es importante estudiar más a fondo la selección y ajuste de los modelos de material y especialmente de la medición de las propiedades, ya que las células son organismos vivos en constante cambio.

En particular, si nos centramos en cada uno de los modelos propuestos en esta Tesis, se abren distintas líneas futuras de cada capítulo por separado que se describen a continuación:

- **Capítulo 2.** Deformación celular producida por la aceleración de un flujo fluido al atravesar un estrechamiento de canal:
 - Generar baterías de simulaciones para diferentes geometrías de canal, caudal, geometrías de célula o propiedades mecánicas de los componentes de la célula, con el objetivo de crear un gemelo digital que sea capaz de correr en tiempo real y combinarlo con trabajos experimentales para tener mayor información de las células que se están estudiando en laboratorio.
- **Capítulo 3.** Migración lobopodial en matriz tridimensional:

6.3. Contribuciones

- Considerar las adhesiones célula-matriz, de manera que no toda la célula esté totalmente unida a la matriz y además pueda generar nuevas adhesiones o soltar las que ya tiene añadiendo modelos existentes en bibliografía de material cohesivo o de tipo clutch (Swaminathan and Waterman (2016)).
 - Incluir la remodelación del citoesqueleto en función de las tensiones u otra variable y acoplar la contracción con la remodelación, generando así contracciones no homogéneas en toda la célula.
- **Capítulo 4.** Formación de montículos de células infectadas por listeria en un cultivo celular en dos dimensiones:
 - Implementar un modelo completamente dinámico para generar una geometría inicial aleatoria (mediante celdas de Voronoi), crear un mallado automático y generación automática de nuevas adhesiones y protrusiones. De esta forma, cada célula tendría un flujo completo de contracción, decisión según el mecanismo mecanosensor y protrusión. El montículo generado de esta forma podría ser comparable al obtenido experimentalmente.
 - Modelar la propagación de la bacteria no supone un gran problema, sin embargo, incorporarlo al modelo dinámico y ser capaces de simular el problema teniendo en cuenta la variable tiempo, aumenta considerablemente la complejidad del modelo y su implementación.

6.3 Contribuciones

Como resultado del trabajo en investigación llevado a cabo en esta Tesis, tres artículos se encuentran actualmente publicados y uno más se encuentra en preparación. Este trabajo también ha resultado en cinco contribuciones a congresos internacionales.

6.3.1 Publicaciones en revistas

Trabajos publicados:

- **Serrano-Alcalde, F.**, Gómez-Benito, M.J. & García-Aznar, J.M. (2017). The role of nuclear mechanics in cell deformation under creeping flows. *Journal of Theoretical Biology*, 432, 25-32. DOI: 10.1016/j.jtbi.2017.07.028
- **Serrano-Alcalde, F.**, Gómez-Benito, M.J. & García-Aznar, J.M. (2020). Cell biophysical stimuli in lobodopodium formation: a computer based approach. *Computer Methods in Biomechanics and Biomedical Engineering*, 1-10. DOI: 10.1080/10255842.2020.1836622
- Bastounis, E., **Serrano-Alcalde, F.**, Radhakrishnan, P., Engström, P., Gómez-Benito, M.J., Oswald, M., Yeh, Y.T., Smith, J.G., Welch, M.D., García-Aznar, J.M. & Theriot, J. (2021). Mechanical competition triggered by innate immune signaling drives the collective extrusion of bacterially infected epithelial cells. *Developmental Cell*, 56(4), 443-460. DOI: 10.1016/j.devcel.2021.01.012

En preparación:

- **Serrano-Alcalde, F.**, Bastounis, E., García-Aznar, J.M., Theriot, J. & Gómez-Benito, M.J. Collective sensing and extrusion of listeria-infected cells.

6.3.2 Congress and conference contributions

- **Serrano-Alcalde, F.**, García-Aznar, J.M. & Gómez-Benito, M.J. The role of matrix stiffness on 3D cell migration. 6th European Conference on Computational Mechanics (ECCM 6), Glasgow, June 2018
- **Serrano-Alcalde, F.**, Gómez-Benito, M.J. & García-Aznar, J.M. Influence of the mechanical properties of cell nucleus on overall deformation of the cell: a computational study. Virtual Physiological Human conference (VPH), Zaragoza, September 2018.
- **Serrano-Alcalde, F.**, Gómez-Benito, M.J. & García-Aznar, J.M. Influence of the mechanical properties of cell nucleus in different 3D conditions. Virtual Physiological Human conference (VPH), París, August 2020.

6.3. Contribuciones

- **Serrano-Alcalde, F.**, Gómez-Benito, M.J., Theriot, J.A., Bastounis, E.E. & García-Aznar, J.M. Collective mechanosensing in infected cell cultures. 26th Congress of the European Society of Biomechanics, Milan, July 2021.

Bibliography

- Allena, R., Thiam, H., Piel, M., and Aubry, D. (2015). A mechanical model to investigate the role of the nucleus during confined cell migration. *Computer methods in biomechanics and biomedical engineering*, 18(sup1):1868–1869.
- Avesani, D., Dumbser, M., Chiogna, G., and Bellin, A. (2016). An alternative smooth particle hydrodynamics formulation to simulate chemotaxis in porous media. *Journal of Mathematical Biology*, pages 1–22.
- Aznar, J. M. G., Valero, C., Borau, C., and Garijo, N. (2016). Computational mechano-chemo-biology: a tool for the design of tissue scaffolds. *Biomanufacturing Reviews*, 1(1):2.
- Bastounis, E. E., Serrano-Alcalde, F., Radhakrishnan, P., Engström, P., Gómez-Benito, M. J., Oswald, M. S., Yeh, Y.-T., Smith, J. G., Welch, M. D., García-Aznar, J. M., and Theriot, J. A. (2021). Mechanical competition triggered by innate immune signaling drives the collective extrusion of bacterially infected epithelial cells. *Developmental Cell*, 56(4):443–460.e11.
- Berthier, J. and Silberzan, P. (2010). *Microfluidics for Biotechnology*. Artech House.
- Biot, M. A. (1941). General theory of three-dimensional consolidation. *Journal of Applied Physics*, 12(2):155–164.
- Bissell, M. J., Weaver, V. M., Lelièvre, S. A., Wang, F., Petersen, O. W., and Schmeichel, K. L. (1999). Tissue structure, nuclear organization, and gene expression in normal and malignant breast. *Cancer research*, 59(7 Supplement):1757s–1764s.
- Borau, C., Kamm, R., and García-Aznar, J. (2011). Mechano-sensing and cell migration: a 3d model approach. *Physical biology*, 8(6):066008.

- Brodland, G. W., Daniel, I., Chen, L., and Veldhuis, J. H. (2006). A cell-based constitutive model for embryonic epithelia and other planar aggregates of biological cells. *International journal of plasticity*, 22(6):965–995.
- Casquero, H., Bona-Casas, C., and Gomez, H. (2017). Nurbs-based numerical proxies for red blood cells and circulating tumor cells in microscale blood flow. *Computer Methods in Applied Mechanics and Engineering*, 316:646–667.
- Cho, S., Irianto, J., and Discher, D. E. (2017). Mechanosensing by the nucleus: From pathways to scaling relationships. *Journal of Cell Biology*, 216(2):305–315.
- Co, J. Y., Margalef-Catala, M., Li, X., Mah, A. T., Kuo, C. J., Monack, D. M., and Amieva, M. R. (2019). Controlling epithelial polarity: a human enteroid model for host-pathogen interactions. *Cell reports*, 26(9):2509–2520.
- Dahl, K. N., Ribeiro, A. J., and Lammerding, J. (2008). Nuclear shape, mechanics, and mechanotransduction. *Circulation Research*, 102(11):1307–1318.
- De Santis, G., Lennon, A. B., Boschetti, F., Verheghe, B., Verdonck, P., and Prendergast, P. J. (2011). How can cells sense the elasticity of a substrate?: an analysis using a cell tensegrity model. *European cells & materials*, 22:202–213.
- DeSimone, D. W. and Horwitz, A. R. (2014). Many modes of motility. *science*, 345(6200):1002–1003.
- Discher, D. E., Janmey, P., and Wang, Y.-l. (2005). Tissue cells feel and respond to the stiffness of their substrate. *Science*, 310(5751):1139–1143.
- Doyle, A. D., Petrie, R. J., Kutys, M. L., and Yamada, K. M. (2013). Dimensions in cell migration. *Current opinion in cell biology*, 25(5):642–649.
- Dupont, S., Morsut, L., Aragona, M., Enzo, E., Giulitti, S., Cordenonsi, M., Zanconato, F., Le Digabel, J., Forcato, M., Bicciato, S., et al. (2011). Role of yap/taz in mechanotransduction. *Nature*, 474(7350):179–183.
- Eisenstecken, T., Hu, J., and Winkler, R. G. (2016). Bacterial swarmer cells in confinement: a mesoscale hydrodynamic simulation study. *Soft Matter*, 12:8316–8326.

Bibliography

- Elosegui-Artola, A., Andreu, I., Beedle, A. E., Lezamiz, A., Uroz, M., Kosmalska, A. J., Oria, R., Kechagia, J. Z., Rico-Lastres, P., Le Roux, A.-L., et al. (2017). Force triggers yap nuclear entry by regulating transport across nuclear pores. *Cell*, 171(6):1397–1410.
- Elsdale, T. and Bard, J. (1972). Collagen substrata for studies on cell behavior. *The Journal of cell biology*, 54(3):626–637.
- Escribano, J., Chen, M. B., Moeendarbary, E., Cao, X., Shenoy, V., Garcia-Aznar, J. M., Kamm, R. D., and Spill, F. (2019). Balance of mechanical forces drives endothelial gap formation and may facilitate cancer and immune-cell extravasation. *PLoS computational biology*, 15(5).
- Escribano, J., Sánchez, M., and García-Aznar, J. (2014). A discrete approach for modeling cell–matrix adhesions. *Computational particle mechanics*, 1(2):117–130.
- Escribano, J., Sánchez, M., and García-Aznar, J. (2015). Modeling the formation of cell-matrix adhesions on a single 3d matrix fiber. *Journal of theoretical biology*, 384:84–94.
- Escribano, J., Sunyer, R., Sánchez, M. T., Trepát, X., Roca-Cusachs, P., and García-Aznar, J. M. (2018). A hybrid computational model for collective cell durotaxis. *Biomechanics and modeling in mechanobiology*, 17(4):1037–1052.
- Faralla, C., Bastounis, E. E., Ortega, F. E., Light, S. H., Rizzuto, G., Nocadello, S., Anderson, W. F., Robbins, J. R., Theriot, J. A., and Bakardjiev, A. I. (2018). *Listeria monocytogenes* inlp interacts with afadin and facilitates basement membrane crossing. *PLoS pathogens*, 14(5):e1007094.
- Farhadifar, R., Röper, J.-C., Aigouy, B., Eaton, S., and Jülicher, F. (2007). The influence of cell mechanics, cell-cell interactions, and proliferation on epithelial packing. *Current Biology*, 17(24):2095–2104.
- Fedosov, D. A., Peltomaki, M., and Gompper, G. (2014). Deformation and dynamics of red blood cells in flow through cylindrical microchannels. *Soft Matter*, 10:4258–4267.
- Fischer, M., Rikeit, P., Knaus, P., and Coirault, C. (2016). Yap-mediated mechanotransduction in skeletal muscle. *Frontiers in physiology*, 7:41.

- Fraley, S. I., Wu, P.-h., He, L., Feng, Y., Krisnamurthy, R., Longmore, G. D., and Wirtz, D. (2015). Three-dimensional matrix fiber alignment modulates cell migration and mt1-mmp utility by spatially and temporally directing protrusions. *Scientific reports*, 5:14580.
- Friedl, P. and Wolf, K. (2010). Plasticity of cell migration: a multiscale tuning model. *The Journal of Cell Biology*, 188(1):11–19.
- Friedl, P., Wolf, K., and Lammerding, J. (2011). Nuclear mechanics during cell migration. *Current Opinion in Cell Biology*, 23(1):55 – 64. Cell structure and dynamics.
- Gasser, T. C., Ogden, R. W., and Holzapfel, G. A. (2006). Hyperelastic modelling of arterial layers with distributed collagen fibre orientations. *Journal of the royal society interface*, 3(6):15–35.
- Gelman, R., Williams, B. R., and Piez, K. (1979). Collagen fibril formation. evidence for a multistep process. *Journal of Biological Chemistry*, 254(1):180–186.
- Giorgi, M., Verbruggen, S. W., and Lacroix, D. (2016). In silico bone mechanobiology: modeling a multifaceted biological system. *Wiley Interdisciplinary Reviews: Systems Biology and Medicine*, 8(6):485–505.
- Giverso, C., Arduino, A., and Preziosi, L. (2017). How nucleus mechanics and ecm microstructure influence the invasion of single cells and multicellular aggregates. *Bulletin of Mathematical Biology*, pages 1–29.
- Giverso, C., Grillo, A., and Preziosi, L. (2014). Influence of nucleus deformability on cell entry into cylindrical structures. *Biomechanics and modeling in mechanobiology*, 13(3):481–502.
- González-Valverde, I. and García-Aznar, J. M. (2018). Mechanical modeling of collective cell migration: An agent-based and continuum material approach. *Computer Methods in Applied Mechanics and Engineering*, 337:246–262.
- Gudipaty, S. A. and Rosenblatt, J. (2017). Epithelial cell extrusion: pathways and pathologies. In *Seminars in cell & developmental biology*, volume 67, pages 132–140. Elsevier.

Bibliography

- Guilak, F. (1995). Compression-induced changes in the shape and volume of the chondrocyte nucleus. *Journal of biomechanics*, 28(12):1529–1541.
- Guillou, L., Dahl, J. B., Lin, J.-M. G., Barakat, A. I., Husson, J., Muller, S. J., and Kumar, S. (2016). Measuring cell viscoelastic properties using a microfluidic extensional flow device. *Biophysical journal*, 111(9):2039–2050.
- Guz, N., Dokukin, M., Kalaparthy, V., and Sokolov, I. (2014). If cell mechanics can be described by elastic modulus: Study of different models and probes used in indentation experiments. *Biophysical Journal*, 107(3):564–575.
- Hervas-Raluy, S., Garcia-Aznar, J., and Gomez-Benito, M. (2019). Modelling actin polymerization: the effect on confined cell migration. *Biomechanics and modeling in mechanobiology*, pages 1–11.
- Hibbit, Karlsson and Sorensen, Inc. (2006). *Theory Manual, v. 6.6*. HKS inc. Pawtucket, RI, USA.
- Hochmuth, R. M., Mohandas, N., and Blackshear, P. L. (1973). Measurement of the elastic modulus for red cell membrane using a fluid mechanical technique. *Biophysical Journal*, 13(8):747–762.
- Hoffman, B. D., Grashoff, C., and Schwartz, M. A. (2011). Dynamic molecular processes mediate cellular mechanotransduction. *Nature*, 475(7356):316–323.
- Holzappel, G. A., Gasser, T. C., and Ogden, R. W. (2000). A new constitutive framework for arterial wall mechanics and a comparative study of material models. *Journal of elasticity and the physical science of solids*, 61(1-3):1–48.
- Hsu, S., Thakar, R., Liepmann, D., and Li, S. (2005). Effects of shear stress on endothelial cell haptotaxis on micropatterned surfaces. *Biochemical and biophysical research communications*, 337(1):401–409.
- Hu, J., Yang, M., Gompper, G., and Winkler, R. G. (2015). Modelling the mechanics and hydrodynamics of swimming e. coli. *Soft matter*, 11(40):7867–7876.
- Hur, S. C., Henderson-MacLennan, N. K., McCabe, E. R. B., and Di Carlo, D. (2011). Deformability-based cell classification and enrichment using inertial microfluidics. *Lab Chip*, 11:912–920.

- Imai, Y., Omori, T., Shimogonya, Y., Yamaguchi, T., and Ishikawa, T. (2016). Numerical methods for simulating blood flow at macro, micro, and multi scales. *Journal of Biomechanics*, 49(11):2221 – 2228. Selected Articles from the International Conference on {CFD} in Medicine and Biology (Albufeira, Portugal – August 30th - September 4th, 2015).
- Inoue, Y., Deji, T., Shimada, Y., Hojo, M., and Adachi, T. (2010). Simulations of dynamics of actin filaments by remodeling them in shearflows. *Computers in Biology and Medicine*, 40(11):876–882.
- Jaalouk, D. E. and Lammerding, J. (2009). Mechanotransduction gone awry. *Nature reviews Molecular cell biology*, 10(1):63–73.
- Jacobs, C. R., Huang, H., and Kwon, R. Y. (2012). *Introduction to cell mechanics and mechanobiology*. Garland Science.
- Janota, C. S., Calero-Cuenca, F. J., and Gomes, E. R. (2020). The role of the cell nucleus in mechanotransduction. *Current opinion in cell biology*, 63:204–211.
- Jiang, H. and Sun, S. X. (2013). Cellular pressure and volume regulation and implications for cell mechanics. *Biophysical journal*, 105(3):609–619.
- Kaunas, R. and Hsu, H.-J. (2009). A kinematic model of stretch-induced stress fiber turnover and reorientation. *Journal of theoretical biology*, 257(2):320–330.
- Knodler, L. A., Vallance, B. A., Celli, J., Winfree, S., Hansen, B., Montero, M., and Steele-Mortimer, O. (2010). Dissemination of invasive salmonella via bacterial-induced extrusion of mucosal epithelia. *Proceedings of the national academy of sciences*, 107(41):17733–17738.
- Kocgozlu, L., Saw, T. B., Le, A. P., Yow, I., Shagirov, M., Wong, E., Mège, R.-M., Lim, C. T., Toyama, Y., and Ladoux, B. (2016). Epithelial cell packing induces distinct modes of cell extrusions. *Current Biology*, 26(21):2942–2950.
- Kubow, K. E., Conrad, S. K., and Horwitz, A. R. (2013). Matrix microarchitecture and myosin {II} determine adhesion in 3d matrices. *Current Biology*, 23(17):1607 – 1619.
- Kuipers, D., Mehonic, A., Kajita, M., Peter, L., Fujita, Y., Duke, T., Charras, G., and Gale, J. E. (2014). Epithelial repair is a two-stage process driven

Bibliography

- first by dying cells and then by their neighbours. *Journal of cell science*, 127(6):1229–1241.
- Ladoux, B. and Mège, R.-M. (2017). Mechanobiology of collective cell behaviours. *Nature reviews Molecular cell biology*, 18(12):743–757.
- Lamason, R. L., Bastounis, E., Kafai, N. M., Serrano, R., Theriot, J. A., Welch, M. D., et al. (2016). Rickettsia sca4 reduces vinculin-mediated intercellular tension to promote spread. *Cell*, 167(3):670–683.
- Lauffenburger, D. A. and Horwitz, A. F. (1996). Cell migration: a physically integrated molecular process. *Cell*, 84(3):359–369.
- Li, Y. and Sun, S. X. (2018). Transition from actin-driven to water-driven cell migration depends on external hydraulic resistance. *Biophysical Journal*, 114(12):2965–2973.
- Lim, C., Zhou, E., and Quek, S. (2006). Mechanical models for living cells—a review. *Journal of biomechanics*, 39(2):195–216.
- Lin, S.-L., Yang, J.-C., Ho, K.-N., Wang, C.-H., Yeh, C.-W., and Huang, H.-M. (2009). Effects of compressive residual stress on the morphologic changes of fibroblasts. *Medical & biological engineering & computing*, 47(12):1273–1279.
- Liu, Y., Shaw, S. K., Ma, S., Yang, L., Luscinskas, F. W., and Parkos, C. A. (2004). Regulation of leukocyte transmigration: cell surface interactions and signaling events. *The Journal of Immunology*, 172(1):7–13.
- Lo, C.-M., Wang, H.-B., Dembo, M., and Wang, Y.-l. (2000). Cell movement is guided by the rigidity of the substrate. *Biophysical journal*, 79(1):144–152.
- Luque, T., Melo, E., Garreta, E., Cortiella, J., Nichols, J., Farré, R., and Navajas, D. (2013). Local micromechanical properties of decellularized lung scaffolds measured with atomic force microscopy. *Acta Biomaterialia*, 9(6):6852–6859.
- Lv, H., Li, L., Sun, M., Zhang, Y., Chen, L., Rong, Y., and Li, Y. (2015). Mechanism of regulation of stem cell differentiation by matrix stiffness. *Stem cell research & therapy*, 6(1):1–11.

- Mach, A. J. and Di Carlo, D. (2010). Continuous scalable blood filtration device using inertial microfluidics. *Biotechnology and Bioengineering*, 107(2):302–311.
- Mahaffy, R., Park, S., Gerde, E., Käs, J., and Shih, C. (2004). Quantitative analysis of the viscoelastic properties of thin regions of fibroblasts using atomic force microscopy. *Biophysical Journal*, 86(3):1777 – 1793.
- Malandrino, A. and Moeendarbary, E. (2019). Poroelasticity of living tissues. In Narayan, R., editor, *Encyclopedia of Biomedical Engineering*, pages 238 – 245. Elsevier, Oxford.
- Maloney, J. M. and Van Vliet, K. J. (2014). Chemoenvironmental modulators of fluidity in the suspended biological cell. *Soft Matter*, 10(40):8031–8042.
- Martins, R. P., Finan, J. D., Guilak, F., and Lee, D. A. (2012). Mechanical regulation of nuclear structure and function. *Annual review of biomedical engineering*, 14:431–455.
- Massai, D., Isu, G., Madeddu, D., Cerino, G., Falco, A., Frati, C., Gallo, D., Deriu, M. A., Labate, G. F. D., Quaini, F., et al. (2016). A versatile bioreactor for dynamic suspension cell culture. application to the culture of cancer cell spheroids. *PloS one*, 11(5):e0154610.
- Mietke, A., Otto, O., Girardo, S., Rosendahl, P., Taubenberger, A., Golfier, S., Ulbricht, E., Aland, S., Guck, J., and Fischer-Friedrich, E. (2015). Extracting cell stiffness from real-time deformability cytometry: Theory and experiment. *Biophysical Journal*, 109(10):2023–2036.
- Mijailovich, S. M., Kojic, M., Zivkovic, M., Fabry, B., and Fredberg, J. J. (2002). A finite element model of cell deformation during magnetic bead twisting. *Journal of Applied Physiology*, 93(4):1429–1436.
- Moeendarbary, E., Valon, L., Fritzsche, M., Harris, A. R., Moulding, D. A., Thrasher, A. J., Stride, E., Mahadevan, L., and Charras, G. T. (2013). The cytoplasm of living cells behaves as a poroelastic material. *Nature materials*, 12(3):253–261.
- Mofrad, M. R. and Kamm, R. D. (2009). *Cellular Mechanotransduction: Diverse Perspectives from Molecules to Tissues*. Cambridge University Press.

Bibliography

- Moreno-Arotzena, O., Borau, C., Movilla, N., Vicente-Manzanares, M., and García-Aznar, J. M. (2015). Fibroblast migration in 3d is controlled by haptotaxis in a non-muscle myosin ii-dependent manner. *Annals of Biomedical Engineering*, 43(12):3025–3039.
- Moreo, P., García-Aznar, J. M., and Doblaré, M. (2008). Modeling mechanosensing and its effect on the migration and proliferation of adherent cells. *Acta Biomaterialia*, 4(3):613–621.
- Müller, S. J., Weigl, F., Bezold, C., Bächer, C., Albrecht, K., and Gekle, S. (2021). A hyperelastic model for simulating cells in flow. *Biomechanics and modeling in mechanobiology*, 20(2):509–520.
- Nelson, D. L., Cox, M. M., and Lehninger, A. L. (2008). *Lehninger principles of biochemistry*. New York : W. H. Freeman and Company, cop. 2008.
- O’Dea, R. D. and King, J. R. (2012). Continuum limits of pattern formation in hexagonal-cell monolayers. *Journal of mathematical biology*, 64(3):579–610.
- Oria, R., Wiegand, T., Escribano, J., Elosegui-Artola, A., Uriarte, J. J., Moreno-Pulido, C., Platzman, I., Delcanale, P., Albertazzi, L., Navajas, D., et al. (2017). Force loading explains spatial sensing of ligands by cells. *Nature*, 552(7684):219.
- Ortega, F. E., Koslover, E. F., and Theriot, J. A. (2019). *Listeria monocytogenes* cell-to-cell spread in epithelia is heterogeneous and dominated by rare pioneer bacteria. *Elife*, 8:e40032.
- Otto, O., Rosendahl, P., Mietke, A., Golfier, S., Herold, C., Klaue, D., Girardo, S., Pagliara, S., Ekpenyong, A., Jacobi, A., et al. (2015). Real-time deformability cytometry: on-the-fly cell mechanical phenotyping. *Nature methods*, 12(3):199–202.
- Pagliara, S., Franze, K., McClain, C. R., Wylde, G. W., Fisher, C. L., Franklin, R. J. M., Kabla, A. J., Keyser, U. F., and Chalut, K. J. (2014). Auxetic nuclei in embryonic stem cells exiting pluripotency. *Nature Materials*, 13(6):638–644.
- Paszek, M. J., Zahir, N., Johnson, K. R., Lakins, J. N., Rozenberg, G. I., Gefen, A., Reinhart-King, C. A., Margulies, S. S., Dembo, M., Boettiger, D., et al. (2005). Tensional homeostasis and the malignant phenotype. *Cancer cell*, 8(3):241–254.

- Pathak, A. and Kumar, S. (2012). Independent regulation of tumor cell migration by matrix stiffness and confinement. *Proceedings of the National Academy of Sciences*, 109(26):10334–10339.
- Peng, Z., Chen, Y.-L., Lu, H., Pan, Z., and Chang, H.-C. (2015). Mesoscale simulations of two model systems in biophysics: from red blood cells to DNAs. *Computational Particle Mechanics*, 2:339–357.
- Peskin, C. S., Odell, G. M., and Oster, G. F. (1993). Cellular motions and thermal fluctuations: the brownian ratchet. *Biophysical journal*, 65(1):316–324.
- Petrie, R. J., Gavara, N., Chadwick, R. S., and Yamada, K. M. (2012). Nonpolarized signaling reveals two distinct modes of 3d cell migration. *The Journal of Cell Biology*, 197(3):439–455.
- Petrie, R. J. and Koo, H. (2014). Direct measurement of intracellular pressure. *Current protocols in cell biology*, 63(1):12–9.
- Petrie, R. J., Koo, H., and Yamada, K. M. (2014). Generation of compartmentalized pressure by a nuclear piston governs cell motility in a 3d matrix. *Science*, 345(6200):1062–1065.
- Petrie, R. J. and Yamada, K. M. (2016). Multiple mechanisms of 3d migration: the origins of plasticity. *Current Opinion in Cell Biology*, 42:7 – 12. Cell dynamics.
- Rajabian, T., Gavicherla, B., Heisig, M., Müller-Altrock, S., Goebel, W., Gray-Owen, S. D., and Ireton, K. (2009). The bacterial virulence factor *inlC* perturbs apical cell junctions and promotes cell-to-cell spread of listeria. *Nature cell biology*, 11(10):1212–1218.
- Ridley, A. J., Schwartz, M. A., Burridge, K., Firtel, R. A., Ginsberg, M. H., Borisy, G., Parsons, J. T., and Horwitz, A. R. (2003). Cell migration: integrating signals from front to back. *Science*, 302(5651):1704–1709.
- Rodriguez, M. L., McGarry, P. J., and Sniadecki, N. J. (2013). Review on cell mechanics: experimental and modeling approaches. *Applied Mechanics Reviews*, 65(6).

Bibliography

- Ronan, W., Deshpande, V. S., McMeeking, R. M., and McGarry, J. P. (2012). Numerical investigation of the active role of the actin cytoskeleton in the compression resistance of cells. *Journal of the Mechanical Behavior of Biomedical Materials*, 14:143–157.
- Rosenblatt, J., Raff, M. C., and Cramer, L. P. (2001). An epithelial cell destined for apoptosis signals its neighbors to extrude it by an actin-and myosin-dependent mechanism. *Current biology*, 11(23):1847–1857.
- Rüberg, T. and Aznar, J. M. G. (2016). Numerical simulation of solid deformation driven by creeping flow using an immersed finite element method. *Advanced Modeling and Simulation in Engineering Sciences*, 3(1):9.
- Safran, S. and De, R. (2009). Nonlinear dynamics of cell orientation. *Physical Review E*, 80(6):060901.
- Schmedt, T., Chen, Y., Nguyen, T. T., Li, S., Bonanno, J. A., and Jurkunas, U. V. (2012). Telomerase immortalization of human corneal endothelial cells yields functional hexagonal monolayers. *PLoS One*, 7(12).
- Schmidt, S. and Friedl, P. (2010). Interstitial cell migration: integrin-dependent and alternative adhesion mechanisms. *Cell and tissue research*, 339(1):83.
- Scianna, M. and Preziosi, L. (2013). Modeling the influence of nucleus elasticity on cell invasion in fiber networks and microchannels. *Journal of Theoretical Biology*, 317:394–406.
- Scianna, M., Preziosi, L., and Wolf, K. (2013). A cellular potts model simulating cell migration on and in matrix environments. *Mathematical Biosciences and Engineering*, 10(1):235–261.
- Serrano-Alcalde, F., García-Aznar, J. M., and Gómez-Benito, M. J. (2017). The role of nuclear mechanics in cell deformation under creeping flows. *Journal of theoretical biology*, 432:25–32.
- Sevink, A., Schmid, F., Kawakatsu, T., and Milano, G. (2017). Combining cell-based hydrodynamics with hybrid particle-field simulations: Efficient and realistic simulation of structuring dynamics. *Soft Matter*.
- Solon, J., Levental, I., Sengupta, K., Georges, P. C., and Janmey, P. A. (2007). Fibroblast adaptation and stiffness matching to soft elastic substrates. *Biophysical Journal*, 93(12):4453 – 4461.

- Sturm, R. (2011). A computer model for the simulation of fiber–cell interaction in the alveolar region of the respiratory tract. *Computers in Biology and Medicine*, 41(7):565–573.
- Sunyer, R., Conte, V., Escribano, J., Elosegui-Artola, A., Labernadie, A., Valon, L., Navajas, D., García-Aznar, J. M., Muñoz, J. J., Roca-Cusachs, P., et al. (2016). Collective cell durotaxis emerges from long-range intercellular force transmission. *Science*, 353(6304):1157–1161.
- Swaminathan, V. and Waterman, C. M. (2016). The molecular clutch model for mechanotransduction evolves. *Nature cell biology*, 18(5):459–461.
- Taber, L., Shi, Y., Yang, L., and Bayly, P. (2011). A poroelastic model for cell crawling including mechanical coupling between cytoskeletal contraction and actin polymerization. *Journal of mechanics of materials and structures*, 6(1):569–589.
- Tamada, M., Perez, T. D., Nelson, W. J., and Sheetz, M. P. (2007). Two distinct modes of myosin assembly and dynamics during epithelial wound closure. *The Journal of cell biology*, 176(1):27–33.
- Tamada, M., Sheetz, M. P., and Sawada, Y. (2004). Activation of a signaling cascade by cytoskeleton stretch. *Developmental cell*, 7(5):709–718.
- Te Boekhorst, V., Preziosi, L., and Friedl, P. (2016). Plasticity of cell migration in vivo and in silico. *Annual review of cell and developmental biology*, 32:491–526.
- Trepat, X., Lenormand, G., and Fredberg, J. J. (2008). Universality in cell mechanics. *Soft Matter*, 4(9):1750–1759.
- Ungai-Salánki, R., Peter, B., Gerecsei, T., Orgovan, N., Horvath, R., and Szabó, B. (2019). A practical review on the measurement tools for cellular adhesion force. *Advances in Colloid and Interface Science*, 269:309–333.
- Van Liedekerke, P., Palm, M., Jagiella, N., and Drasdo, D. (2015). Simulating tissue mechanics with agent-based models: concepts, perspectives and some novel results. *Computational particle mechanics*, 2(4):401–444.
- Vaughan, T., Mullen, C., Verbruggen, S., and McNamara, L. (2015). Bone cell mechanosensation of fluid flow stimulation: a fluid-structure interaction

Bibliography

- model characterising the role integrin attachments and primary cilia. *Biomech Model Mechanobiol*, 14:703–718.
- Vaziri, A., Lee, H., and Mofrad, M. K. (2006). Deformation of the cell nucleus under indentation: mechanics and mechanisms. *Journal of materials research*, 21(08):2126–2135.
- Verdier, C., Couzon, C., Duperray, A., and Singh, P. (2008). Modeling cell interactions under flow. *Journal of Mathematical Biology*, 58(1):235.
- Vermolen, F. J. and Gefen, A. (2013). A phenomenological model for chemico-mechanically induced cell shape changes during migration and cell–cell contacts. *Biomechanics and Modeling in Mechanobiology*, 12(2):301–323.
- Vernerey, F. J. and Farsad, M. (2011). A constrained mixture approach to mechano-sensing and force generation in contractile cells. *Journal of the mechanical behavior of biomedical materials*, 4(8):1683–1699.
- Wang, N. (2017). Review of cellular mechanotransduction. *Journal of physics D: Applied physics*, 50(23):233002.
- Wang, N., Tytell, J. D., and Ingber, D. E. (2009). Mechanotransduction at a distance: mechanically coupling the extracellular matrix with the nucleus. *Nature reviews Molecular cell biology*, 10(1):75–82.
- Wolf, K. and Friedl, P. (2006). Molecular mechanisms of cancer cell invasion and plasticity. *British journal of dermatology*, 154:11–15.
- Wolf, K., Te Lindert, M., Krause, M., Alexander, S., Te Riet, J., Willis, A. L., Hoffman, R. M., Figdor, C. G., Weiss, S. J., and Friedl, P. (2013). Physical limits of cell migration: control by ecm space and nuclear deformation and tuning by proteolysis and traction force. *Journal of Cell Biology*, 201(7):1069–1084.
- Wolf, K., Wu, Y. I., Liu, Y., Geiger, J., Tam, E., Overall, C., Stack, M. S., and Friedl, P. (2007). Multi-step pericellular proteolysis controls the transition from individual to collective cancer cell invasion. *Nature cell biology*, 9(8):893–904.

- Xavier, M., Rosendahl, P., Herbig, M., Kräter, M., Spencer, D., Bornhäuser, M., Oreffo, R. O., Morgan, H., Guck, J., and Otto, O. (2016). Mechanical phenotyping of primary human skeletal stem cells in heterogeneous populations by real-time deformability cytometry. *Integrative Biology*, 8(5):616–623.
- Ye, T., Phan-Thien, N., and Lim, C. T. (2016). Particle-based simulations of red blood cells—a review. *Journal of Biomechanics*, 49(11):2255 – 2266. Selected Articles from the International Conference on {CFD} in Medicine and Biology (Albufeira, Portugal – August 30th - September 4th, 2015).
- Zaman, M. H., Trapani, L. M., Sieminski, A. L., MacKellar, D., Gong, H., Kamm, R. D., Wells, A., Lauffenburger, D. A., and Matsudaira, P. (2006). Migration of tumor cells in 3d matrices is governed by matrix stiffness along with cell-matrix adhesion and proteolysis. *Proceedings of the National Academy of Sciences*, 103(29):10889–10894.
- Zemel, A., Bischofs, I., and Safran, S. (2006). Active elasticity of gels with contractile cells. *Physical review letters*, 97(12):128103.
- Zhang, B., Luo, Q., Chen, Z., Shi, Y., Ju, Y., Yang, L., and Song, G. (2016). Increased nuclear stiffness via fak-erk1/2 signaling is necessary for synthetic mechano-growth factor e peptide-induced tenocyte migration. *Scientific reports*, 6.
- Zhao, F., Vaughan, T. J., and McNamara, L. M. (2016). Quantification of fluid shear stress in bone tissue engineering scaffolds with spherical and cubical pore architectures. *Biomechanics and Modeling in Mechanobiology*, 15(3):561–577.
- Zhou, E., Xu, F., Quek, S., and Lim, C. (2012). A power-law rheology-based finite element model for single cell deformation. *Biomechanics and modeling in mechanobiology*, 11(7):1075–1084.
- Zhou, E. H., Lim, C. T., and Quek, S. T. (2005). Finite element simulation of the micropipette aspiration of a living cell undergoing large viscoelastic deformation. *Mechanics of Advanced Materials and Structures*, 12(6):501–512.
- Zink, D., Fischer, A. H., and Nickerson, J. A. (2004). Nuclear structure in cancer cells. *Nature reviews cancer*, 4(9):677–687.